THE EUROPEAN
PHYSICAL JOURNAL C

Regular Article - Experimental Physics

Measurement of the energy asymmetry in $t\bar{t}j$ production at 13 TeV with the ATLAS experiment and interpretation in the SMEFT framework

ATLAS Collaboration[*]

CERN, 1211 Geneva 23, Switzerland

Abstract A measurement of the energy asymmetry in jet-associated top-quark pair production is presented using 139 fb^{-1} of data collected by the ATLAS detector at the Large Hadron Collider during pp collisions at $\sqrt{s} = 13$ TeV. The observable measures the different probability of top and anti-top quarks to have the higher energy as a function of the jet scattering angle with respect to the beam axis. The energy asymmetry is measured in the semileptonic $t\bar{t}$ decay channel, and the hadronically decaying top quark must have transverse momentum above 350 GeV. The results are corrected for detector effects to particle level in three bins of the scattering angle of the associated jet. The measurement agrees with the SM prediction at next-to-leading-order accuracy in quantum chromodynamics in all three bins. In the bin with the largest expected asymmetry, where the jet is emitted perpendicular to the beam, the energy asymmetry is measured to be -0.043 ± 0.020, in agreement with the SM prediction of -0.037 ± 0.003. Interpreting this result in the framework of the Standard Model effective field theory (SMEFT), it is shown that the energy asymmetry is sensitive to the top-quark chirality in four-quark operators and is therefore a valuable new observable in global SMEFT fits.

Contents

1 Introduction

In searches for physics beyond the Standard Model (SM) at the Large Hadron Collider (LHC), quantum effects of virtual new heavy particles in high-energy observables play a crucial role. In the framework of the Standard Model effective field theory (SMEFT), such effects can be described by effective couplings that modify and extend the interactions of SM particles at energies within the reach of the LHC [1–3]. Extensions of the Standard Model at high energies, referred to as UV ('ultraviolet') theories, typically leave a pattern of effects in several observables. To pin down the structure of a UV theory, sensitive observables that probe complementary directions in the large parameter space of effective couplings have to be combined in a global analysis.

Top-quark physics at the LHC is very well suited to deciphering possible UV theories, both in sensitivity and in complementarity. Top-quark pair production provides a large number of precise observables, allowing the detection of even small deviations from SM predictions in the presence of new physics. Among these observables, the charge asymmetry, based on the different probability for top and antitop quarks to be emitted in a considered phase-space region, is particularly sensitive to new physics. In QCD, the charge asymmetry in $t\bar{t}$ production first occurs at next-to-leading order (NLO)

* e-mail: atlas.publications@cern.ch

[4]; in $t\bar{t}j$ production it is induced at tree level due to the presence of the additional jet [5–8]. Contributions from new particles can lead to significant modifications of the asymmetry compared to the SM prediction [9–12].

At the LHC, the charge asymmetry has been measured as a rapidity asymmetry[1] in top-quark pair production and is found to be in good agreement with the SM prediction [13–15]. Alternatively, the charge asymmetry can be measured as an *energy asymmetry* in top-quark pair production in association with a high transverse momentum (high p_T) jet [16]. The energy asymmetry is an important test of the charge asymmetry at leading order in QCD. By construction, the energy asymmetry is sensitive to the charge asymmetry in a different phase-space region than the rapidity asymmetry. In combination, the two asymmetries are therefore powerful probes of physics beyond the Standard Model in SMEFT. In this article, the energy asymmetry is measured with the 13 TeV proton-proton collision data collected by the ATLAS experiment during Run 2 in 2015-2018 of the LHC.

The energy asymmetry in $t\bar{t}j$ production is defined as

$$A_E(\theta_j) \equiv \frac{\sigma^{\mathrm{opt}}(\theta_j|\Delta E > 0) - \sigma^{\mathrm{opt}}(\theta_j|\Delta E < 0)}{\sigma^{\mathrm{opt}}(\theta_j|\Delta E > 0) + \sigma^{\mathrm{opt}}(\theta_j|\Delta E < 0)}, \quad (1)$$

with the *optimised cross section*

$$\sigma^{\mathrm{opt}}(\theta_j) = \sigma(\theta_j|y_{t\bar{t}j} > 0) + \sigma(\pi - \theta_j|y_{t\bar{t}j} < 0),$$
$$\theta_j \in [0, \pi], \quad (2)$$

where $\sigma(\theta_j)$ is the differential cross section as a function of θ_j, and $y_{t\bar{t}j}$ is the rapidity of the $t\bar{t}j$ system.

To measure the energy asymmetry the difference of the top and antitop energies $\Delta E = E_t - E_{\bar{t}}$ is determined as a function of the jet angle θ_j. Both ΔE and θ_j are defined in the $t\bar{t}j$ rest frame, which corresponds to the partonic centre-of-mass frame in tree-level processes. The angle θ_j is defined as the angle between the jet direction and the positive z-axis, i.e., the direction of parton p_1 in the process $p_1 p_2 \rightarrow t\bar{t}j$. The orientation of the z-axis can be chosen in either direction along the beam line, due to the symmetry in proton-proton collisions. The energy asymmetry is mainly generated in the partonic process $qg \rightarrow t\bar{t}q$, as illustrated in Fig. 1. The outgoing quark-jet is boosted in the direction of the incoming valence quark. This boost is reflected in the rapidity of the $t\bar{t}j$ system in the laboratory frame, $y_{t\bar{t}j}$. By combining 'forward' events having $y_{t\bar{t}j} > 0$ with 'backward' events having $y_{t\bar{t}j} < 0$ in the optimised cross section $\sigma^{\mathrm{opt}}(\theta_j)$, the statistical sensitivity to the energy asymmetry is optimised [17,18].

The energy asymmetry in $t\bar{t}j$ production is measured in three bins of the jet angle θ_j in a fiducial phase space defined at particle level. The analysis selects events with a high-p_T jet, one leptonic W decay from one of the top quarks (called in the following the leptonically decaying top quark) and one hadronic W decay from the other top quark (called in the following the hadronically decaying top quark). The decay products of the hadronically decaying top are required to be collimated in one large-radius jet, as is characteristic of the boosted regime. By focusing on this boosted regime, the additional jet is easily distinguished from the top-quark decay products. Moreover, the energy asymmetry increases with the transverse momentum of the associated jet [18].

The energy asymmetry is highly sensitive to the chirality of the top and antitop quarks [19], which allows the detection of even small potential deviations from the SM prediction. In SMEFT, such effects are described by four-quark operators that involve quarks with different chiralities. The detection of the additional jet in $t\bar{t}j$ production modifies the relative contributions of effective operators to the observables. As a consequence, observables in $t\bar{t}j$ production probe the parameter space of effective couplings in new directions beyond those sensitive to the rapidity asymmetry and other $t\bar{t}$ observables [19]. The energy asymmetry is therefore a valuable new observable in global SMEFT fits [20–24], and thus the results of this measurement are interpreted in SMEFT to derive bounds on four-quark operator contributions.

This paper is organised as follows: a short description of the ATLAS detector is given in Sect. 2, followed by the object definitions at detector and particle level in Sect. 3; event selection and reconstruction are discussed in Sect. 4, while the simulated samples used to model signal and background events are described in Sect. 5. Sections 6 and 7 deal with the unfolding method and the considered systematic uncertainties, respectively; the measurement results are presented in Sect. 8 and interpreted in the context of SMEFT in Sect. 9. Section 10 provides a summary of the analysis.

2 ATLAS detector

The ATLAS detector [25] at the LHC covers nearly the entire solid angle around the collision point.[2] It consists of an inner tracking detector surrounded by a thin superconducting solenoid, electromagnetic and hadron calorimeters, and a

---

[1] In the literature, 'charge asymmetry' is often used as a synonym for 'rapidity asymmetry'. This paper distinguishes between 'charge asymmetry' as a feature of $t\bar{t}$ production in a theory, and 'rapidity asymmetry' and 'energy asymmetry' as observables sensitive to this feature.

[2] ATLAS uses a right-handed coordinate system with its origin at the nominal interaction point (IP) in the centre of the detector and the z-axis along the beam pipe. The x-axis points from the IP to the centre of the LHC ring, and the y-axis points upwards. Cylindrical coordinates (r, ϕ) are used in the transverse plane, ϕ being the azimuthal angle around the z-axis. The pseudorapidity is defined in terms of the polar angle θ as $\eta = -\ln\tan(\theta/2)$, and the rapidity is defined as $y = (1/2)[(E + p_z)/(E - p_z)]$. Angular distance is measured in units of $\Delta R \equiv \sqrt{(\Delta\eta)^2 + (\Delta\phi)^2}$.
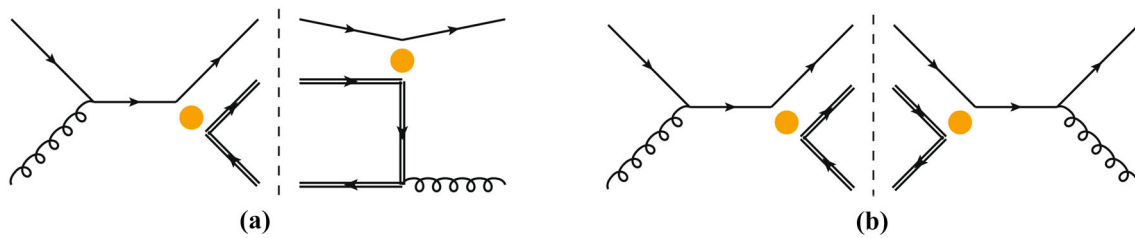
Fig. 1 Examples of contributions to the energy asymmetry in terms of Feynman diagrams. The double lines indicate top quarks; the orange filled circles stand for possible insertions of four-quark operators in SMEFT. The dashed line symbolizes the interference $\mathcal{M}_1\mathcal{M}_2^*$ of the two $qg \to t\bar{t}q$ amplitudes $\mathcal{M}_1$ and $\mathcal{M}_2^*$ to its left and right sides.

Contributions to the asymmetry in QCD are obtained by replacing the orange filled circles in the left diagram by gluons. Further details about the QCD prediction and SMEFT contributions can be found in Ref. [18] and Ref. [19], respectively

muon spectrometer incorporating three large superconducting air-core toroidal magnets.

The inner-detector system (ID) is immersed in a 2 T axial magnetic field and provides charged-particle tracking in the range $|\eta| < 2.5$. The high-granularity silicon pixel detector covers the vertex region and typically provides four measurements per track, the first hit normally being in the insertable B-layer installed before Run 2 [26,27]. It is followed by the silicon microstrip tracker, which usually provides eight measurements per track. These silicon detectors are complemented by the transition radiation tracker, which enables radially extended track reconstruction up to $|\eta| = 2.0$. It also provides electron identification information based on the fraction of hits (typically 30 in total) above a higher energy-deposit threshold corresponding to transition radiation.

The calorimeter system covers the pseudorapidity range $|\eta| < 4.9$. Within the region $|\eta| < 3.2$, electromagnetic calorimetry is provided by barrel and endcap high-granularity lead/liquid-argon (LAr) calorimeters, with an additional thin LAr presampler covering $|\eta| < 1.8$ to correct for energy loss in material upstream of the calorimeters. Hadron calorimetry is provided by the steel/scintillator-tile calorimeter, segmented into three barrel structures within $|\eta| < 1.7$, and two copper/LAr hadron endcap calorimeters. The solid angle coverage is completed with forward copper/LAr and tungsten/LAr calorimeter modules optimised for electromagnetic and hadronic energy measurements respectively.

The muon spectrometer (MS) comprises separate trigger and high-precision tracking chambers measuring the deflection of muons in a magnetic field generated by the superconducting air-core toroidal magnets. The field integral of the toroids ranges between 2.0 and 6.0 Tm across most of the detector. A set of precision chambers covers the region $|\eta| < 2.7$ with three layers of monitored drift tubes, complemented by cathode-strip chambers in the forward region, where the background is highest. The muon trigger system covers the range $|\eta| < 2.4$ with resistive-plate chambers in the barrel, and thin-gap chambers in the endcap regions.

Interesting events are selected by the first-level trigger system implemented in custom hardware, followed by selections made by algorithms implemented in software in the high-level trigger [28]. The first-level trigger accepts events from the 40 MHz bunch crossings at a rate below 100 kHz, which the high-level trigger reduces in order to record events to disk at about 1 kHz.

An extensive software suite [29] is used in the reconstruction and analysis of real and simulated data, in detector operations, and in the trigger and data acquisition systems of the experiment.

3 Object definition

This section defines the final state objects at detector and particle levels. The particle-level objects are used to define the fiducial phase space for the measurement.

3.1 Detector-level objects

The primary vertex of an event is the vertex which has the highest sum of squared transverse momenta from associated tracks with $p_T > 0.5$ GeV [30]. The primary vertex is required to have at least two tracks.

Electron candidates are reconstructed from clusters of energy deposits in the electromagnetic calorimeter that are matched to a track in the ID [31]. They are required to have a transverse energy greater than 25 GeV and $|\eta| < 2.47$. Electron candidates are excluded if their calorimeter energy clusters lie within the transition region between the barrel and the endcap of the electromagnetic calorimeter ($1.37 < |\eta| < 1.52$). Electron tracks must satisfy $|z_0 \sin \theta| < 0.5$ mm and $|d_0|/\sigma(d_0) < 5$, where z_0 is the longitudinal impact parameter relative to the reconstructed primary vertex, d_0 is the transverse impact parameter relative to the beam axis, and $\sigma(d_0)$ is the uncertainty in d_0. 'Baseline' electron candidates are required to satisfy the 'Loose' likelihood-based quality criterion of a multivariate algorithm [32] based on shower

shape and track selection requirements. 'Tight' electron candidates are required to satisfy the 'Tight' quality criterion and to pass p_T- and η-dependent isolation requirements based on their tracks and energy clusters, defined for the 'Tight' isolation working point [32].

Muons are reconstructed by combining track information from the MS with tracks found in the ID. 'Baseline' muon candidates must satisfy $p_T > 25\,\text{GeV}$, $|\eta| < 2.5$ and the 'Medium' identification criterion defined in Ref. [33]. This criterion uses requirements on the number of hits in the various ID and MS subsystems and the q/p compatibility between the MS and ID measurements. In addition, the track associated with the muon candidate must have $|z_0 \sin\theta| < 0.5\,\text{mm}$ and $|d_0|/\sigma(d_0) < 3$. 'Tight' muon candidates are furthermore required to be isolated from additional activity in the event according to the 'Tight' isolation definition using particle-flow objects [33].

Small-radius (small-R) jets are reconstructed from particle-flow objects [34], using the anti-k_t jet clustering algorithm [35] as implemented in the FastJet package [36], with a radius parameter of $R = 0.4$. The impact of additional pp interactions (pile-up) is mitigated by using the jet-area method to correct the jet p_T [37]. Jets are calibrated to ensure a consistent jet energy scale and resolution between data and simulation as described in Ref. [38]. Only jet candidates with $p_T > 25\,\text{GeV}$ and $|\eta| < 2.5$ are considered in this analysis. To mitigate the impact of pile-up, an additional selection criterion using a likelihood-based 'jet-vertex-tagger' (JVT) discriminant is applied to jets with $p_T < 60\,\text{GeV}$ and $|\eta| < 2.4$ [39].

Small-R jets containing b-hadrons (b-jets) are identified (b-tagged) using the deep neural network (DNN) based algorithm, DL1r [40]. This neural network is based on distinctive features of b-hadrons in terms of the impact parameters of tracks and the displaced vertices reconstructed in the inner detector. The inputs of the DL1r network also include discriminating variables constructed by a recurrent neural network, which exploits the spatial and kinematic correlations between tracks originating from the same b-hadron. A selection requirement on the DNN discriminant output is used to identify b-jets. The chosen value provides an 85% average efficiency for identifying b-jets in simulated $t\bar{t}$ events and c-jet and light-flavour jet rejection factors of 2.6 and 29, respectively.

Large-radius (large-R) jets are reconstructed with the anti-k_t algorithm from locally calibrated topological cell clusters [41] with radius parameter $R = 1.0$, and then trimmed using parameters $R_{sub} = 0.2$ and $f_{cut} = 0.05$ [42]. The jet mass resolution is improved by combining the jet mass measurement in the calorimeter with the measurement of the charged component of the jet within the ID [43]. The p_T and mass calibrations of large-R jets are based on 13 TeV data and simulation [43]. Only large-R jets with $|\eta| < 2.0$ are selected.

A large-R jet is considered to be b-tagged if there is at least one b-tagged small-R jet within $\Delta R = 1.0$ of its axis.

Large-R jets containing top quarks are identified (top-tagged) with a DNN using jet substructure variables [44] as input. The top-tagger has an efficiency of 80% for large-R jets that are matched to a particle-level jet, which is in turn matched to a 'truth' top-quark in the MC generator's event record, that has jet mass above 140 GeV and at least one ghost-associated [37] b-hadron. The rejection factor for jets not matched to a top quark ranges from ≈ 10 to ≈ 50 for large-R jets with transverse momenta of 2000 GeV and 350 GeV, respectively. To avoid correlations with additional analysis-specific selection criteria (see Sect. 4), b-tagging information is not included as input to the DNN tagger.

Ambiguities can arise from the independent reconstruction of electron, muon and jet candidates in the detector. A sequential procedure (overlap removal) is applied to avoid double-counting of physics objects, using the same algorithm as in Ref. [45].

The missing transverse momentum vector $\vec{E}_T^{\text{miss}}$ (with magnitude E_T^{miss}) is calculated from the negative vector sum of the p_T of all reconstructed electrons, muons and small-R jets after overlap removal, as well as the p_T of soft activity comprising tracks not associated with those reconstructed objects [46].

3.2 Particle-level objects

Particle-level objects are defined according to ATLAS common practices for 'truth' particle observable definitions as outlined in Ref. [47]. These are specified as close as possible to the definition used for experimentally reconstructed objects using only physical particles that enter the detector to minimise model-dependent corrections. Particle-level objects in simulated $t\bar{t}$ events are defined using quasi-stable particles with a mean lifetime $\tau > 30\,\text{ps}$. They are selected after hadronisation but before the interaction of these particles with the detector components. Particles from pile-up effects are not included.

Electrons and muons must originate (either directly or from leptonic τ decays) from the W bosons from top-quark decays, without requiring a direct match with the parent boson, excluding electrons and muons from hadron decays. The 4-momenta of the 'truth' charged leptons are modified ('dressed') by adding the 4-momenta of all radiated photons within a cone of size $\Delta R = 0.1$ around the lepton, excluding photons from hadron decays, to take into account final-state photon radiation. Small-R and large-R particle-level jets are reconstructed with the same jet algorithms as at detector level using all stable particles, but excluding the charged leptons and neutrinos not from hadron decays and also the photons used to dress the charged leptons. The b-hadrons with $p_T > 5\,\text{GeV}$ are included in the clusters

forming stable-particle jets with their energies set to a negligible positive value (ghost-association) [37]. Particle-level small-R jets containing one or more of these b-hadrons are considered to originate from a b-quark and are called b-flavoured at particle level. A particle-level large-R jet is considered to be b-flavoured if there is at least one b-flavoured small-R jet within $\Delta R = 1.0$ of its axis. A particle-level large-R jet is considered to be top-labelled if it is b-flavoured and the jet mass satisfies is greater than 140 GeV. Charged leptons and small-R jets must have $p_T > 25$ GeV and $|\eta| < 2.5$. The particle-level missing transverse momentum is defined as the vector sum of the transverse momenta of all neutrinos found in the simulation history of the event, excluding those originating from hadron decays.

Particle-level objects are subject to an overlap removal procedure similar to that applied for the detector-level objects as described in Ref. [45].

4 Event selection and reconstruction

This analysis focuses on events with one leptonically and one hadronically decaying top quark in the boosted topology plus an additional hard jet. In this topology, almost all decay products of the hadronically decaying top quark are expected to be collimated into a single large-R jet. The signature for the leptonically decaying top quark is an isolated charged lepton (electron or muon), missing transverse momentum and a b-tagged jet.

Data used in this analysis were collected by the ATLAS detector between 2015 and 2018 at $\sqrt{s} = 13$ Tev. Only events for which all detector subsystems were operational are considered. The data set corresponds to an integrated luminosity of 139 fb^{-1}.

Only events passing a single-electron or single-muon trigger [48,49] are considered. The lowest-threshold triggers use isolation requirements to reduce the trigger rate. These have p_T thresholds of 20 GeV for muons and 24 GeV for electrons in 2015 data, and 26 GeV for both lepton types in 2016, 2017 and 2018 data. They are complemented by additional triggers with a higher p_T threshold of 50 GeV but no isolation requirements in order to increase the event acceptance.

The following event selection criteria were optimised to yield the highest expected sensitivity to the energy asymmetry for jet emission perpendicular to the beam axis. If not stated otherwise, the same criteria are applied for detector-level objects and particle-level objects:

- **Lepton candidate** (ℓ) – Exactly one tight lepton (muon or electron) with $p_T > 27$ GeV is required. This lepton is considered the candidate to be the one originated by the top quark via the W decay and is therefore called the lep-

ton candidate (ℓ). Events containing additional baseline leptons with $p_T > 25$ GeV are rejected. At particle level, exactly one particle-level lepton with $p_T > 27$ GeV is required, and events containing an additional lepton with $p_T > 25$ GeV are rejected.

- **E_T^{miss} and W boson transverse mass (m_T^W)** – To suppress events containing a fake or non-prompt lepton at detector level, it is required that $E_T^{\mathrm{miss}} \geq 20$ GeV and $E_T^{\mathrm{miss}} + m_T^W \geq 60$ GeV.[3] At particle level, no E_T^{miss} or m_T^W cuts are applied.

- **Hadronic top candidate (j_h)** – At least one top-tagged large-R jet fulfilling $p_T > 350$ GeV, and which is separated from the lepton, $\Delta\phi(j_h, \ell) > 1.0$, is required. From the large-R jets fulfilling these conditions, the hadronic top candidate is defined as the one with the highest p_T. At particle level, the top-tagging criterion is replaced by the top-labelling criterion defined in Sect. 3.2, while the kinematic requirements remain unchanged.

- **Leptonic top b-jet candidate (j_l)** – At least one small-R jet close to the lepton candidate, $\Delta R(j_l, \ell) < 2.0$, and isolated from the hadronic top candidate, $\Delta R(j_l, j_h) > 1.5$, is required. From the small-R jets fulfilling these conditions, the leptonic top b-jet candidate is defined as the highest-p_T identified b-jet. If no identified b-jet fulfils these conditions, the highest-p_T small-R jet is taken.

- **Associated jet candidate (j_a)** – At least one small-R jet with $p_T > 100$ GeV separated from the large jet, $\Delta R(j_a, j_h) > 1.5$, and the lepton, $\Delta R(j_a, \ell) > 0.4$, and different from the leptonic jet candidate is required. From the small-R jets fulfilling these conditions, the associated jet candidate is defined as the one with the highest p_T. The p_T cut was chosen such as to optimise the sensitivity to the energy asymmetry in the central θ_j bin, which includes events where the jet is emitted perpendicular to the beam axis and the asymmetry is largest. The optimisation is a trade-off between increased asymmetries for higher p_T values [18] and increased statistical precision for smaller p_T values.

- **Identified b-jet** – At least one small-R jet is required to be identified as a b-jet. The b-jet must either be the leptonic jet candidate j_l or be close to the hadronic top candidate j_h within $\Delta R < 1.0$. If two or more small-R jets are identified as b-jets, the leptonic jet candidate j_l must be identified as a b-jet and the hadronic top candidate must be close to an identified b-jet.

The missing transverse momentum is used as the estimate of the transverse components of the neutrino momentum. The longitudinal component of the neutrino momentum is

---

[3] $m_T^W = \sqrt{p_T^\ell E_T^{\mathrm{miss}}(1 - \cos\Delta\phi)}$, where $\Delta\phi$ is the angle between the lepton candidate and $\vec{E}_T^{\mathrm{miss}}$ in the plane transverse to the beam axis.

obtained by requiring that the invariant mass of the lepton–neutrino system equals the W boson mass. If the resulting quadratic equation has more than one real solution, the solution with the smaller absolute longitudinal momentum is taken. If no real solution is found, the $E_{\mathrm{T}}^{\mathrm{miss}}$ vector is varied minimally in length and direction to obtain one real solution.

The W boson candidate from the leptonic top quark is defined as the 4-momentum sum of the lepton candidate and the reconstructed neutrino. The leptonic top candidate is defined as the 4-momentum sum of the lepton candidate ℓ, reconstructed neutrino, and leptonic jet candidate j_l. The charge of the leptonic top candidate is given by the lepton charge, and the opposite charge is assigned to the hadronic top candidate.

Signal events that pass the selection at both the particle level and the detector level are classified as fiducial signal, while events that pass the detector-level selection but not the particle-level selection are classified as non-fiducial signal.

5 Signal and background modelling

All signal and background processes are modelled using Monte Carlo (MC) simulations, with the exception of backgrounds with fake or non-prompt leptons, which are estimated from data (see Sect. 5.2.2). All simulated samples used EVTGEN 1.6.0 [50] to model the decays of heavy hadrons, with the exception of the background samples generated with SHERPA [51]. Most of the MC samples were passed through a full simulation of the detector response with the GEANT4 toolkit [52,53]. The samples used to estimate modelling systematic uncertainties are either obtained by reweighting the default full simulation samples, or produced using the fast simulation software ATLFAST-II [54], where sample comparisons are always performed using the same type of detector simulation. To model additional pp interactions from the same or neighbouring bunch crossings, the hard scattering events were overlaid with a set of minimum-bias interactions generated using PYTHIA 8 [55] and the MSTW2008LO [56] parton distribution function (PDF) set with a set of tuned parameters called the A3 [57] tune. Finally, the simulated MC events are reconstructed using the same software as the data.

5.1 Signal modelling

All $t\bar{t}$ samples are normalised to the inclusive production cross section calculated by TOP++ 2.0 [58] at next-to-next-to-leading order (NNLO) in QCD including the resummation of next-to-next-to-leading-logarithm (NNLL) soft-gluon terms [59–64]. This corresponds to $\sigma(t\bar{t}) = 832 \pm 51$ pb at a top-quark mass of $m_t = 172.5$ GeV, which is assumed for all $t\bar{t}$ samples unless stated otherwise. The uncertainties

in the cross section due to the choice of PDF and α_{s} are calculated using the PDF4LHC prescription [65] with the MSTW2008NNLO 68% CL [56,66], CT10NNLO [67,68] and NNPDF2.3 5f FFN [69] PDF sets; these uncertainties are added in quadrature to the effect of the scale uncertainty.

The nominal $t\bar{t}$ events were generated with the POWHEG BOX [70–73] v2 generator which provides matrix elements (MEs) at NLO in the strong coupling constant α_{s}, with the NNPDF3.0NLO [74] PDF and the h_{damp} parameter[4] set to $1.5m_t$ [75]. The functional form of the renormalisation and factorisation scales (μ_{r} and μ_{f}) was set to the nominal scale of $\sqrt{m_t^2 + p_{\mathrm{T}}^2}$. The events were interfaced with PYTHIA 8.230 for the parton shower (PS) and hadronisation, using the A14 tune [76] and the NNPDF2.3LO PDF set.

Various alternative $t\bar{t}$ samples are used to estimate the systematic uncertainties associated with the modelling of $t\bar{t}$ production. To simulate more (less) initial-state radiation (ISR), μ_r and μ_f were varied independently by a factor of 0.5 (2.0) in the ME and the up (down) Var3c variations [76] of the A14 tune were used. Samples with the renormalisation scale for QCD emission in final-state radiation (FSR) altered by a factors of 0.5 and 2.0 were used as well. To test the dependence of the measurement on the PS and hadronisation model, POWHEG BOX was interfaced with HERWIG 7.04 [77,78] instead of PYTHIA 8.230, using the H7UE tune [78] and the MMHT2014LO PDF set [79]. The uncertainty in the matching between the ME and PS is evaluated with a sample similar to the nominal $t\bar{t}$ signal sample but where the h_{damp} parameter is set to $3m_t$, as well as a sample based on MADGRAPH5_AMC@NLO (referred to as MG5_AMC in the following) [80] interfaced with PYTHIA 8. The calculation of the hard-scattering uses MG5_AMC 2.6.0 with the NNPDF3.0NLO PDF set. Events were interfaced with PYTHIA 8.230, using the A14 tune and the NNPDF2.3LO PDF. The shower starting scale has the functional form $\mu_{\mathrm{q}} = H_{\mathrm{T}}/2$ [81], where H_{T} is defined as the scalar sum of the p_{T} of all outgoing partons. The choice for μ_{r} and μ_{f} is the same as used with POWHEG BOX. Two dedicated samples with the same settings as in the nominal $t\bar{t}$ signal sample (POWHEG BOX + PYTHIA 8) have m_t set to either 172 GeV or 173 GeV to study the impact of mass uncertainties.

The $t\bar{t}j$ events for the SM and SMEFT predictions used in Sects. 8 and 9 were generated with MG5_AMC interfaced with PYTHIA 8. The calculation of the hard-scattering uses MG5_AMC 2.7.2 with the NNPDF3.0NLO PDF set. Events were interfaced with PYTHIA 8.244 for PS and hadronisation, using the A14 tune and the NNPDF2.3LO PDF set.

---

[4] The h_{damp} parameter controls the transverse momentum p_{T} of the first additional emission beyond the leading order (LO) Feynman diagram in the parton shower (PS) and therefore regulates the high-p_{T} emission against which the $t\bar{t}$ system recoils.

The renormalisation and factorisation scales were chosen as $\mu_r = \mu_f = m_t$. The SM prediction is obtained from matrix elements at NLO in the strong coupling constant α_s. The SM–EFT interference and squared EFT–EFT contributions were generated separately at leading order in α_s using the SMEFT@NLO [82] package. Scale uncertainties in the SM and SMEFT predictions are obtained from the envelope of nine different scale variations by varying μ_r and μ_f independently by factors of 0.5 and 2.0.

5.2 Background modelling

There are two sources of background events: events with electrons and muons produced in W or $Z/\gamma^\star$ boson decays (prompt leptons, Sect. 5.2.1) and events that have one lepton arising from another source (fake and non-prompt leptons, Sect. 5.2.2). In the latter case, electrons and muons originate from heavy-flavour hadron decays, photon conversions, or improper reconstruction of other physics objects such as hadronic jets.

5.2.1 Backgrounds with prompt leptons

Background contributions with prompt leptons originate from a wide range of processes, which are estimated from simulation using the samples described below. The systematic uncertainties in the modelling of these processes by the simulation are discussed in Sect. 7.

Single-top Wt associated production was modelled using the POWHEG BOX [71–73,83] v2 generator to provide MEs at NLO in α_s, using the five-flavour scheme with the NNPDF3.0NLO PDF set. The functional form of μ_r and μ_f was set to the nominal scale of $\sqrt{m_t^2 + p_T^2}$. The diagram removal scheme [84] was employed to treat the interference with $t\bar{t}$ production [75]. Dedicated samples produced with a diagram subtraction (DS) scheme [84] are used to evaluate the uncertainty due to the treatment of the overlap with $t\bar{t}$ production.

Single-top s-channel (t-channel) production was modelled using the POWHEG BOX [71–73,85,86] v2 generator to provide MEs at NLO in α_s, using the five-flavour (four-flavour) scheme with the NNPDF3.0NLO PDF set. The functional form of μ_r and μ_r was set to $\sqrt{m_b^2 + p_{T,b}^2}$ [85]. For these processes, the events were interfaced with PYTHIA 8.230 using the A14 tune and the NNPDF2.3LO PDF set.

Single-top uncertainties due to ISR are estimated using varied weights in the ME and in the PS. To evaluate this μ_r and μ_f were varied by a factor of 2.0 up and down. The impact of increased or decreased FSR is evaluated using PS weights, which vary the renormalisation scale for QCD emission in the FSR by a factor of 0.5 and 2.0, respectively. The impact of the PS and hadronisation model is evaluated by

comparing the nominal generator sample with events produced with the POWHEG BOX v2 generator at NLO in QCD. These use the five-flavour (four-flavour) scheme for tW and s-channel (t-channel) processes, and the NNPDF3.0NLO PDF set. The events are interfaced with HERWIG 7.04, using the H7UE tune and the MMHT2014LO PDF set [79]. To assess the uncertainty due to the choice of matching scheme, the nominal sample is compared with a sample generated with the MG5_AMC 2.6.2 generator at NLO in QCD in the five-flavour (four-flavour) scheme for tW and s-channel (t-channel) processes, using the NNPDF3.0NLO PDF set. The events were interfaced with PYTHIA 8.230, using the A14 tune and the NNPDF2.3LO PDF.

QCD V+jets (W+jets and Z+jets) production was simulated with the SHERPA v2.2.1 MC generator. In this set-up, NLO MEs for up to two jets, and leading order (LO) MEs for up to four jets, were calculated with the OpenLoops [87,88] and Comix [89] libraries. All SHERPA samples use the nominal SHERPA PS [90], based on Catani–Seymour dipoles and the cluster hadronisation model [91], which employs a dedicated set of tuned parameters developed by the SHERPA for use with the NNPDF3.0NNLO PDF set. The V+jets samples are normalised to a NNLO prediction [92].

Diboson (VV) samples were simulated with the SHERPA 2.2.1 and SHERPA 2.2.2 PS MC generators. SHERPA 2.2.2 was used for two- and three-lepton samples. Matrix element and PS matching [93] was applied to the various jet multiplicities, which were then merged into an inclusive sample using an improved CKKW matching procedure [94,95]. The procedure was extended to NLO using the MEPS@NLO prescription [96]. These simulations are at NLO for up to one additional parton and at LO for up to three additional parton emissions using factorised on-shell decays. The virtual QCD corrections for matrix elements at NLO were provided by the OpenLoops library [87,88]. The calculation was performed in the G_μ scheme, ensuring an optimal description of pure electroweak interactions at the electroweak scale.

The production of $t\bar{t}V$ and $t\bar{t}H$ events was modelled using the MG5_AMC 2.3.3 and POWHEG BOX generators, respectively. The generators provide matrix elements at NLO in α_s, with the NNPDF3.0NLO PDF set. For $t\bar{t}V$ and $t\bar{t}H$ production, the events were interfaced with PYTHIA 8.210 and PYTHIA 8.230, respectively. Each uses the A14 tune and the NNPDF2.3LO PDF set.

5.2.2 Backgrounds with fake or non-prompt leptons

To estimate the total contribution of events with fake or non-prompt leptons a data-driven "matrix-method" [97] is used. Two categories of events are selected, satisfying 'baseline' (identification only) and 'tight' (identification and isolation) lepton selection requirements as described in Sect. 3.1. The real (fake/non-prompt) lepton efficiency, ε_{real} (ε_{fake}), is

defined as the ratio of the number of real (fake/non-prompt) leptons satisfying the tight selection to the number of real (fake/non-prompt) leptons satisfying the baseline selection.

The efficiencies for real and fake/non-prompt leptons are parametrised with respect to the p_T and $|\eta|$ of the leptons and are measured separately for electrons and muons in control regions that are statistically independent of the signal region. The fake/non-prompt efficiencies are estimated using single-lepton events from data, where criteria are imposed to suppress the contribution from real leptons. The requirement on the missing transverse momentum is reversed relative to the signal region, to $E_T^{miss} < 20$ GeV, to reduce the contribution from W boson and $t\bar{t}$ events. The residual contribution from real prompt-lepton events in the selected sample is estimated using a MC simulation and subtracted separately from both the tight and baseline samples before the ratio of these samples is calculated to measure the efficiency. The efficiency for fake/non-prompt electrons (muons) ranges from 23% (13%) to 59% (23%), depending on the lepton p_T, $|\eta|$ and data taking period. Any differences between the fake/non-prompt lepton efficiencies in the control region with $E_T^{miss} < 20$ GeV and a validation region with $E_T^{miss} > 20$ GeV have been found to be well within the normalisation uncertainty applied on fake/non-prompt lepton backgrounds as described in Sect. 7. The prompt- or real-lepton efficiencies are evaluated from the simulated $t\bar{t}$ sample, corrected with scale factors measured in data [32,33], in a control region with zero b-tagged jets. The efficiency for real electrons (muons) ranges from 83% (77%) to 95% (95%), depending on the lepton p_T, $|\eta|$ and data taking period.

The sample of events with fake or non-prompt leptons is estimated from the weighted data events, where the weight depends on the real- and fake-lepton efficiencies. As the dominant source of these events is expected to be QCD multijet production, this background is hereafter referred to as 'Multijet'.

5.3 Event yields

Table 1 summarizes the event yields for the signal and background predictions before unfolding (pre-marginalisation) in comparison with those observed in data. The expected yield is in agreement with the observed number of events within uncertainties. The $t\bar{t}$ signal purity is 87%, out of which 70% are fiducial signal. The non-fiducial signal consists mainly of events in which the hadronic top candidate does not pass the p_T, mass and b-flavour requirements. The most important background is W boson production in association with jets (W+jets) which contributes at the level of 5% due to the similarity of its final state and kinematics to the signal. Single-top production contributes at the level of 3% and is dominated by the Wt-channel. The Multijet yield fraction in the signal region is found to be below 2%. The uncertainty of

Table 1 Event yields for the simulated signal and background predictions with uncertainties as described in Sect. 7, compared with the event yield in the signal region as observed in data. The uncertainties do not add up in quadrature to the total uncertainty, due systematic uncertainties being correlated between event samples

	Events
$t\bar{t}$ fiducial	$18{,}000 \pm 3700$
$t\bar{t}$ non-fiducial	8000 ± 1700
W+jets	1600 ± 860
Single-top Wt	680 ± 340
Multijet	580 ± 300
$t\bar{t}V$	400 ± 200
Z+jets	210 ± 110
VV	168 ± 85
$t\bar{t}H$	147 ± 74
Single-top t-channel	82 ± 40
Single-top s-channel	8 ± 3
Total	$30{,}000 \pm 5300$
Data	$27\,265$

21% in the $t\bar{t}$ signal prediction originates mainly from signal modelling effects, where the corresponding impact on the signal yield cancels out for the energy asymmetry observables. Most backgrounds are expected to be symmetric and this is seen within the statistical uncertainty of the simulated samples. For W+jets events the expected asymmetry is negative due to the combination of a higher cross section for W^+ than for W^- production and the selected phase space preferring hadronically decaying top candidates with a larger energy than the leptonically decaying ones, which mostly include the real W bosons.

Figure 2 shows the level of agreement between the data and the detector-level prediction for the top-quark energy and the antitop-quark energy and θ_j. All systematic uncertainties listed in Sect. 7 are included in these comparisons. The data are consistent with the predictions within uncertainties, with a predicted rate about 10% larger than the observed data due to an overestimation of the $t\bar{t}$ yield in the boosted phase space, as reported in Refs. [45,98]. As the charge asymmetry observable is independent of the $t\bar{t}$ cross-section, it is not sensitive to any mismodelling in the rate of $t\bar{t}$ production.

6 Asymmetry extraction and unfolding

Based on the selection criteria defined in Sect. 4, the *optimised event rates* $N^{opt}(\theta_j, \Delta E)$ are extracted from the data in bins of the jet scattering angle, θ_j, and the top–antitop energy difference, $\Delta E = E_t - E_{\bar{t}}$. Here $N^{opt}(\theta_j)$ is defined
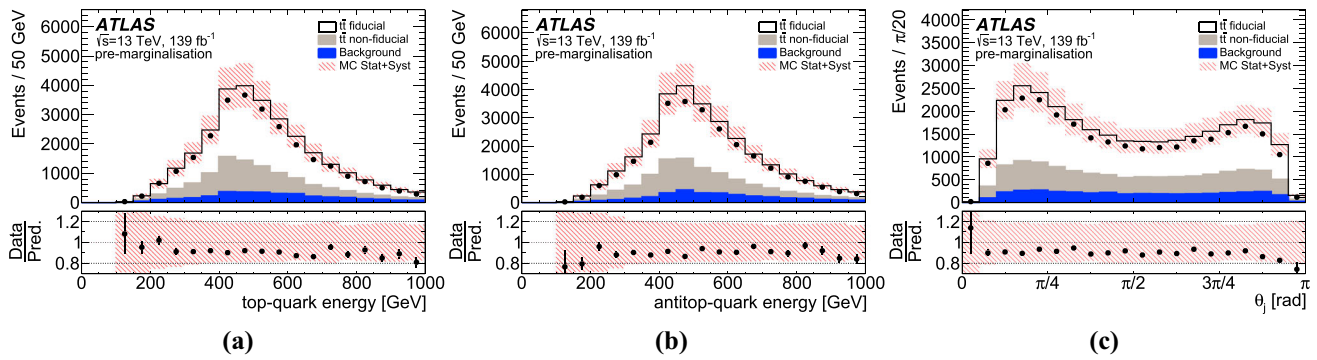
(a)   **(b)**   **(c)**

Fig. 2 Comparison of observed data with the predicted distribution of **a** the top-quark energy, **b** the antitop-quark energy, and **c** the angle θ_j before unfolding (pre-marginalisation). The expectations for the $t\bar{t}$ fiducial and non-fiducial signal are represented by the white and grey areas, respectively, while all non-$t\bar{t}$ backgrounds are added up in the blue area. The shaded red bands correspond to the total uncertainty of the prediction, while the statistical uncertainty on the data is indicated by the black error bars, that are mostly smaller than the size of the marker

as

$$N^{\mathrm{opt}}(\theta_j) = N(\theta_j | y_{t\bar{t}j} > 0) + N(\pi - \theta_j | y_{t\bar{t}j} < 0),$$

in analogy with the optimised cross section $\sigma^{\mathrm{opt}}(\theta_j)$ from Eq. (2). The selected data events are divided into three bins in θ_j, $[0, \pi/4, 3/5\pi, \pi]$, and four bins in ΔE, $[-\infty, -100, 0, 100, \infty]$ GeV. The choice of binning in θ_j optimizes the significance of the energy asymmetry in the central bin at particle level. The binning in ΔE was chosen to account for different migration behaviour for small and large energy differences, while at the same time maintaining a high event rate in each bin. Each of the three θ_j bins is subdivided into four ΔE bins for a total of 12 bins as illustrated in Fig. 3. The chosen configuration shows the best response in linearity tests with different asymmetries in pseudo-data. To obtain $N^{\mathrm{opt}}(\theta_j | \Delta E > 0)$ and $N^{\mathrm{opt}}(\theta_j | \Delta E < 0)$ used in Eq. 4 the content of the corresponding pairs of bins are later summed.

The sample in the 12 bins measured at the detector level is corrected for detector effects (unfolded) to particle-level fiducial phase space defined in Sect. 4. The unfolding is performed with the Fully Bayesian Unfolding (FBU) [14,99] method, which applies Bayesian inference to obtain a full posterior probability density distribution of the unfolded asymmetry.
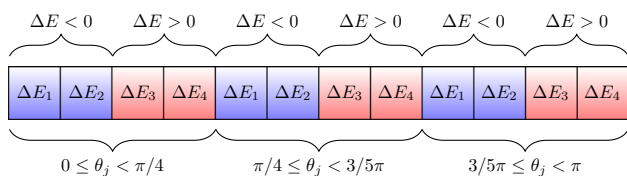

Fig. 3 Concatenation of optimised event rates $N^{\mathrm{opt}}(\theta_j, \Delta E)$ in three bins of θ_j, $[0, \pi/4, 3\pi/5, \pi]$, and four bins in ΔE, $[-\infty, -100, 0, 100, \infty]$ GeV. For each bin in θ_j, the bins coloured blue have $\Delta E < 0$, while the bins coloured red have $\Delta E > 0$. The binning is used both at the reconstruction level R and truth level T

Given an observed spectrum $D \in \mathbb{N}^{N_r}$ with N_r reconstructed bins, a 'truth' spectrum $T \in \mathbb{R}^{N_t}$ with N_t bins and a response matrix $\mathcal{M} \in \mathbb{R}^{N_r} \times \mathbb{R}^{N_t}$, the posterior probability density of the true spectrum T is calculated using Bayes' theorem:

$$P(T|D, \mathcal{M}) \propto \mathcal{L}(D|T, \mathcal{M})\pi(T),$$

where $\mathcal{L}(D|T, \mathcal{M})$ is the likelihood function of D for a given T and $\mathcal{M}$, and $\pi(T)$ is the prior probability density for T. While the response matrix is estimated from the simulated sample of $t\bar{t}$ events, a uniform prior probability density in all bins is chosen as $\pi(T)$, such that equal probabilities are assigned to all T spectra within a wide range between zero and twice the SM prediction.

The likelihood of observing data D for various predictions of signal $R \in \mathbb{R}^{N_r}$ and background $B \in \mathbb{R}^{N_r}$ is given by the product of Poisson probabilities for each bin of the spectrum:

$$\mathcal{L}(D|T, \mathcal{M}, B) = \prod_{i=1}^{N_r} \frac{(r_i + b_i)^{d_i}}{d_i!} e^{-(r_i + b_i)},$$

where r_i and b_i are the expected signal and background yields and d_i is the observed data yield in bin i. The true distribution T is related to the reconstructed signal distribution R via the response matrix $\mathcal{M}$:

$$r_i(T, \mathcal{M}) = \sum_{j=1}^{N_t} m_{ij} t_j, \qquad m_{ij} = \frac{\epsilon_{t_j} P(r_i|t_j)}{f_{\mathrm{acc},r_i}} \tag{3}$$

with efficiency ϵ_{t_j}, migration $P(r_i|t_j)$ and acceptance f_{acc,r_i}. The efficiency ϵ_{t_j} is the probability for an event produced in 'truth' bin t_j to be reconstructed in any bin, i.e. the combined detector acceptance, reconstruction efficiency and selection efficiency. The migration $P(r_i|t_j)$ is the probability for an event produced in the 'truth' bin j to be reconstructed in bin i, given that it is reconstructed in any bin. The acceptance f_{acc,r_i} is the fraction of events passing the detector-level selection
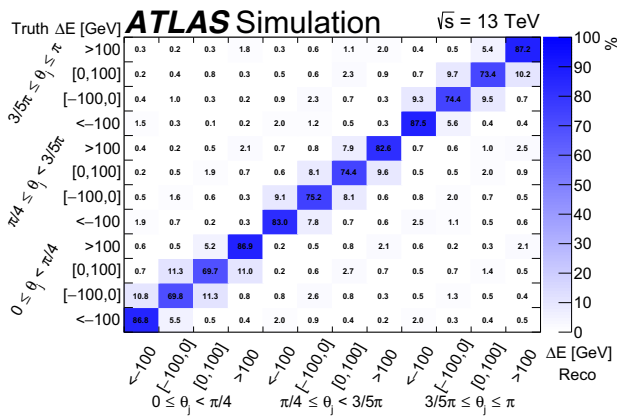
Fig. 4 Migration matrix, normalised to 100% in each truth bin. This gives the probability of a reconstructed event created in truth bin j to be reconstructed in bin i

in bin i that also satisfy the fiducial phase-space selection at particle level.

The migration matrix shown in Fig. 4 is mostly diagonal, with the smallest diagonal entry being 69.7%, indicating that the reconstruction is performing well. The average efficiencies and acceptances are $\epsilon = 34.4\%$ and $f_{\rm acc} = 69.6\%$, respectively.

Systematic uncertainties are included in the FBU via marginalisation, i.e. by introducing $N_{\rm np}$ nuisance parameters which are integrated out to obtain the marginal likelihood:

$$\mathcal{L}(D|T) = \int \mathcal{L}(D|R(T;\boldsymbol{\theta}_s), B(\boldsymbol{\theta}_s, \boldsymbol{\theta}_b))G(\boldsymbol{\theta}_s)G(\boldsymbol{\theta}_b)\mathrm{d}\boldsymbol{\theta}_s\mathrm{d}\boldsymbol{\theta}_b,$$

where $\boldsymbol{\theta}_s$ are nuisance parameters for uncertainties in the modelling, object identification, reconstruction and calibration affecting both the signal prediction $R(T;\boldsymbol{\theta}_s)$ and background prediction $B(\boldsymbol{\theta}_s, \boldsymbol{\theta}_b)$ and $\boldsymbol{\theta}_b$ are the nuisance parameters for background normalisation uncertainties. The priors $G(\boldsymbol{\theta_s})$ and $G(\boldsymbol{\theta_b})$ are Gaussian and truncated Gaussian distributions, respectively, with $\mu = 0$ and $\sigma = 1$. The truncation is applied to avoid a non-physical negative number of events in the background estimate.

The posterior probability distribution $P(T|D)$ is determined by sampling the $(N_{\rm t} + N_{\rm np})$-dimensional parameter space, evaluating the likelihood $\mathcal{L}(D|T, \mathcal{M})\pi(T)$ for each point, and projecting the samples to the T-parameter space. The unfolded asymmetry $A_E(\theta_j)$ is computed from $P(T|D)$ as

$$P(A_E(\theta_j)|D) = \int \delta(A_E(\theta_j) - A_E(\theta_j, T))P(T|D)\,\mathrm{d}T$$

where $A_E(\theta_j, T)$ is defined as in Eq. (1):

$$A_E(\theta_j, T) \equiv \frac{N^{\rm opt}(\theta_j|\Delta E > 0) - N^{\rm opt}(\theta_j|\Delta E < 0)}{N^{\rm opt}(\theta_j|\Delta E > 0) + N^{\rm opt}(\theta_j|\Delta E < 0)} \quad (4)$$

where for $\Delta E > 0$ and $\Delta E < 0$ the sum over the two corresponding bins is taken. The estimate and variance of the

energy asymmetry A_E are given by the mean and variance of the posterior distribution. The marginalised posterior distributions of the nuisance parameters are given by projections on the corresponding one-dimensional nuisance parameter space. The sampling is based on Markov Chain Monte Carlo methods [100] with the *No-U-turn sampler* algorithm [101] in four Markov chains each with 10,000 sampling steps and 2500 tuning steps. The technical implementation uses the PYFBU code [102], which uses the PYMC3 package [103].

The unfolding method was found to be robust against various reweightings of the input distributions, varying the energy asymmetry in a range between -0.15 and 0.15, and with respect to the impact of SMEFT operators within current global limits. As expected, any difference between the unfolded and input asymmetries in these tests is covered by the uncertainties of the response matrix. The final result was also found to be stable with respect to the chosen flat prior. A Gaussian prior with the SM prediction as the mean and a 20% uncertainty changes the central values by 2%–6% and results in approximately 4% smaller uncertainties, supporting the argument that the flat prior is a conservative choice.

7 Systematic uncertainties

Various experimental and theoretical systematic uncertainties affecting both the signal and background predictions are considered. A nuisance parameter with a Gaussian prior is assigned to each systematic uncertainty, unless otherwise specified, and their effect on the measurement is directly included in the unfolding procedure as described in Sect. 6. The smoothing and symmetrisation procedures are described in Sect. 7.3.

7.1 Experimental uncertainties

The uncertainty in the combined 2015–2018 integrated luminosity is 1.7% [104], obtained using the LUCID-2 detector [105] for the primary luminosity measurements. This uncertainty affects only the backgrounds estimated from simulation, since the luminosity uncertainty in the signal cancels out when measuring the energy asymmetry. A reweighting procedure based on the mean number of interactions is used to correct the pile-up profile in MC simulation to match the data. A systematic uncertainty is assigned to the weights. Lepton (e, μ) identification, reconstruction, isolation and trigger performance [48,49] can differ slightly between data and simulation such that scale factors are applied to correct for these differences. The scale factors were obtained by a tag-and-probe method in Z boson and J/ψ decays [32,33]. Systematic uncertainties are assigned to each of these scale factors. The lepton momentum scale and resolution are corrected for

the differences between data and simulation, and the systematic uncertainties for these corrections are taken into account.

For jets, the jet energy scale and resolution uncertainties are applied to both the small-R and large-R jets, taking correlations into account [43,106,107]. Further uncertainties are considered for the JVT [39], the jet mass calibration [43], and the top-tagging scale factors [44,108] for tagged and mistagged jets.

Eigenvector variations for b-, c- and light-jet b-tagging efficiencies [109] are applied to the flavour-tagging scale factors, together with the uncertainty on the p_T extrapolation to the regions in which they could not be determined directly. The uncertainties of all the E_T^{miss} components associated with reconstructed objects are propagated in a fully correlated way. Additional uncertainties in the scale and resolution of the soft-track components are considered [46].

Three kinds of uncertainties are considered for the non-prompt- and fake-lepton backgrounds: the uncertainty in the prediction, due to the limited number of data events and large applied weights, which is uncorrelated for each unfolded bin; the statistical uncertainties of the real- and fake-lepton efficiencies for electrons and muons (four parameters); and a 50% normalisation uncertainty for this background [45].

7.2 Theoretical uncertainties

The relative uncertainties in the inclusive cross sections of backgrounds estimated from simulation are 5.3% for single-top [110,111] and 5% for W+jets [112]. A conservative 50% normalisation uncertainty is applied for the remaining Z+jets, diboson, $t\bar{t}V$ and $t\bar{t}H$ background samples [45], which together represent only 3% of the total expected event yield. In data/MC comparison plots, a relative uncertainty of 6.1% is applied to the $t\bar{t}$ cross section [58]. In the unfolding the amount of signal is unconstrained and not affected by this systematic uncertainty.

The effect of signal modelling uncertainties on the signal distribution R is estimated by varying the response matrix in Eq. (3) for the fixed nominal 'truth' distribution, since the unfolding procedure depends only on the response matrix and is performed without any assumption about the underlying 'truth' distribution.

Signal modelling uncertainties account for the following possible sources of systematic uncertainty:

- parton shower and hadronisation model, estimated as the symmetrised difference between PYTHIA 8 and HERWIG 7, both interfaced to POWHEG BOX;
- matching between matrix element and parton shower, evaluated from the difference between the POWHEG BOX and the MG5_AMC predictions, both interfaced to PYTHIA 8, and from variations of the h_{damp} parameter;
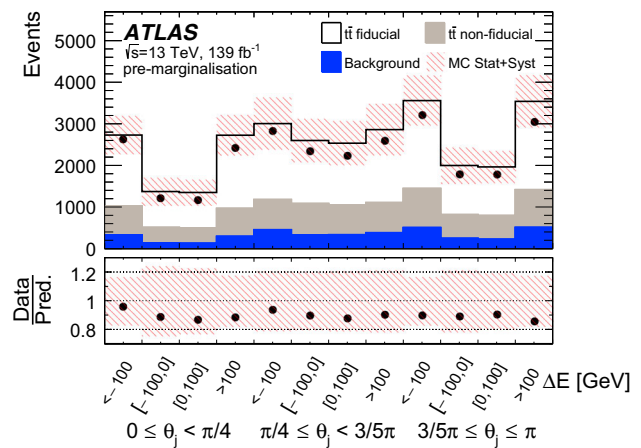

Fig. 5 Comparison of data to the prior (pre-marginalisation) prediction for the ΔE vs. θ_j distribution used in the unfolding. The 3 differential bins in θ_j and 4 ΔE bins are concatenated to give 12 bins as shown in Fig. 3. The shaded red bands correspond to the total uncertainty of the prediction

- initial-state radiation, derived from varied weights in the matrix element and in the parton shower obtained in simulations with μ_r and μ_f values different from the nominal one;
- final-state radiation, based on the variation of parton shower weights corresponding to different renormalisation scales;
- top-quark mass used in the simulation.

The samples used to estimate these uncertainties are described in Sect. 5.1.

The uncertainties in parton distribution functions are evaluated using a set of 30 nuisance parameters described in the PDF4LHC15 prescription [113]. The PDF variations are obtained using alternative MC generator weights stored within the nominal POWHEG + PYTHIA 8 $t\bar{t}$ sample. The uncertainty from the limited size of the MC signal sample is estimated using a bootstrapping method outlined in Ref. [114] from the covariance matrix of the ensemble of repeated unfolding results with varied response matrices.

The single-top systematic uncertainties are decorrelated between the s-, t- and Wt-channel, except for the PDF uncertainties, which are fully correlated across the different channels and with $t\bar{t}$. Both the differences in shape and normalisation are taken into account, except for the PDF uncertainties, since their effect on the normalisation is already included in the cross-section uncertainty. The modelling uncertainties are the same ones as considered for $t\bar{t}$ and are estimated with the same methods. In addition, the difference between the predictions for the Wt-channel obtained with diagram subtraction or removal is considered as a systematic uncertainty [84].

For the W+jets background, modelling uncertainties are estimated by varying the renormalisation and factorisation
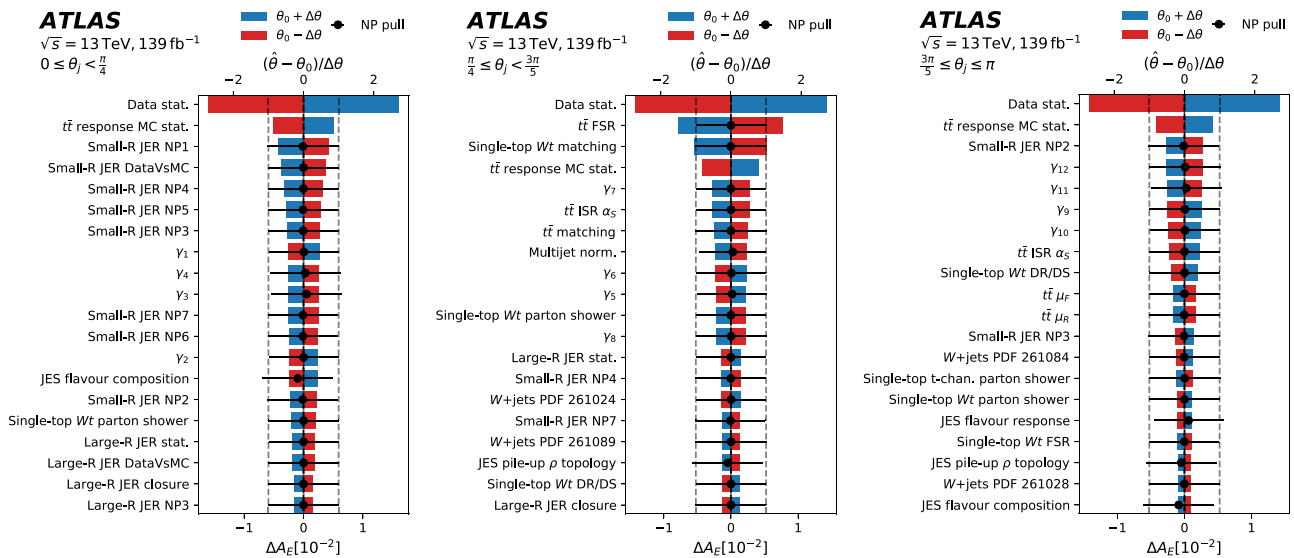
Fig. 6 Ranking of systematic uncertainties in the three θ_j bins. The black dots and error bars (upper scale) denote the mean and standard deviation of the posterior distribution of the nuisance parameter, normalised to its pre-marginalisation standard deviation. The blue and red boxes (lower scale) show the impact on the energy asymmetry from a 1σ variation in its influencing nuisance parameter. The γ variations denote the statistical uncertainties of the background predictions in the corresponding bin of the ΔE vs θ_j distribution. The numbers appended to the W+jets PDF variations denote the corresponding NNPDF3.0 [74] PDF sets

scales up and down by a factor of 2, varying the matrix element to parton shower matching scale up and down by factors of 1.5 and 1.33, respectively, and varying the parton shower resummation scale up and down by a factor of 4, in each case relative to scale(s) for the nominal sample described in Sect. 5.2.1 (see Ref. [81] for further details). The uncertainties in the parton distribution functions are evaluated using a set of 100 PDF variations included in the NNPDF3.0 description [74], obtained using alternative MC generator weights stored within the nominal SHERPA 2.2.1 W+jets samples. To account for the systematic uncertainty in the fraction of W+jets events containing jets originating from b- or c-quarks, these events are filtered into separate samples and their individual normalisation is varied up and down by 30% [115].

7.3 Smoothing and symmetrisation

In order to mitigate effects due to statistical fluctuations in the MC samples used to estimate systematic uncertainties, a bootstrapping method [114] is used to remove statistically insignificant effects in the $t\bar{t}$, single-top and W+jets modelling uncertainties. A variation in a detector-level bin corresponding to one standard deviation of the systematic uncertainty is considered to be statistically significant if it is more than twice as large as the statistical uncertainty of the expected yield in the bin. If at least one of the four ΔE bins in a θ_j interval has a significant variation, all four are left unchanged and no smoothing is applied. Same-sign ΔE

bins are merged and kept if the variation is statistically significant after adding them up, but no variation in the single bins is itself statistically significant. Otherwise, all four bins are combined and the same significance criterion is applied to the combination. If it is significant, all four bins are set to this combined value, effectively dropping the shape of the systematic uncertainty, but keeping its normalisation. If it is still not significant, the systematic uncertainty is neglected in the unfolding.

Since a nuisance parameter with a Gaussian prior is assigned to each of them, the uncertainties are symmetrised in each bin of the reconstruction-level distribution. For one-sided systematic uncertainties, the difference between the nominal yield and the varied yield is used as the standard deviation of the Gaussian prior. For two-sided systematic uncertainties, the average absolute difference between the nominal yield and the upper- and lower-side varied yields is used as the standard deviation.

8 Measurement results

The distribution of the data events at detector level binned in ΔE and θ_j is compared with the SM expectation in Fig. 5. The data are consistent with the predictions within uncertainties. This distribution is the input to the unfolding procedure. With the same number of detector-level bins as 'truth' level bins, the posterior prediction agrees with the data distribution and is thus not shown.

Table 2 Impact of systematic uncertainties by category. The impact of the individual uncertainties is estimated from the posterior distribution as the effect on a bin i of a 1σ variation in its influencing nuisance parameter j, $\sigma_i^{(j)} = c_{ij}/\sqrt{c_{jj}}$. The impact of a group of uncertainties is calculated with Gaussian error propagation, taking into account correlations between uncertainties. The uncertainties in the luminosity and the cross sections of Z+jets, VV, $t\bar{t}V$ and $t\bar{t}H$ backgrounds are found to be negligible and are not shown in the table

Scenario	ΔA_E [10^{-2}]		
	$0 \leq \theta_j < \frac{\pi}{4}$	$\frac{\pi}{4} < \theta_j \leq \frac{3\pi}{5}$	$\frac{3\pi}{5} \leq \theta_j \leq \pi$
Data statistical uncertainty	1.60	1.40	1.40
$t\bar{t}$ modelling	0.08	0.87	0.34
$t\bar{t}$ response MC statistics	0.51	0.42	0.42
W+jets modelling and PDF	0.29	0.49	0.42
Single-top modelling	0.28	0.60	0.29
$t\bar{t}$ and single-top PDF	0.08	0.10	0.07
Multijet	0.53	0.54	0.51
Jet energy resolution	0.98	0.40	0.36
Other detector uncertainties	0.42	0.43	0.30
Total	2.10	2.00	1.80

To determine the impact of each systematic uncertainty, a method of ranking is employed in Fig. 6. For each bin, the effects of 1σ variations in its influencing nuisance parameters are calculated. These effects are then used to rank each systematic uncertainty for the three θ_j bins individually. The effects are extracted from the samples of the posterior distribution with $\sigma_i^{(j)} = c_{ij}/\sqrt{c_{jj}}$ being the estimated shift of bin i due to a shift of nuisance parameter j, where c_{ij} denotes the covariance of the posterior distributions. The impact of systematic uncertainties is largest in the central bin due to the $t\bar{t}$ FSR variation and the choice of matching scheme in the single-top Wt channel being significant compared to the statistical precision of the MC samples, whereas the impact is negligible in the outer bins and therefore ignored in accord with the smoothing procedure described in Sect. 7.3. The different size of the systematic effects is explained by the difference in the relative populations of the ΔE bins in each angu-

lar interval, causing bin-to-bin migrations produced by the systematic variations to affect the asymmetry most strongly in the central θ_j bin. The statistical uncertainties displayed in Fig. 6 are given by the uncertainty from unfolding with all nuisance parameters fixed to their post-marginalisation values. The MC statistical uncertainty of the response matrix is derived with the bootstrapping method described in Sect. 7. The impact of systematic uncertainties by category is calculated with Gaussian error propagation and shown in Table 2. The measurement is dominated by the data statistical uncertainty; the largest systematic uncertainties are from the jet energy resolution, the $t\bar{t}$ modelling and the statistical uncertainty of the multijet estimate in the first, second and third bins, in that order. The first θ_j bin preferentially selects jets closer to the beamline as compared to the other bins; the jet energy resolution uncertainty is therefore larger, as this uncertainty increases with the absolute value of η within the analysis fiducial volume [38].

The measured A_E is obtained from the unfolded ΔE distributions in the three θ_j bins and is shown in Table 3 and in Fig. 7 together with the SM prediction including MC statistical and scale uncertainties obtained as described in Sect. 5.1. In the highest θ_j bin the uncertainty in the SM prediction is similar to the expected sensitivity of the measurement and dominated by scale uncertainties. The measured energy asymmetry is in good agreement with the SM prediction with a combined p-value of 0.80. In the central bin, the measured (expected) energy asymmetry differs from zero by 2.1 (1.9) standard deviations. While the systematic uncertainties of the total cross section dominate for the ΔE and θ_j distribution in Fig. 5, these uncertainties cancel out in the A_E measurement. The correlations between A_E values measured in pairs θ_j bins are always smaller than 5% in magnitude.

9 SMEFT interpretation

The sensitivity of the energy asymmetry to new physics above a scale Λ is investigated in the framework of the Standard Model effective field theory (SMEFT). To this end, the SM Lagrangian $\mathcal{L}_{\mathrm{SM}}$ is extended by a series of local operators

Table 3 The measurement ('Data') of the energy asymmetry in three bins of the jet angle θ_j is compared with the 'SM prediction' obtained from simulations of $t\bar{t}j$ events with MADGRAPH5_AMC@NLO + PYTHIA 8 at NLO in QCD for $t\bar{t}j$ + PS, including MC statistical and scale uncertainties as described in Sect. 5.1. The table also shows the expected measurement values and uncertainties in the case of observing exactly the 'SM prediction' (labelled as 'SM expectation')
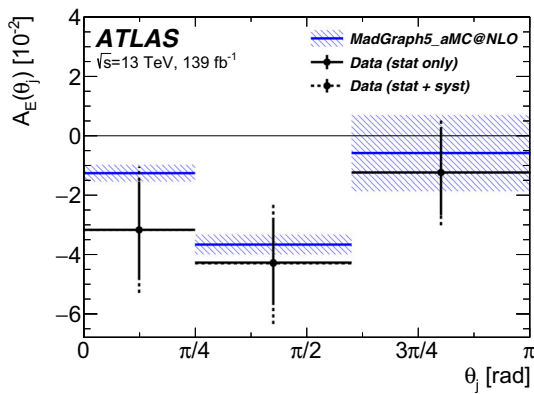
Scenario	$A_E \pm \Delta A_E$ [10^{-2}]		
	$0 \leq \theta_j \leq \frac{\pi}{4}$	$\frac{\pi}{4} \leq \theta_j \leq \frac{3\pi}{5}$	$\frac{3\pi}{5} \leq \theta_j \leq \pi$
Data	-3.2 ± 2.1	-4.3 ± 2.0	-1.3 ± 1.8
SM prediction (MADGRAPH5_AMC@NLO)	-1.3 ± 0.3	-3.7 ± 0.3	-0.6 ± 1.3
SM expectation	-1.3 ± 2.1	-3.7 ± 2.0	-0.6 ± 1.6

Fig. 7 Data measurements (black points with errors) and predictions (blue lines) of the energy asymmetry in three bins of the jet angle θ_j. The SM prediction was obtained from simulations of $t\bar{t}j$ events with MADGRAPH5_AMC@NLO + PYTHIA 8 at NLO in QCD for $t\bar{t}j$ + PS, including MC statistical and scale uncertainties (blue shaded bands) as described in Sect. 5.1

$$O_k,$$

$$\mathcal{L}_{\mathrm{SMEFT}} = \mathcal{L}_{\mathrm{SM}} + \sum_k \frac{C_k}{\Lambda^2} O_k + \dots . \tag{5}$$

The sum runs over all SM gauge-invariant operators of mass dimension six. The ellipsis indicates higher-dimensional operators in the SMEFT expansion, which are neglected in this analysis. The analysis also assumes CP invariance, which implies that all Wilson coefficients C_k are real. Setting all the Wilson coefficients to zero corresponds to the SM. The cut-off scale of this effective theory is set to $\Lambda = 1$ TeV throughout the analysis.

In the Warsaw basis [116], 15 dimension-six operators affect $t\bar{t}j$ production at tree level [19]. The energy asymmetry is particularly sensitive to the chirality and the colour charges of the involved quark fields. To demonstrate this sensitivity, the focus of this numerical analysis is on six selected four-quark operators [117]

$$O_{Qq}^{1,8} = (\bar{Q}_L \gamma_\mu T^A Q_L)(\bar{q}_L \gamma^\mu T^A q_L)$$
$$O_{Qq}^{1,1} = (\bar{Q}_L \gamma_\mu Q_L)(\bar{q}_L \gamma^\mu q_L)$$
$$O_{tu}^8 = (\bar{t}_R \gamma_\mu T^A t_R)(\bar{u}_R \gamma^\mu T^A u_R)$$
$$O_{tu}^1 = (\bar{t}_R \gamma_\mu t_R)(\bar{u}_R \gamma^\mu u_R)$$
$$O_{tq}^8 = (\bar{q}_L \gamma_\mu T^A q_L)(\bar{t}_R \gamma^\mu T^A t_R)$$
$$O_{tq}^1 = (\bar{q}_L \gamma_\mu q_L)(\bar{t}_R \gamma^\mu t_R) . \tag{6}$$

Left-handed quark doublets of the first two generations and the third generation are denoted by

$$q_L = (u_L, d_L)^\top, \ (c_L, s_L)^\top, \qquad Q_L = (t_L, b_L)^\top,$$

reflecting an assumed flavour symmetry among couplings of the first and second quark generations. These six operators feature different chiral structures (LL, RR, LR) and colour structures (singlet (1) and octet (8)), thus covering the relevant properties that can be tested with the energy asymmetry. Operators with right-handed down-type quarks d_R would affect the energy asymmetry very similarly to those with up-type quarks and are therefore not included in this analysis. Up- and down-quark operators can be resolved for instance with $t\bar{t}Z$ or $t\bar{t}W$ observables, which are sensitive to the weak isospin of the quarks [22].

The Wilson coefficients in the effective Lagrangian in Eq. (5) parameterize possible effects of virtual new heavy particles in the cross section σ and in asymmetry observables A according to

$$\sigma = \sigma_S^{\mathrm{SM}} + \sum_k C_k \sigma_S^k + \sum_{k \leq l} C_k C_l \, \sigma_S^{kl},$$

$$A = \frac{\sigma_A}{\sigma_S} = \frac{\sigma_A^{\mathrm{SM}} + \sum_k C_k \sigma_A^k + \sum_{k \leq l} C_k C_l \, \sigma_A^{kl}}{\sigma_S^{\mathrm{SM}} + \sum_k C_k \sigma_S^k + \sum_{k \leq l} C_k C_l \, \sigma_S^{kl}}. \tag{7}$$

The cross sections $\sigma_{S,A}^{\mathrm{SM}}$ denote the SM contributions, while $\sigma_{S,A}^k$ and $\sigma_{S,A}^{kl}$ correspond to the interference of a SMEFT amplitude with the SM amplitude at $\mathcal{O}(\Lambda^{-2})$ and the pure SMEFT amplitudes at $\mathcal{O}(\Lambda^{-4})$, respectively. For the energy asymmetry the charge-symmetric and charge-asymmetric cross sections σ_S and σ_A are defined as

$$\sigma_S = \sigma^{\mathrm{opt}}(\theta_j | \Delta E > 0) + \sigma^{\mathrm{opt}}(\theta_j | \Delta E < 0)$$
$$\sigma_A = \sigma^{\mathrm{opt}}(\theta_j | \Delta E > 0) - \sigma^{\mathrm{opt}}(\theta_j | \Delta E < 0),$$

with σ^{opt} defined as in Eq. (2). The SM prediction and SMEFT contributions are computed in $t\bar{t}j$ production at NLO and LO in QCD, respectively, as described in Sect. 5.1. Relative to the SM predictions $\sigma_{S,A}^{\mathrm{SM}}$, the four-quark operator contributions $\sigma_{S,A}^k$ and $\sigma_{S,A}^{kl}$ grow at high energies as $(m_{t\bar{t}}/2m_t)^2$ and $(m_{t\bar{t}}/2m_t)^4$, respectively [22]. In this analysis, the energy asymmetry is defined in the boosted regime, which probes invariant masses in the range $600 \lesssim m_{t\bar{t}} \lesssim 1200$ Gev, well above the $t\bar{t}$ threshold. The energy enhancement partially cancels out in the normalised asymmetry, but is still present due to the growth of the charge-asymmetric cross section σ_A in ΔE at high energies.

Figure 8 shows the energy asymmetry as a function of individual Wilson coefficients; A_E^1, A_E^2 and A_E^3 correspond to the three bins in θ_j, $[0, \pi/4, 3/5\pi, \pi]$, respectively. To assess the sensitivity of the energy asymmetry to the various operator contributions, χ^2 fits of the SMEFT predictions x^{SMEFT} to the measured energy asymmetry x^{d} in the three jet-angle bins $x = (A_E^1, A_E^2, A_E^3)^\top$ are performed, fitting one or two coefficients at a time, using

$$\chi^2 = (x^{\mathrm{d}} - x^{\mathrm{SMEFT}})^\top C^{-1} (x^{\mathrm{d}} - x^{\mathrm{SMEFT}}) .$$
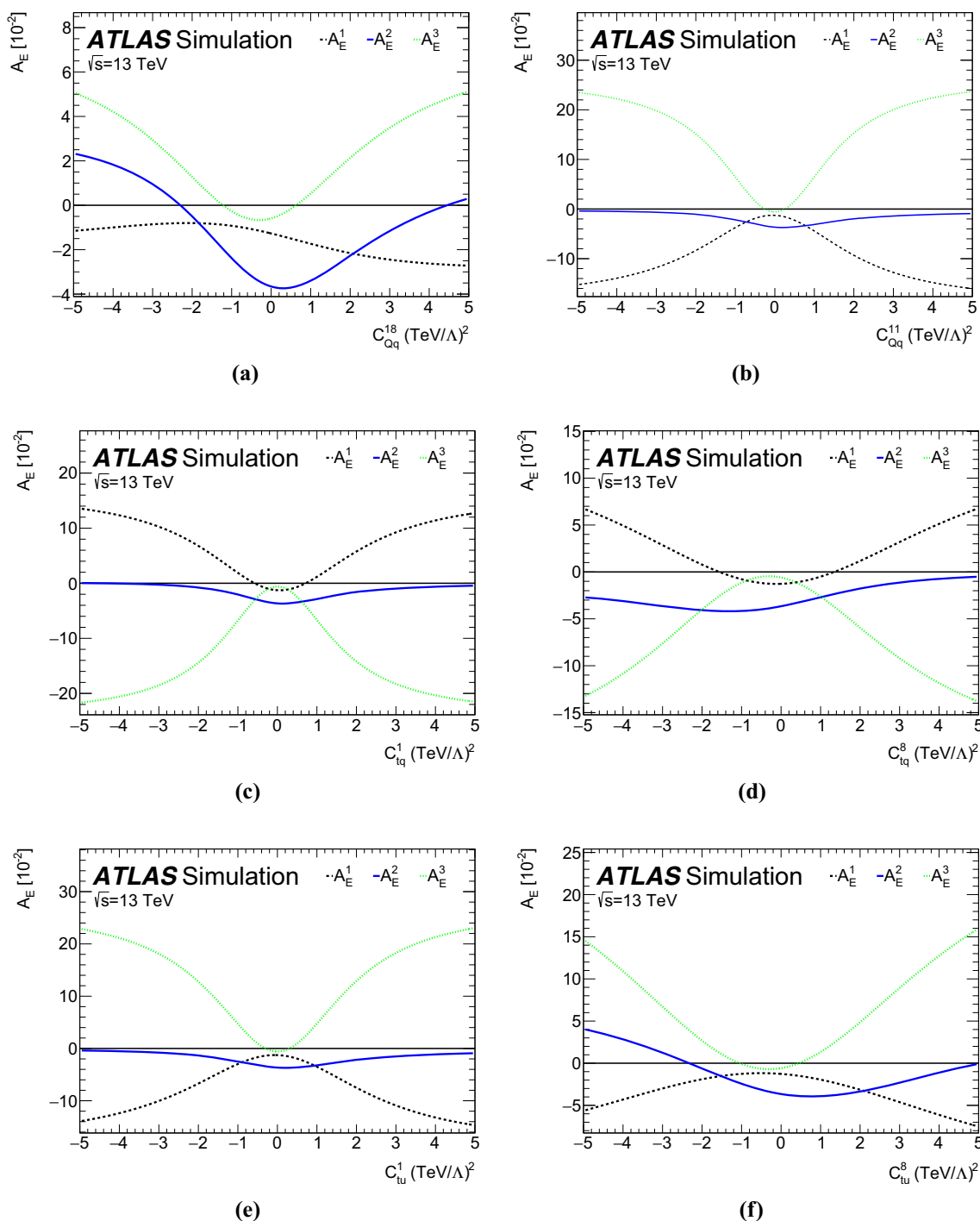
Fig. 8 Energy asymmetry A_E in three θ_j bins, A_E^1 (black, dashed), A_E^2 (blue, solid) and A_E^3 (green, dotted), as a function of individual Wilson coefficients. In each sub-figure, only one coefficient is considered, while all other coefficients are set to zero

Correlations among the measurements and among the predictions are taken into account by the covariance matrix

$$C = C^{\text{d}} + C^{\text{t}}, \qquad C^{\text{t}} = C^{\text{MC stat}} + C^{\text{scale}},$$

which contains the measurement uncertainties C^{d} and the prediction's theoretical uncertainties C^{t} due to both the MC sample size, $C^{\text{MC stat}}$, and the renormalisation and factorisation scale uncertainties, C^{scale}. The predictions x^{SMEFT} are functions of the Wilson coefficients C_k, shown in Eq. (7), that enter the fit as parameters. The corresponding uncertainties associated with $\sigma_{\text{S,A}}^k$ and $\sigma_{\text{S,A}}^{kl}$ are contained in $C^{\text{MC stat}}$ and C^{scale}. The covariance matrix for the scale uncertainties in the SM and SMEFT contributions to x^{SMEFT} in each θ_j bin is obtained from the envelope of nine differ-
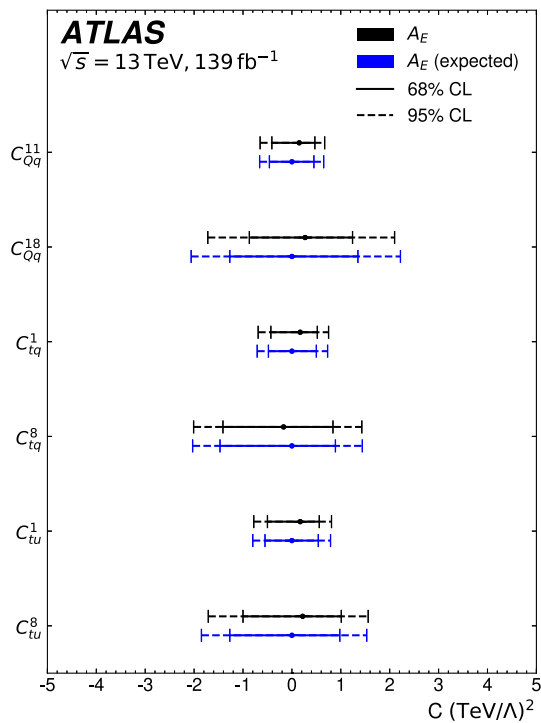
Fig. 9 Bounds on individual Wilson coefficients from the energy asymmetry, obtained from a combined fit to the measured (black) and expected (blue) energy asymmetry in all three θ_j bins. The bounds on $C\,(\mathrm{TeV}/\Lambda)^2$ are reported at the 68% CL (solid) and 95% CL (dashed)

ent settings for the renormalisation and factorisation scales, varied independently by factors of 0.5 and 2.0 and assuming no correlation between the bins. The choice of no bin-to-bin correlation has negligible impact on the result, since theoretical uncertainties have only a small impact on this observable, except in the last θ_j bin.

Figure 9 shows the bounds on individual Wilson coefficients obtained from combined fits to A_E in all three θ_j bins with only one operator contributing at a time. The corresponding 68% and 95% confidence level (CL) intervals are listed in Table 4. Overall, the energy asymmetry is sensitive to four-quark operator coefficients in the range of $[-2, 2]\,(\mathrm{TeV}/\Lambda)^2$ at 95% CL, with the precise bounds varying for individual operators.

To estimate the relative impact of $\mathcal{O}(\Lambda^{-2})$ versus $\mathcal{O}(\Lambda^{-4})$ operator contributions, Table 4 shows the bounds obtained from the energy asymmetry when including operator contributions to the charge-symmetric and charge-asymmetric cross sections σ_S and σ_A up to $\mathcal{O}(\Lambda^{-4})$ (left two columns) and up to $\mathcal{O}(\Lambda^{-2})$ (right two columns). Comparing these two scenarios, it is clear that the bounds are dominated by the $\mathcal{O}(\Lambda^{-4})$ contributions $\sigma_{S,A}^{kl}$. The results at $\mathcal{O}(\Lambda^{-2})$ are listed here only to assess the relevance of the various operator contributions.

Due to its sensitivity to four-quark operators the energy asymmetry will provide additional constraining power when

included in global SMEFT fits. Recent global fits of top-quark observables lead to stronger bounds on four-quark coefficients, see for instance Figure 5.7 in Ref. [21], Figure 13 in Ref. [22] or Figure 5 in Ref. [23]. This is due to charge-symmetric observables such as the invariant mass distribution $d\sigma/dm_{t\bar{t}}$, where the sensitivity to four-quark operators is strongly enhanced at high energy.

The main asset of the energy asymmetry is its ability to resolve new directions in the SMEFT parameter space. In particular, charge asymmetries are very sensitive to the quark chiralities and the colour structure of effective interactions. The analytic dependence of the energy asymmetry has been studied in detail in Ref. [19]. To explore the numerical sensitivity to the chiral and colour structure of the six operators from Eq. (6), fits to pairs of Wilson coefficients were performed. Figure 10 shows the bounds on these coefficients from a combined fit of the energy asymmetry in all three jet-angle bins. Most bounds are centred near (0, 0), due to good agreement between the measurement and the SM prediction.

The various pairs of operators have been chosen in order to investigate their chiral structure and colour structure separately. Figure 10a, b show colour-singlet operators with different quark chiralities. Figure 10c, d show the same chirality scenarios as in Fig. 10a, b, but for colour-octet operators. Figure 10e, f show operators that differ only in their colour structure. The main features observed are discussed below; details about the operator dependence of the asymmetry can be found in Ref. [19].

In Fig. 10a, b, the two operators differ only by the chirality of the top quark (left) and the chirality of the up quark (right). For operators with left- versus right-handed tops (left), a blind direction is observed along $C_{Qq}^{11} = \pm C_{tq}^1$. This blind direction is slightly broken by the linear SMEFT contribution of $\mathcal{O}(\Lambda^{-2})$ (see Equation (3.17) in Ref. [19]). For operators with different initial quark chiralities (right), the blind direction is broken at $\mathcal{O}(\Lambda^{-4})$, because the operators $O_{Qq}^{1,1}$ and O_{tu}^1 do not interfere with each other in the limit of massless incoming quarks. Colour-octet operators, shown in Fig. 10c, d, interfere with QCD. This effect lifts the blind direction in the (C_{Qq}^{18}, C_{tq}^8) plane.

The bounds for colour singlets are generally stronger than for colour octets. This can be seen by comparing the bounds in Fig. 10a, b with those in Fig. 10c, d or by comparing the bounds on each of the coefficients in Fig. 10e, f. The different sensitivity is due to colour factors in the amplitude, which lead to a larger contribution of colour-singlet coefficients to the asymmetry.

Due to the extra jet in $t\bar{t}j$ production, the QCD structure of the energy asymmetry is not the same as for the rapidity asymmetry in $t\bar{t}$ production. Indeed, the two asymmetries probe different directions in chiral and colour space. This complementarity can be estimated by comparing Fig. 10 with
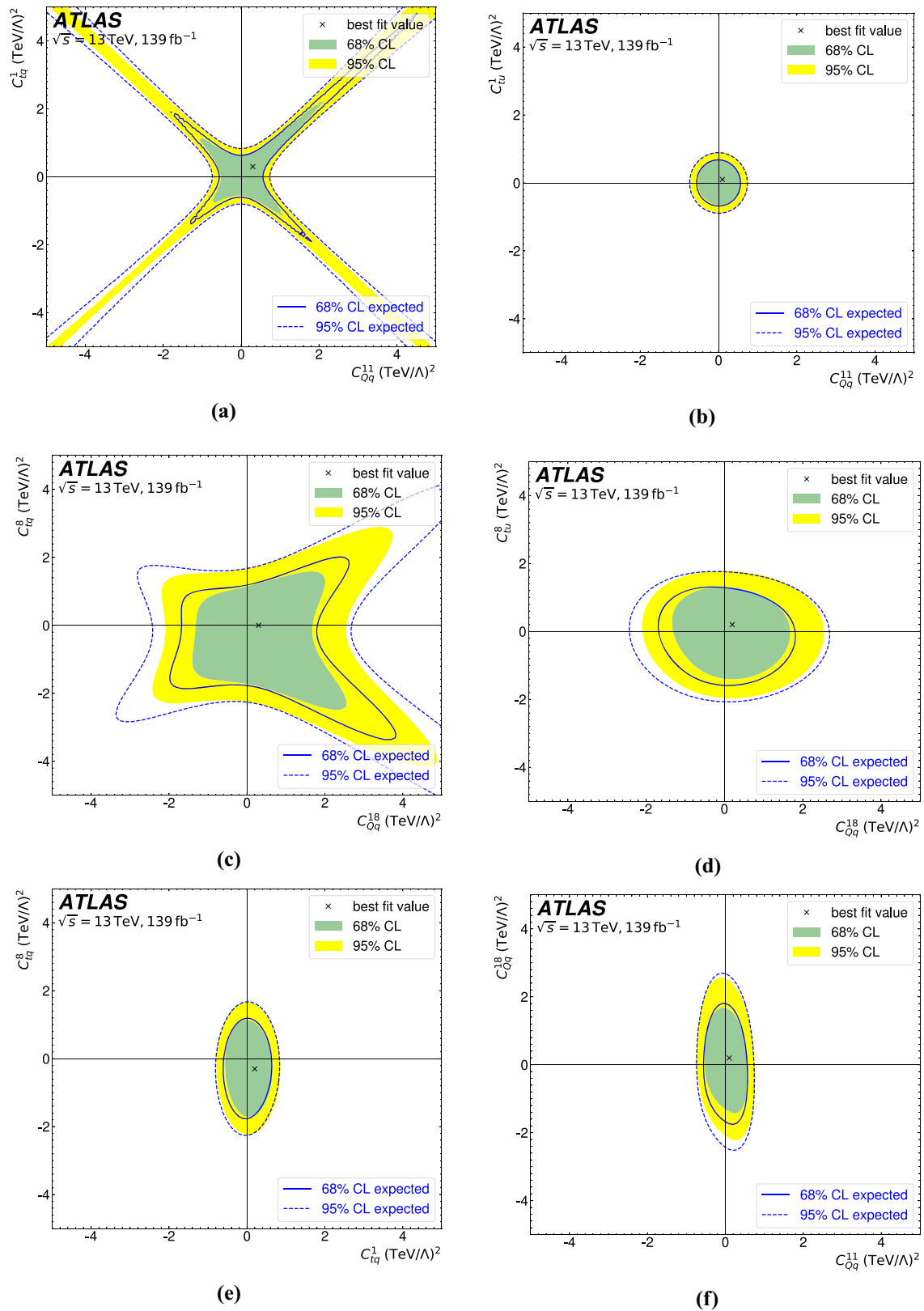
Fig. 10 Bounds on Wilson coefficients from two-parameter fits of the energy asymmetry A_E in all three θ_j bins. The inner green and outer yellow areas show the 68% and 95% CL limits obtained from the measured energy asymmetry, respectively. The black cross denotes the minimum of the χ^2 fit. Solid and dashed blue contours show the expected 68% and 95% CL limits from the energy asymmetry, respectively

Table 4 Bounds on individual Wilson coefficients C (TeV/Λ)^2 from the energy asymmetry, obtained from a combined fit to its values in all three θ_j bins: A_E^1, A_E^2, and A_E^3. The SMEFT predictions include operator contributions to σ_S and σ_A up to $\mathcal{O}(\Lambda^{-4})$ (left) and up to $\mathcal{O}(\Lambda^{-2})$ (right)

C (TeV/Λ)^2	A_E (Λ^{-4})		A_E (Λ^{-2})	
	68% CL	95% CL	68% CL	95% CL
C_{Qq}^{11}	[−0.41, 0.47]	[−0.65, 0.67]	[−0.68, 4.06]	[−3.36, 6.16]
C_{Qq}^{18}	[−0.87, 1.24]	[−1.72, 2.10]	[−1.26, 4.76]	[−3.24, 9.64]
C_{tq}^{1}	[−0.43, 0.52]	[−0.69, 0.75]	[−0.60, 5.76]	[−3.42, 9.36]
C_{tq}^{8}	[−1.41, 0.84]	[−2.01, 1.43]	[−1.86, 1.70]	[−3.30, 3.98]
C_{tu}^{1}	[−0.50, 0.56]	[−0.78, 0.81]	[−0.96, 5.82]	[−4.72, 8.88]
C_{tu}^{8}	[−1.00, 1.01]	[−1.71, 1.56]	[−1.30, 2.52]	[−3.02, 4.66]

Figure 6 in Ref. [19], which shows the expected bounds from the energy asymmetry compared with the expected bounds from the rapidity asymmetry. For the colour-singlet operators in Fig. 10a, b, the two asymmetries probe similar areas in the parameter space. For the colour-octet operators in Fig. 10c, d, however, the shapes of the bounds look very different. In particular, the rapidity asymmetry leaves a blind direction in the $(C_{Qq}^{18}, C_{tq}^{8})$ plane, which is broken by the energy asymmetry due to operator interference with the QCD amplitude as shown in Fig. 10c. The different shapes of the bounds in Fig. 10e, f are due to the colour-singlet and colour-octet contributions differing between $t\bar{t}$ and ttj production, which is probed by the asymmetries with a high sensitivity.

This comparison demonstrates once more the relevance of the energy asymmetry for global fits. Combining the energy and rapidity asymmetries in a joint fit would result in a better resolution of the Wilson coefficients in the SMEFT parameter space. Moreover, the energy asymmetry resolves remaining blind or nearly blind directions left by the rapidity asymmetry and other top-quark observables. In global analyses the energy asymmetry can thus be a useful tool to gain information about the chiral and colour structure of possible UV theories.

10 Summary

This paper reports the first measurement of the energy asymmetry in jet-associated top-quark pair production in the boosted topology in the lepton+jets decay channel, using 139 fb^{-1} of $\sqrt{s} = 13$ TeV proton-proton collision data collected by the ATLAS experiment at the LHC. The measurement was performed differentially in three bins of the jet scattering angle θ_j. A fully Bayesian unfolding method was used to correct for detector resolution and acceptance effects.

The differential measurements of the energy asymmetry in all three θ_j bins are consistent with the SM predictions calculated at NLO in QCD, including effects of parton showering and hadronisation. In the second bin, $\pi/4 < \theta_j < 3\pi/5$, with jet emission perpendicular to the beam axis, the energy asymmetry is measured as $A_E^2 = -0.043 \pm 0.020$, in good agreement with the QCD prediction of -0.037 ± 0.003. The measurement uncertainty is dominated by the limited data sample in the boosted phase-space region.

To determine the sensitivity of the energy asymmetry to new physics, this observable was analyzed within the SMEFT framework. The energy asymmetry is highly sensitive to the chiral and colour structure of four-quark operators with top quarks. Based on SMEFT predictions in terms of dimension-six operators, bounds on the Wilson coefficients of individual operators are extracted.

The energy asymmetry in $t\bar{t}j$ production has a sensitivity to some individual four-quark operators that is similar to that of other observables in the top sector and probes new directions in the parameter space of Wilson coefficients. The sensitivity to these new directions is illustrated in the two-parameter fits of operator pairs with different chiral and colour structures. These results show that the energy asymmetry complements the sensitivity of other observables, such as differential cross sections and the rapidity asymmetry, and hence that the energy asymmetry is a valuable new observable in global SMEFT fits.

References

1. W. Buchmuller, D. Wyler, Effective Lagrangian analysis of new interactions and flavour conservation. Nucl. Phys. B **268**, 621 (1986). https://doi.org/10.1016/0550-3213(86)90262-2

2. C.N. Leung, S.T. Love, S. Rao, Low-energy manifestations of a new interactions scale: operator analysis. Z. Phys. C **31**, 433 (1986). https://doi.org/10.1007/BF01588041

3. I. Brivio, M. Trott, The standard model as an effective field theory. Phys. Rep. **793**, 1 (2019). https://doi.org/10.1016/j.physrep.2018.11.002 arXiv:1706.08945 [hep-ph]

4. J.H. Kuhn, G. Rodrigo, Charge asymmetry of heavy quarks at hadron colliders. Phys. Rev. D **59**, 054017 (1999). https://doi.org/10.1103/PhysRevD.59.054017 arXiv:hep-ph/9807420

5. M.T. Bowen, S.D. Ellis, D. Rainwater, Standard model top quark asymmetry at the Fermilab Tevatron. Phys. Rev. D **73**, 014008 (2006). https://doi.org/10.1103/PhysRevD.73.014008 arXiv:hep-ph/0509267

6. S. Dittmaier, P. Uwer, S. Weinzierl, Next-to-leading-order QCD corrections to $t\bar{t} + jet$ production at hadron colliders. Phys. Rev. Lett. **98**, 262002 (2007). https://doi.org/10.1103/PhysRevLett.98.262002 arXiv:hep-ph/0703120

7. S. Dittmaier, P. Uwer, S. Weinzierl, Hadronic top-quark pair production in association with a hard jet at next-to-leading order QCD: phenomenological studies for the Tevatron and the LHC. Eur. Phys. J. C **59**, 625 (2009). https://doi.org/10.1140/epjc/s10052-008-0816-y arXiv:0810.0452 [hep-ph]

8. K. Melnikov, M. Schulze, NLO QCD corrections to top quark pair production in association with one hard jet at hadron colliders. Nucl. Phys. B **840**, 129 (2010). https://doi.org/10.1016/j.nuclphysb.2010.07.003 arXiv:1004.3284 [hep-ph]

9. O. Antunano, J.H. Kuhn, G. Rodrigo, Top quarks, axigluons, and charge asymmetries at hadron colliders. Phys. Rev. D **77**, 014003 (2008). https://doi.org/10.1103/PhysRevD.77.014003 arXiv:0709.1652 [hep-ph]

10. M. Bauer, F. Goertz, U. Haisch, T. Pfoh, S. Westhoff, Top-quark forward-backward asymmetry in Randall–Sundrum models beyond the leading order. JHEP **11**, 039 (2010). https://doi.org/10.1007/JHEP11(2010)039 arXiv:1008.0742 [hep-ph]

11. U. Haisch, S. Westhoff, Massive color-octet bosons: bounds on effects in top-quark pair production. JHEP **08**, 088 (2011). https://doi.org/10.1007/JHEP08(2011)088 arXiv:1106.0529 [hep-ph]

12. J.F. Kamenik, J. Shu, J. Zupan, Review of new physics effects in $t\bar{t}$ production. Eur. Phys. J. C **72**, 2102 (2012). https://doi.org/10.1140/epjc/s10052-012-2102-2 arXiv:1107.5257 [hep-ph]

13. ATLAS and CMS Collaborations, Combination of inclusive and differential $t\bar{t}$ charge asymmetry measurements using ATLAS and CMS data at $\sqrt{s} = 7\,TeV$ and 8 TeV. JHEP **04**, 033 (2018). https://doi.org/10.1007/JHEP04(2018)033. arXiv:1709.05327 [hep-ex]

14. ATLAS Collaboration, Measurement of the charge asymmetry in top-quark pair production in the lepton-plus-jets final state in pp collision data at $\sqrt{s} = 8$ TeV with the ATLAS detector. Eur. Phys. J. C **76**, 87 (2016). https://doi.org/10.1140/epjc/s10052-016-3910-6. arXiv:1509.02358 [hep-ex] [Erratum: Eur. Phys. J. C **77**, 564 (2017)]

15. CMS Collaboration, Inclusive and differential measurements of the $t\bar{t}$ charge asymmetry in pp collisions at $\sqrt{s} = 8$ TeV. Phys. Lett. B **757** (2016) 154. https://doi.org/10.1016/j.physletb.2016.03.060. arXiv: 1507.03119 [hep-ex]

16. S. Berge, S. Westhoff, Top-quark charge asymmetry goes forward: two new observables for hadron colliders. JHEP **07**, 179 (2013). https://doi.org/10.1007/JHEP07(2013)179 arXiv:1305.3272 [hep-ph]

17. S. Alte, S. Berge, H. Spiesberger, Top quark charge asymmetry: searching for light axigluons in $t\bar{t} + jet$ production at the LHC. JHEP **09**, 084 (2014). https://doi.org/10.1007/JHEP09(2014)084 arXiv:1406.0501 [hep-ph]

18. S. Berge, S. Westhoff, Observing the top energy asymmetry at the LHC. Phys. Rev. D **95**, 014035 (2017). https://doi.org/10.1103/PhysRevD.95.014035 arXiv:1608.00574 [hep-ph]

19. A. Basan, P. Berta, L. Masetti, E. Vryonidou, S. Westhoff, Measuring the top energy asymmetry at the LHC: QCD and SMEFT interpretations. JHEP **03**, 184 (2020). https://doi.org/10.1007/JHEP03(2020)184 arXiv:2001.07225 [hep-ph]

20. A. Buckley et al., Constraining top quark effective theory in the LHC Run II era. JHEP **04**, 015 (2016). https://doi.org/10.1007/JHEP04(2016)015 arXiv:1512.03360 [hep-ph]

21. N.P. Hartland et al., A Monte Carlo global analysis of the Standard Model Effective Field Theory: the top quark sector. JHEP **04**, 100 (2019). https://doi.org/10.1007/JHEP04(2019)100 arXiv:1901.05965 [hep-ph]

22. I. Brivio et al., O new physics, where art thou? A global search in the top sector. JHEP **02**, 131 (2020). https://doi.org/10.1007/JHEP02(2020)131 arXiv:1910.03606 [hep-ph]

23. J. Ellis, M. Madigan, K. Mimasu, V. Sanz, T. You, Top, Higgs, diboson and electroweak fit to the Standard Model effective field theory. JHEP **04**, 279 (2021). https://doi.org/10.1007/JHEP04(2021)279 arXiv:2012.02779 [hep-ph]

24. J.J. Ethier et al., Combined SMEFT interpretation of Higgs, diboson, and top quark data from the LHC (2021). arXiv:2105.00006 [hep-ph]

25. ATLAS Collaboration, The ATLAS Experiment at the CERN Large Hadron Collider. JINST **3**, S08003 (2008). https://doi.org/10.1088/1748-0221/3/08/S08003

26. ATLAS Collaboration, ATLAS Insertable B-Layer: Technical Design Report, ATLAS-TDR-19; CERN-LHCC-2010-013 (2010). https://cds.cern.ch/record/1291633 [Addendum: ATLAS-TDR-19-ADD-1; CERN-LHCC-2012-009, https://cds.cern.ch/record/1451888 (2012)]

27. B. Abbott et al., Production and integration of the ATLAS Insertable B-Layer. JINST **13**, T05008 (2018). https://doi.org/10.1088/1748-0221/13/05/T05008 arXiv:1803.00844 [physics.ins-det]

28. ATLAS Collaboration, Performance of the ATLAS trigger system in 2015. Eur. Phys. J. C **77**, 317 (2017). https://doi.org/10.1140/epjc/s10052-017-4852-3. arXiv:1611.09661 [hep-ex]

29. ATLAS Collaboration, ATLAS Computing Acknowledgements, ATL-SOFT-PUB-2020-001. https://cds.cern.ch/record/2717821

30. ATLAS Collaboration, Vertex reconstruction performance of the ATLAS detector at $\sqrt{s} = 13$ TeV, ATL-PHYS-PUB-2015-026 (2015). https://cds.cern.ch/record/2037717

31. ATLAS Collaboration, Electron and photon performance measurements with the ATLAS detector using the 2015–2017 LHC proton–proton collision data. JINST **14**, P12006 (2019). https://doi.org/10.1088/1748-0221/14/12/P12006. arXiv:1908.00005 [hep-ex]

32. ATLAS Collaboration, Electron reconstruction and identification in the ATLAS experiment using the 2015 and 2016 LHC proton–proton collision data at $\sqrt{s} = 13$ TeV. Eur. Phys. J. C **79**, 639 (2019)https://doi.org/10.1140/epjc/s10052-019-7140-6. arXiv:1902.04655 [hep-ex]

33. ATLAS Collaboration, Muon reconstruction and identification efficiency in ATLAS using the full Run 2 pp collision data set at $\sqrt{s} = 13$ TeV. Eur. Phys. J. C **81**, 578 (2020). https://doi.org/10.1140/epjc/s10052-021-09233-2. arXiv:2012.00578 [hep-ex]

34. ATLAS Collaboration, Jet reconstruction and performance using particle flow with the ATLAS Detector. Eur. Phys. J. C **77**, 466 (2017). https://doi.org/10.1140/epjc/s10052-017-5031-2. arXiv:1703.10485 [hep-ex]

35. M. Cacciari, G.P. Salam, G. Soyez, The anti-k_t jet clustering algorithm. JHEP **04**, 063 (2008). https://doi.org/10.1088/1126-6708/2008/04/063 arXiv:0802.1189 [hep-ph]

36. M. Cacciari, G.P. Salam, G. Soyez, FastJet user manual. Eur. Phys. J. C **72**, 1896 (2012). https://doi.org/10.1140/epjc/s10052-012-1896-2 arXiv:1111.6097 [hep-ph]

37. M. Cacciari, G.P. Salam, G. Soyez, The catchment area of jets. JHEP **04**, 005 (2008). https://doi.org/10.1088/1126-6708/2008/04/005 arXiv:0802.1188 [hep-ph]

38. ATLAS Collaboration, Jet energy scale and resolution measured in proton–proton collisions at $\sqrt{s} = 13$ TeV with the ATLAS detector. Eur. Phys. J. C **81**, 689 (2020). https://doi.org/10.1140/epjc/s10052-021-09402-3. arXiv:2007.02645 [hep-ex]

39. ATLAS Collaboration, Performance of pile-up mitigation techniques for jets in pp collisions at $\sqrt{s} = 8$ TeV using the ATLAS detector. Eur. Phys. J. C **76**, 581 (2016). https://doi.org/10.1140/epjc/s10052-016-4395-z. arXiv:1510.03823 [hep-ex]

40. ATLAS Collaboration, ATLAS b-jet identification performance and efficiency measurement with $t\bar{t}$ events in pp collisions at $\sqrt{s} = 13$ TeV. Eur. Phys. J. C **79**, 970 (2019). https://doi.org/10.1140/epjc/s10052-019-7450-8. arXiv:1907.05120 [hep-ex]

41. ATLAS Collaboration, Topological cell clustering in the ATLAS calorimeters and its performance in LHC Run 1. Eur. Phys. J. C **77**, 490 (2017). https://doi.org/10.1140/epjc/s10052-017-5004-5. arXiv:1603.02934 [hep-ex]

42. D. Krohn, J. Thaler, L.-T. Wang, Jet trimming. JHEP **02**, 084 (2010). https://doi.org/10.1007/JHEP02(2010)084 arXiv:0912.1342 [hep-ph]

43. ATLAS Collaboration, In situ calibration of large-radius jet energy and mass in 13 TeV proton–proton collisions with the ATLAS detector. Eur. Phys. J. C **79**, 135 (2019). https://doi.org/10.1140/epjc/s10052-019-6632-8. arXiv:1807.09477 [hep-ex]

44. ATLAS Collaboration, Performance of top-quark and W-boson tagging with ATLAS in Run 2 of the LHC. Eur. Phys. J. C **79**, 375 (2019). https://doi.org/10.1140/epjc/s10052-019-6847-8. arXiv:1808.07858 [hep-ex]

45. ATLAS Collaboration, Measurements of top-quark pair differential and double-differential cross-sections in the ℓ+jets channel with pp collisions at $\sqrt{s} = 13$ TeV using the ATLAS detector. Eur. Phys. J. C **79**, 1028 (2019). https://doi.org/10.1140/epjc/s10052-019-7525-6. arXiv:1908.07305 [hep-ex] [Erratum: Eur. Phys. J. C **80**, 1092 (2020)]

46. ATLAS Collaboration, Performance of missing transverse momentum reconstruction with the ATLAS detector using proton–proton collisions at $\sqrt{s} = 13$ TeV. Eur. Phys. J. C **78**, 903 (2018). https://doi.org/10.1140/epjc/s10052-018-6288-9. arXiv:1802.08168 [hep-ex]

47. ATLAS Collaboration, Proposal for particle-level object and observable definitions for use in physics measurements at the LHC, ATL-PHYS-PUB-2015-013 (2015). https://cds.cern.ch/record/2022743

48. ATLAS Collaboration, Performance of electron and photon triggers in ATLAS during LHC Run 2. Eur. Phys. J. C **80**, 47 (2020). https://doi.org/10.1140/epjc/s10052-019-7500-2. arXiv:1909.00761 [hep-ex]

49. ATLAS Collaboration, Performance of the ATLAS muon triggers in Run 2. JINST **15**, P09015 (2020). https://doi.org/10.1088/1748-0221/15/09/p09015. arXiv:2004.13447 [hep-ex]

50. D.J. Lange, The EvtGen particle decay simulation package. Nucl. Instrum. Meth. A **462**, 152 (2001). https://doi.org/10.1016/S0168-9002(01)00089-4

51. E. Bothmann et al., Event generation with Sherpa 2.2. SciPost Phys. **7**, 034 (2019). https://doi.org/10.21468/SciPostPhys.7.3.034 arXiv:1905.09127 [hep-ph]

52. GEANT4 Collaboration, S. Agostinelli et al., GEANT4—a simulation toolkit. Nucl. Instrum. Meth. A **506**, 250 (2003). https://doi.org/10.1016/S0168-9002(03)01368-8

53. ATLAS Collaboration, The ATLAS Simulation Infrastructure. Eur. Phys. J. C **70**, 823 (2010). https://doi.org/10.1140/epjc/s10052-010-1429-9. arXiv:1005.4568 [physics.ins-det]

54. ATLAS Collaboration, The simulation principle and performance of the ATLAS fast calorimeter simulation FastCaloSim, ATL-PHYS-PUB-2010-013 (2010). https://cds.cern.ch/record/1300517

55. T. Sjöstrand et al., An introduction to PYTHIA 8.2. Comput. Phys. Commun. **191**, 159 (2015). https://doi.org/10.1016/j.cpc.2015.01.024 arXiv:1410.3012 [hep-ph]

56. A.D. Martin, W.J. Stirling, R.S. Thorne, G. Watt, Parton distributions for the LHC. Eur. Phys. J. C **63**, 189 (2009). https://doi.org/10.1140/epjc/s10052-009-1072-5 arXiv:0901.0002 [hep-ph]

57. ATLAS Collaboration, The Pythia 8 A3 tune description of ATLAS minimum bias and inelastic measurements incorporating
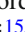
the Donnachie–Landshoff diffractive model, ATL-PHYS-PUB-2016-017. https://cds.cern.ch/record/2206965 (2016)

58. M. Czakon, A. Mitov, Top++: a program for the calculation of the top-pair cross-section at hadron colliders. Comput. Phys. Commun. 185, 2930 (2014). https://doi.org/10.1016/j.cpc.2014.06.021 arXiv:1112.5675 [hep-ph]

59. M. Beneke, P. Falgari, S. Klein, C. Schwinn, Hadronic top-quark pair production with NNLL threshold resummation. Nucl. Phys. B 855, 695 (2012). https://doi.org/10.1016/j.nuclphysb.2011.10.021 arXiv:1109.1536 [hep-ph]

60. M. Cacciari, M. Czakon, M. Mangano, A. Mitov, P. Nason, Top-pair production at hadron colliders with next-to-next-to-leading logarithmic soft-gluon resummation. Phys. Lett. B 710, 612 (2012). https://doi.org/10.1016/j.physletb.2012.03.013 arXiv:1111.5869 [hep-ph]

61. P. Bärnreuther, M. Czakon, A. Mitov, Percent-level-precision physics at the Tevatron: next-to-next-to-leading order QCD corrections to $q\bar{q} \rightarrow t\bar{t} + X$. Phys. Rev. Lett. 109, 132001 (2012). https://doi.org/10.1103/PhysRevLett.109.132001 arXiv:1204.5201 [hep-ph]

62. M. Czakon, A. Mitov, NNLO corrections to top-pair production at hadron colliders: the all-fermionic scattering channels. JHEP 12, 054 (2012). https://doi.org/10.1007/JHEP12(2012)054 arXiv:1207.0236 [hep-ph]

63. M. Czakon, A. Mitov, NNLO corrections to top pair production at hadron colliders: the quark-gluon reaction. JHEP 01, 080 (2013). https://doi.org/10.1007/JHEP01(2013)080 arXiv:1210.6832 [hep-ph]

64. M. Czakon, P. Fiedler, A. Mitov, Total top-quark pair-production cross section at hadron colliders through $O(\alpha_S^4)$. Phys. Rev. Lett. 110, 252004 (2013). https://doi.org/10.1103/PhysRevLett.110.252004 arXiv:1303.6254 [hep-ph]

65. M. Botje et al., The PDF4LHC Working Group Interim Recommendations (2011). arXiv:1101.0538 [hep-ph]

66. A.D. Martin, W.J. Stirling, R.S. Thorne, G. Watt, Uncertainties on α_S in global PDF analyses and implications for predicted hadronic cross sections. Eur. Phys. J. C 64, 653 (2009). https://doi.org/10.1140/epjc/s10052-009-1164-2 arXiv:0905.3531 [hep-ph]

67. H.-L. Lai et al., New parton distributions for collider physics. Phys. Rev. D 82, 074024 (2010). https://doi.org/10.1103/PhysRevD.82.074024 arXiv:1007.2241 [hep-ph]

68. J. Gao et al., CT10 next-to-next-to-leading order global analysis of QCD. Phys. Rev. D 89, 033009 (2014). https://doi.org/10.1103/PhysRevD.89.033009 arXiv:1302.6246 [hep-ph]

69. R.D. Ball et al., Parton distributions with LHC data. Nucl. Phys. B 867, 244 (2013). https://doi.org/10.1016/j.nuclphysb.2012.10.003 arXiv:1207.1303 [hep-ph]

70. S. Frixione, P. Nason, G. Ridolfi, A positive-weight next-to-leading-order Monte Carlo for heavy flavour hadroproduction. JHEP 09, 126 (2007). https://doi.org/10.1088/1126-6708/2007/09/126 arXiv:0707.3088 [hep-ph]

71. P. Nason, A new method for combining NLO QCD with shower Monte Carlo algorithms. JHEP 11, 040 (2004). https://doi.org/10.1088/1126-6708/2004/11/040 arXiv:hep-ph/0409146

72. S. Frixione, P. Nason, C. Oleari, Matching NLO QCD computations with parton shower simulations: the POWHEG method. JHEP 11, 070 (2007). https://doi.org/10.1088/1126-6708/2007/11/070 arXiv:0709.2092 [hep-ph]

73. S. Alioli, P. Nason, C. Oleari, E. Re, A general framework for implementing NLO calculations in shower Monte Carlo programs: the POWHEG BOX. JHEP 06, 043 (2010). https://doi.org/10.1007/JHEP06(2010)043 arXiv:1002.2581 [hep-ph]

74. R.D. Ball et al., Parton distributions for the LHC run II. JHEP 04, 040 (2015). https://doi.org/10.1007/JHEP04(2015)040 arXiv:1410.8849 [hep-ph]

75. ATLAS Collaboration, Studies on top-quark Monte Carlo modelling for Top2016, ATL-PHYS-PUB-2016-020 (2016). https://cds.cern.ch/record/2216168

76. ATLAS Collaboration, ATLAS Pythia 8 tunes to 7 TeV data, ATL-PHYS-PUB-2014-021 (2014). https://cds.cern.ch/record/1966419

77. M. Bähr et al., Herwig++ physics and manual. Eur. Phys. J. C 58, 639 (2008). https://doi.org/10.1140/epjc/s10052-008-0798-9 arXiv:0803.0883 [hep-ph]

78. J. Bellm et al., Herwig 7.0/Herwig++ 3.0 release note. Eur. Phys. J. C 76, 196 (2016). https://doi.org/10.1140/epjc/s10052-016-4018-8 arXiv:1512.01178 [hep-ph]

79. L. Harland-Lang, A. Martin, P. Motylinski, R. Thorne, Parton distributions in the LHC era: MMHT 2014 PDFs. Eur. Phys. J. C 75, 204 (2015). https://doi.org/10.1140/epjc/s10052-015-3397-6 arXiv:1412.3989 [hep-ph]

80. J. Alwall et al., The automated computation of tree-level and next-to-leading order differential cross sections, and their matching to parton shower simulations. JHEP 07, 079 (2014). https://doi.org/10.1007/JHEP07(2014)079 arXiv:1405.0301 [hep-ph]

81. ATLAS Collaboration, Studies on top-quark Monte Carlo modelling with Sherpa and MG5_aMC@NLO, ATL-PHYS-PUB-2017-007 (2017). https://cds.cern.ch/record/2261938

82. C. Degrande et al., Automated one-loop computations in the standard model effective field theory. Phys. Rev. D 103, 096024 (2021). https://doi.org/10.1103/PhysRevD.103.096024 arXiv:2008.11743 [hep-ph]

83. E. Re, Single-top Wt-channel production matched with parton showers using the POWHEG method. Eur. Phys. J. C 71, 1547 (2011). https://doi.org/10.1140/epjc/s10052-011-1547-z arXiv:1009.2450 [hep-ph]

84. S. Frixione, E. Laenen, P. Motylinski, C. White, B.R. Webber, Single-top hadroproduction in association with a W boson. JHEP 07, 029 (2008). https://doi.org/10.1088/1126-6708/2008/07/029 arXiv:0805.3067 [hep-ph]

85. R. Frederix, E. Re, P. Torrielli, Single-top t-channel hadroproduction in the four-flavour scheme with POWHEG and aMC@NLO. JHEP 09, 130 (2012). https://doi.org/10.1007/JHEP09(2012)130 arXiv:1207.5391 [hep-ph]

86. S. Alioli, P. Nason, C. Oleari, E. Re, NLO single-top production matched with shower in POWHEG: s-and t-channel contributions. JHEP 09, 111 (2009). https://doi.org/10.1088/1126-6708/2009/09/111. arXiv:0907.4076 [hep-ph] [Erratum: JHEP 02, 011 (2010)]

87. F. Cascioli, P. Maierhöfer, S. Pozzorini, Scattering amplitudes with open loops. Phys. Rev. Lett. 108, 111601 (2012). https://doi.org/10.1103/PhysRevLett.108.111601 arXiv:1111.5206 [hep-ph]

88. A. Denner, S. Dittmaier, L. Hofer, COLLIER: a fortran-based complex one-loop library in extended regularizations. Comput. Phys. Commun. 212, 220 (2017). https://doi.org/10.1016/j.cpc.2016.10.013 arXiv:1604.06792 [hep-ph]

89. T. Gleisberg, S. Höche, Comix, a new matrix element generator. JHEP 12, 039 (2008). https://doi.org/10.1088/1126-6708/2008/12/039 arXiv:0808.3674 [hep-ph]

90. S. Schumann, F. Krauss, A parton shower algorithm based on Catani–Seymour dipole factorisation. JHEP 03, 038 (2008). https://doi.org/10.1088/1126-6708/2008/03/038 arXiv:0709.1027 [hep-ph]

91. J.-C. Winter, F. Krauss, G. Soff, A modified cluster-hadronization model. Eur. Phys. J. C 36, 381 (2004). https://doi.org/10.1140/epjc/s2004-01960-8 arXiv:hep-ph/0311085

92. C. Anastasiou, L.J. Dixon, K. Melnikov, F. Petriello, High precision QCD at hadron colliders: electroweak gauge boson rapidity distributions at next-to-next-to leading order. Phys.

Rev. D **69**, 094008 (2004). https://doi.org/10.1103/PhysRevD.69.094008 arXiv:hep-ph/0312266

93. S. Höche, F. Krauss, M. Schönherr, F. Siegert, A critical appraisal of $NLO + PS$ matching methods. JHEP **09**, 049 (2012). https://doi.org/10.1007/JHEP09(2012)049 arXiv:1111.1220 [hep-ph]

94. S. Catani, F. Krauss, B.R. Webber, R. Kuhn, QCD matrix elements + parton showers. JHEP **11**, 063 (2001). https://doi.org/10.1088/1126-6708/2001/11/063 arXiv:hep-ph/0109231

95. S. Höche, F. Krauss, S. Schumann, F. Siegert, QCD matrix elements and truncated showers. JHEP **05**, 053 (2009). https://doi.org/10.1088/1126-6708/2009/05/053 arXiv:0903.1219 [hep-ph]

96. S. Höche, F. Krauss, M. Schönherr, F. Siegert, QCD matrix elements + parton showers. The NLO case. JHEP **04**, 027 (2013). https://doi.org/10.1007/JHEP04(2013)027 arXiv:1207.5030 [hep-ph]

97. ATLAS Collaboration, Estimation of non-prompt and fake lepton backgrounds in final states with top quarks produced in proton–proton collisions at $\sqrt{s} = 8$ TeV with the ATLAS Detector, ATLAS-CONF-2014-058 (2014). https://cds.cern.ch/record/1951336

98. ATLAS Collaboration, Study of top-quark pair modelling and uncertainties using ATLAS measurements at $\sqrt{s} = 13$ TeV, ATL-PHYS-PUB-2020-023 (2020). https://cds.cern.ch/record/2730443

99. G.Choudalakis, Fully Bayesian Unfolding (2012). arXiv:1201.4612 [hep-ex]

100. P. Diaconis, The Markov chain Monte Carlo revolution. Bull. Am. Math. Soc. (N.S.) **46**, 179 (2009)

101. M.D. Hoffman, A. Gelman, The No-U-Turn sampler: adaptively setting path lengths in Hamiltonian Monte Carlo (2011). arXiv:1111.4246 [stat.CO]

102. C. Helsens, F. Rubbo, D. Gerbaudo, Implementation of the fully Bayesian unfolding algorithm. https://github.com/pyFBU/fbu [Online; accessed: 05/09/2020]. https://doi.org/10.7717/peerj-cs.55

103. J. Salvatier, T.V. Wiecki, C. Fonnesbeck, Probabilistic programming in Python using PyMC3. PeerJ Comput. Sci. **2**, e55 (2016). https://doi.org/10.7717/peerj-cs.55

104. ATLAS Collaboration, Luminosity determination in pp collisions at $\sqrt{s} = 13$ TeV using the ATLAS detector at the LHC, ATLAS-CONF-2019-021 (2019). https://cds.cern.ch/record/2677054

105. G. Avoni et al., The new LUCID-2 detector for luminosity measurement and monitoring in ATLAS. JINST **13**, P07017 (2018). https://doi.org/10.1088/1748-0221/13/07/P07017

106. ATLAS Collaboration, Jet energy scale measurements and their systematic uncertainties in proton–proton collisions at $\sqrt{s} = 13$ TeV with the ATLAS detector. Phys. Rev. D **96**, 072002 (2017). https://doi.org/10.1103/PhysRevD.96.072002. arXiv:1703.09665 [hep-ex]

107. ATLAS Collaboration, Determination of jet calibration and energy resolution in proton–proton collisions at $\sqrt{s} = 8$ TeV using the ATLAS detector. Eur. Phys. J. C **80**, 1104 (2020). https://doi.org/10.1140/epjc/s10052-020-08477-8. arXiv:1910.04482 [hep-ex]

108. ATLAS Collaboration, Boosted hadronic vector boson and top quark tagging with ATLAS using Run 2 data, ATL-PHYS-PUB-2020-017 (2020). https://cds.cern.ch/record/2724149

109. ATLAS Collaboration, Measurements of b-jet tagging efficiency with the ATLAS detector using $t\bar{t}$ events at $\sqrt{s} = 13$ TeV. JHEP **08**, 089 (2018). https://doi.org/10.1007/JHEP08(2018)089. arXiv:1805.01845 [hep-ex]

110. M. Aliev et al., HATHOR—HAdronic Top and Heavy quarks crOss section calculatoR. Comput. Phys. Commun. **182**, 1034 (2011). https://doi.org/10.1016/j.cpc.2010.12.040 arXiv:1007.1327 [hep-ph]

111. P. Kant et al., HatHor for single top-quark production: updated predictions and uncertainty estimates for single top-quark production in hadronic collisions. Comput. Phys. Commun. **191**, 74 (2015). https://doi.org/10.1016/j.cpc.2015.02.001 arXiv:1406.4403 [hep-ph]

112. ATLAS Collaboration, Measurement of $W^{\pm}$ and Z-boson production cross sections in pp collisions at $\sqrt{s} = 13$ TeV with the ATLAS detector. Phys. Lett. B **759**, 601 (2016). https://doi.org/10.1016/j.physletb.2016.06.023. arXiv:1603.09222 [hep-ex]

113. J. Rojo, PDF4LHC recommendations for Run II. PoS **DIS2016**, 018 (2016). arXiv:1606.08243 [hep-ph]

114. G. Bohm, G. Zech, Introduction to Statistics and Data Analysis for Physicists; 2nd rev. ed. Hamburg: Verlag Deutsches Elektronen-Synchrotron (2014). ISBN: 978-3-935702-88-1, http://bib-pubdb1.desy.de/record/169869

115. ATLAS Collaboration, ATLAS simulation of boson plus jets processes in Run 2, ATL-PHYS-PUB-2017-006. https://cds.cern.ch/record/2261937 (2017)

116. B. Grzadkowski, M. Iskrzynski, M. Misiak, J. Rosiek, Dimension-six terms in the Standard Model Lagrangian. JHEP **10**, 085 (2010). https://doi.org/10.1007/JHEP10(2010)085 arXiv:1008.4884 [hep-ph]

117. D. Barducci et al., Interpreting top-quark LHC measurements in the standard-model effective field theory, ed. by J.A. Aguilar-Saavedra et al. arXiv:1802.07237 [hep-ph] (2018)

118. ATLAS Collaboration, ATLAS Computing Acknowledgements, ATL-SOFT-PUB-2021-003. https://cds.cern.ch/record/2776662

ATLAS Collaboration

G. Aad[98], B. Abbott[124], D. C. Abbott[99], A. Abed Abud[34], K. Abeling[51], D. K. Abhayasinghe[91], S. H. Abidi[27], A. Aboulhorma[33e], H. Abramowicz[157], H. Abreu[156], Y. Abulaiti[5], A. C. Abusleme Hoffman[142a], B. S. Acharya[64a,64b,o], B. Achkar[51], L. Adam[96], C. Adam Bourdarios[4], L. Adamczyk[81a], L. Adamek[162], S. V. Addepalli[24], J. Adelman[116], A. Adiguzel[11c,ab], S. Adorni[52], T. Adye[139], A. A. Affolder[141], Y. Afik[34], C. Agapopoulou[62], M. N. Agaras[12], J. Agarwala[68a,68b], A. Aggarwal[114], C. Agheorghiesei[25c], J. A. Aguilar-Saavedra[135a,135f,aa], A. Ahmad[34], F. Ahmadov[77], W. S. Ahmed[100], X. Ai[44], G. Aielli[71a,71b], I. Aizenberg[175], S. Akatsuka[83], M. Akbiyik[96], T. P. A. Åkesson[94], A. V. Akimov[107], K. Al Khoury[37], G. L. Alberghi[21b], J. Albert[171], P. Albicocco[49], M. J. Alconada Verzini[86], S. Alderweireldt[48], M. Aleksa[34], I. N. Aleksandrov[77], C. Alexa[25b], T. Alexopoulos[9], A. Alfonsi[115], F. Alfonsi[21b], M. Alhroob[124], B. Ali[137], S. Ali[154], M. Aliev[161], G. Alimonti[66a], C. Allaire[34], B. M. M. Allbrooke[152], P. P. Allport[19], A. Aloisio[67a,67b], F. Alonso[86], C. Alpigiani[144], E. Alunno Camelia[71a,71b], M. Alvarez Estevez[95], M. G. Alviggi[67a,67b], Y. Amaral Coutinho[78b], A. Ambler[100], L. Ambroz[130], C. Amelung[34], D. Amidei[102], S. P. Amor Dos Santos[135a], S. Amoroso[44], K. R. Amos[169], C. S. Amrouche[52], V. Ananiev[129], C. Anastopoulos[145], N. Andari[140], T. Andeen[10], J. K. Anders[18], S. Y. Andrean[43a,43b], A. Andreazza[66a,66b], S. Angelidakis[8], A. Angerami[37], A. V. Anisenkov[117a,117b], A. Annovi[69a], C. Antel[52], M. T. Anthony[145], E. Antipov[125], M. Antonelli[49], D. J. A. Antrim[16], F. Anulli[70a], M. Aoki[79], J. A. Aparisi Pozo[169], M. A. Aparo[152], L. Aperio Bella[44], N. Aranzabal[34], V. Araujo Ferraz[78a], C. Arcangeletti[49], A. T. H. Arce[47], E. Arena[88], J-F. Arguin[106], S. Argyropoulos[50], J.-H. Arling[44], A. J. Armbruster[34], A. Armstrong[166], O. Arnaez[162], H. Arnold[34], Z. P. Arrubarrena Tame[110], G. Artoni[130], H. Asada[112], K. Asai[122], S. Asai[159], N. A. Asbah[57], E. M. Asimakopoulou[167], L. Asquith[152], J. Assahsah[33d], K. Assamagan[27], R. Astalos[26a], R. J. Atkin[31a], M. Atkinson[168], N. B. Atlay[17], H. Atmani[58b], P. A. Atmasiddha[102], K. Augsten[137], S. Auricchio[67a,67b], V. A. Austrup[177], G. Avner[156], G. Avolio[34], M. K. Ayoub[13c], G. Azuelos[106,ah], D. Babal[26a], H. Bachacou[140], K. Bachas[158], A. Bachiu[32], F. Backman[43a,43b], A. Badea[57], P. Bagnaia[70a,70b], H. Bahrasemani[148], A. J. Bailey[169], V. R. Bailey[168], J. T. Baines[139], C. Bakalis[9], O. K. Baker[178], P. J. Bakker[115], E. Bakos[14], D. Bakshi Gupta[7], S. Balaji[153], R. Balasubramanian[115], E. M. Baldin[117a,117b], P. Balek[138], E. Ballabene[66a,66b], F. Balli[140], L. M. Baltes[59a], W. K. Balunas[130], J. Balz[96], E. Banas[82], M. Bandieramonte[134], A. Bandyopadhyay[22], S. Bansal[22], L. Barak[157], E. L. Barberio[101], D. Barberis[53a,53b], M. Barbero[98], G. Barbour[92], K. N. Barends[31a], T. Barillari[111], M-S. Barisits[34], J. Barkeloo[127], T. Barklow[149], B. M. Barnett[139], R. M. Barnett[16], A. Baroncelli[58a], G. Barone[27], A. J. Barr[130], L. Barranco Navarro[43a,43b], F. Barreiro[95], J. Barreiro Guimarães da Costa[13a], U. Barron[157], S. Barsov[133], F. Bartels[59a], R. Bartoldus[149], G. Bartolini[98], A. E. Barton[87], P. Bartos[26a], A. Basalaev[44], A. Basan[96], M. Baselga[44], I. Bashta[72a,72b], A. Bassalat[62], M. J. Basso[162], C. R. Basson[97], R. L. Bates[55], S. Batlamous[33e], J. R. Batley[30], B. Batool[147], M. Battaglia[141], M. Bauce[70a,70b], F. Bauer[140,*], P. Bauer[22], H. S. Bawa[29], A. Bayirli[11c], J. B. Beacham[47], T. Beau[131], P. H. Beauchemin[165], F. Becherer[50], P. Bechtle[22], H. P. Beck[18,q], K. Becker[173], C. Becot[44], A. J. Beddall[11c], V. A. Bednyakov[77], C. P. Bee[151], T. A. Beermann[34], M. Begalli[78b], M. Begel[27], A. Behera[151], J. K. Behr[44], C. Beirao Da Cruz E Silva[34], J. F. Beirer[51,34], F. Beisiegel[22], M. Belfkir[4], G. Bella[157], L. Bellagamba[21b], A. Bellerive[32], P. Bellos[19], K. Beloborodov[117a,117b], K. Belotskiy[108], N. L. Belyaev[108], D. Benchekroun[33a], Y. Benhammou[157], D. P. Benjamin[27], M. Benoit[27], J. R. Bensinger[24], S. Bentvelsen[115], L. Beresford[34], M. Beretta[49], D. Berge[17], E. Bergeaas Kuutmann[167], N. Berger[4], B. Bergmann[137], L. J. Bergsten[24], J. Beringer[16], S. Berlendis[6], G. Bernardi[131], C. Bernius[149], F. U. Bernlochner[22], T. Berry[91], P. Berta[138], A. Berthold[46], I. A. Bertram[87], O. Bessidskaia Bylund[177], S. Bethke[111], A. Betti[40], A. J. Bevan[90], S. Bhatta[151], D. S. Bhattacharya[172], P. Bhattarai[24], V. S. Bhopatkar[5], R. Bi[134], R. Bi[27], R. M. Bianchi[134], O. Biebel[110], R. Bielski[127], N. V. Biesuz[69a,69b], M. Biglietti[72a], T. R. V. Billoud[137], M. Bindi[51], A. Bingul[11d], C. Bini[70a,70b], S. Biondi[21a,21b], A. Biondini[88], C. J. Birch-sykes[97], G. A. Bird[19,139], M. Birman[175], T. Bisanz[34], J. P. Biswal[2], D. Biswas[176,j], A. Bitadze[97], C. Bittrich[46], K. Bjørke[129], I. Bloch[44], C. Blocker[24], A. Blue[55], U. Blumenschein[90], J. Blumenthal[96], G. J. Bobbink[115], V. S. Bobrovnikov[117a,117b], M. Boehler[50], D. Bogavac[12], A. G. Bogdanchikov[117a,117b], C. Bohm[43a], V. Boisvert[91], P. Bokan[44], T. Bold[81a], M. Bomben[131], M. Bona[90], M. Boonekamp[140], C. D. Booth[91], A. G. Borbély[55], H. M. Borecka-Bielska[106], L. S. Borgna[92], G. Borissov[87], D. Bortoletto[130], D. Boscherini[21b], M. Bosman[12], J. D. Bossio Sola[34], K. Bouaouda[33a], J. Boudreau[134], E. V. Bouhova-Thacker[87], D. Boumediene[36],

R. Bouquet[131], A. Boveia[123], J. Boyd[34], D. Boye[27], I. R. Boyko[77], A. J. Bozson[91], J. Bracinik[19], N. Brahimi[58c,58d], G. Brandt[177], O. Brandt[30], F. Braren[44], B. Brau[99], J. E. Brau[127], W. D. Breaden Madden[55], K. Brendlinger[44], R. Brener[175], L. Brenner[34], R. Brenner[167], S. Bressler[175], B. Brickwedde[96], D. Britton[55], D. Britzger[111], I. Brock[22], R. Brock[103], G. Brooijmans[37], W. K. Brooks[142e], E. Brost[27], P. A. Bruckman de Renstrom[82], B. Brüers[44], D. Bruncko[26b], A. Bruni[21b], G. Bruni[21b], M. Bruschi[21b], N. Bruscino[70a,70b], L. Bryngemark[149], T. Buanes[15], Q. Buat[151], P. Buchholz[147], A. G. Buckley[55], I. A. Budagov[77], M. K. Bugge[129], O. Bulekov[108], B. A. Bullard[57], S. Burdin[88], C. D. Burgard[44], A. M. Burger[125], B. Burghgrave[7], J. T. P. Burr[30], C. D. Burton[10], J. C. Burzynski[148], E. L. Busch[37], V. Büscher[96], P. J. Bussey[55], J. M. Butler[23], C. M. Buttar[55], J. M. Butterworth[92], W. Buttinger[139], C. J. Buxo Vazquez[103], A. R. Buzykaev[117a,117b], G. Cabras[21b], S. Cabrera Urbán[169], D. Caforio[54], H. Cai[134], V. M. M. Cairo[149], O. Cakir[3a], N. Calace[34], P. Calafiura[16], G. Calderini[131], P. Calfayan[63], G. Callea[55], L. P. Caloba[78b], D. Calvet[36], S. Calvet[36], T. P. Calvet[98], M. Calvetti[69a,69b], R. Camacho Toro[131], S. Camarda[34], D. Camarero Munoz[95], P. Camarri[71a,71b], M. T. Camerlingo[72a,72b], D. Cameron[129], C. Camincher[171], M. Campanelli[92], A. Camplani[38], V. Canale[67a,67b], A. Canesse[100], M. Cano Bret[75], J. Cantero[125], Y. Cao[168], F. Capocasa[24], M. Capua[39a,39b], A. Carbone[66a,66b], R. Cardarelli[71a], J. C. J. Cardenas[7], F. Cardillo[169], G. Carducci[39a,39b], T. Carli[34], G. Carlino[67a], B. T. Carlson[134], E. M. Carlson[163a,171], L. Carminati[66a,66b], M. Carnesale[70a,70b], R. M. D. Carney[149], S. Caron[114], E. Carquin[142e], S. Carrá[44], G. Carratta[21a,21b], J. W. S. Carter[162], T. M. Carter[48], D. Casadei[31c], M. P. Casado[12,g], A. F. Casha[162], E. G. Castiglia[178], F. L. Castillo[59a], L. Castillo Garcia[12], V. Castillo Gimenez[169], N. F. Castro[135a,135e], A. Catinaccio[34], J. R. Catmore[129], A. Cattai[34], V. Cavaliere[27], N. Cavalli[21a,21b], V. Cavasinni[69a,69b], E. Celebi[11c], F. Celli[130], M. S. Centonze[65a,65b], K. Cerny[126], A. S. Cerqueira[78a], A. Cerri[152], L. Cerrito[71a,71b], F. Cerutti[16], A. Cervelli[21b], S. A. Cetin[11b], Z. Chadi[33a], D. Chakraborty[116], M. Chala[135f], J. Chan[176], W. S. Chan[115], W. Y. Chan[88], J. D. Chapman[30], B. Chargeishvili[155b], D. G. Charlton[19], T. P. Charman[90], M. Chatterjee[18], S. Chekanov[5], S. V. Chekulaev[163a], G. A. Chelkov[77,ad], A. Chen[102], B. Chen[157], B. Chen[171], C. Chen[58a], C. H. Chen[76], H. Chen[13c], H. Chen[27], J. Chen[58c], J. Chen[24], S. Chen[132], S. J. Chen[13c], X. Chen[58c], X. Chen[13b], Y. Chen[58a], Y-H. Chen[44], C. L. Cheng[176], H. C. Cheng[60a], A. Cheplakov[77], E. Cheremushkina[44], E. Cherepanova[77], R. Cherkaoui El Moursli[33e], E. Cheu[6], K. Cheung[61], L. Chevalier[140], V. Chiarella[49], G. Chiarelli[69a], G. Chiodini[65a], A. S. Chisholm[19], A. Chitan[25b], Y. H. Chiu[171], M. V. Chizhov[77], K. Choi[10], A. R. Chomont[70a,70b], Y. Chou[99], Y. S. Chow[115], T. Chowdhury[31f], L. D. Christopher[31f], M. C. Chu[60a], X. Chu[13a,13d], J. Chudoba[136], J. J. Chwastowski[82], D. Cieri[111], K. M. Ciesla[82], V. Cindro[89], I. A. Cioară[25b], A. Ciocio[16], F. Cirotto[67a,67b], Z. H. Citron[175,k], M. Citterio[66a], D. A. Ciubotaru[25b], B. M. Ciungu[162], A. Clark[52], P. J. Clark[48], J. M. Clavijo Columbie[44], S. E. Clawson[97], C. Clement[43a,43b], L. Clissa[21a,21b], Y. Coadou[98], M. Cobal[64a,64c], A. Coccaro[53b], J. Cochran[76], R. F. Coelho Barrue[135a], R. Coelho Lopes De Sa[99], S. Coelli[66a], H. Cohen[157], A. E. C. Coimbra[34], B. Cole[37], J. Collot[56], P. Conde Muiño[135a,135g], S. H. Connell[31c], I. A. Connelly[55], E. I. Conroy[130], F. Conventi[67a,ai], H. G. Cooke[19], A. M. Cooper-Sarkar[130], F. Cormier[170], L. D. Corpe[34], M. Corradi[70a,70b], E. E. Corrigan[94], F. Corriveau[100,x], M. J. Costa[169], F. Costanza[4], D. Costanzo[145], B. M. Cote[123], G. Cowan[91], J. W. Cowley[30], K. Cranmer[121], S. Crépé-Renaudin[56], F. Crescioli[131], M. Cristinziani[147], M. Cristoforetti[73a,73b,b], V. Croft[165], G. Crosetti[39a,39b], A. Cueto[34], T. Cuhadar Donszelmann[166], H. Cui[13a,13d], A. R. Cukierman[149], W. R. Cunningham[55], F. Curcio[39a,39b], P. Czodrowski[34], M. M. Czurylo[59b], M. J. Da Cunha Sargedas De Sousa[58a], J. V. Da Fonseca Pinto[78b], C. Da Via[97], W. Dabrowski[81a], T. Dado[45], S. Dahbi[31f], T. Dai[102], C. Dallapiccola[99], M. Dam[38], G. D'amen[27], V. D'Amico[72a,72b], J. Damp[96], J. R. Dandoy[132], M. F. Daneri[28], M. Danninger[148], V. Dao[34], G. Darbo[53b], S. Darmora[5], A. Dattagupta[127], S. D'Auria[66a,66b], C. David[163b], T. Davidek[138], D. R. Davis[47], B. Davis-Purcell[32], I. Dawson[90], K. De[7], R. De Asmundis[67a], M. De Beurs[115], S. De Castro[21a,21b], N. De Groot[114], P. de Jong[115], H. De la Torre[103], A. De Maria[13c], D. De Pedis[70a], A. De Salvo[70a], U. De Sanctis[71a,71b], M. De Santis[71a,71b], A. De Santo[152], J. B. De Vivie De Regie[56], D. V. Dedovich[77], J. Degens[115], A. M. Deiana[40], J. Del Peso[95], Y. Delabat Diaz[44], F. Deliot[140], C. M. Delitzsch[6], M. Della Pietra[67a,67b], D. Della Volpe[52], A. Dell'Acqua[34], L. Dell'Asta[66a,66b], M. Delmastro[4], P. A. Delsart[56], S. Demers[178], M. Demichev[77], S. P. Denisov[118], L. D'Eramo[116], D. Derendarz[82], J. E. Derkaoui[33d], F. Derue[131], P. Dervan[88], K. Desch[22], K. Dette[162], C. Deutsch[22], P. O. Deviveiros[34], F. A. Di Bello[70a,70b], A. Di Ciaccio[71a,71b], L. Di Ciaccio[4], A. Di Domenico[70a,70b], C. Di Donato[67a,67b], A. Di Girolamo[34], G. Di Gregorio[69a,69b], A. Di Luca[73a,73b,b], B. Di Micco[72a,72b], R. Di Nardo[72a,72b], C. Diaconu[98], F. A. Dias[115], T. Dias Do Vale[135a], M. A. Diaz[142a],

F. G. Diaz Capriles[22], J. Dickinson[16], M. Didenko[169], E. B. Diehl[102], J. Dietrich[17], S. Díez Cornell[44], C. Diez Pardos[147], C. Dimitriadi[22,167], A. Dimitrievska[16], W. Ding[13b], J. Dingfelder[22], I-M. Dinu[25b], S. J. Dittmeier[59b], F. Dittus[34], F. Djama[98], T. Djobava[155b], J. I. Djuvsland[15], M. A. B. Do Vale[143], D. Dodsworth[24], C. Doglioni[94], J. Dolejsi[138], Z. Dolezal[138], M. Donadelli[78c], B. Dong[58c], J. Donini[36], A. D'onofrio[13c], M. D'Onofrio[88], J. Dopke[139], A. Doria[67a], M. T. Dova[86], A. T. Doyle[55], E. Drechsler[148], E. Dreyer[148], T. Dreyer[51], A. S. Drobac[165], D. Du[58a], T. A. du Pree[115], F. Dubinin[107], M. Dubovsky[26a], A. Dubreuil[52], E. Duchovni[175], G. Duckeck[110], O. A. Ducu[25b,34], D. Duda[111], A. Dudarev[34], M. D'uffizi[97], L. Duflot[62], M. Dührssen[34], C. Dülsen[177], A. E. Dumitriu[25b], M. Dunford[59a], S. Dungs[45], K. Dunne[43a,43b], A. Duperrin[98], H. Duran Yildiz[3a], M. Düren[54], A. Durglishvili[155b], B. Dutta[44], G. I. Dyckes[16], M. Dyndal[81a], S. Dysch[97], B. S. Dziedzic[82], B. Eckerova[26a], M. G. Eggleston[47], E. Egidio Purcino De Souza[78b], L. F. Ehrke[52], G. Eigen[15], K. Einsweiler[16], T. Ekelof[167], Y. El Ghazali[33b], H. El Jarrari[33e], A. El Moussaouy[33a], V. Ellajosyula[167], M. Ellert[167], F. Ellinghaus[177], A. A. Elliot[90], N. Ellis[34], J. Elmsheuser[27], M. Elsing[34], D. Emeliyanov[139], A. Emerman[37], Y. Enari[159], J. Erdmann[45], A. Ereditato[18], P. A. Erland[82], M. Errenst[177], M. Escalier[62], C. Escobar[169], O. Estrada Pastor[169], E. Etzion[157], G. Evans[135a], H. Evans[63], M. O. Evans[152], A. Ezhilov[133], S. Ezzarqtouni[33a], F. Fabbri[55], L. Fabbri[21a,21b], G. Facini[173], V. Fadeyev[141], R. M. Fakhrutdinov[118], S. Falciano[70a], P. J. Falke[22], S. Falke[34], J. Faltova[138], Y. Fan[13a], Y. Fang[13a], Y. Fang[13a], G. Fanourakis[42], M. Fanti[66a,66b], M. Faraj[58c], A. Farbin[7], A. Farilla[72a], E. M. Farina[68a,68b], T. Farooque[103], S. M. Farrington[48], P. Farthouat[34], F. Fassi[33e], D. Fassouliotis[8], M. Faucci Giannelli[71a,71b], W. J. Fawcett[30], L. Fayard[62], O. L. Fedin[133,p], G. Fedotov[133], M. Feickert[168], L. Feligioni[98], A. Fell[145], C. Feng[58b], M. Feng[13b], M. J. Fenton[166], A. B. Fenyuk[118], S. W. Ferguson[41], J. Ferrando[44], A. Ferrari[167], P. Ferrari[115], R. Ferrari[68a], D. Ferrere[52], C. Ferretti[102], F. Fiedler[96], A. Filipčič[89], F. Filthaut[114], M. C. N. Fiolhais[135a,135c,a], L. Fiorini[169], F. Fischer[147], W. C. Fisher[103], T. Fitschen[19], I. Fleck[147], P. Fleischmann[102], T. Flick[177], B. M. Flierl[110], L. Flores[132], M. Flores[31d], L. R. Flores Castillo[60a], F. M. Follega[73a,73b], N. Fomin[15], J. H. Foo[162], B. C. Forland[63], A. Formica[140], F. A. Förster[12], A. C. Forti[97], E. Fortin[98], M. G. Foti[130], L. Fountas[8], D. Fournier[62], H. Fox[87], P. Francavilla[69a,69b], S. Francescato[57], M. Franchini[21a,21b], S. Franchino[59a], D. Francis[34], L. Franco[4], L. Franconi[18], M. Franklin[57], G. Frattari[70a,70b], A. C. Freegard[90], P. M. Freeman[19], W. S. Freund[78b], E. M. Freundlich[45], D. Froidevaux[34], J. A. Frost[130], Y. Fu[58a], M. Fujimoto[122], E. Fullana Torregrosa[169], J. Fuster[169], A. Gabrielli[21a,21b], A. Gabrielli[34], P. Gadow[44], G. Gagliardi[53a,53b], L. G. Gagnon[16], G. E. Gallardo[130], E. J. Gallas[130], B. J. Gallop[139], R. Gamboa Goni[90], K. K. Gan[123], S. Ganguly[159], J. Gao[58a], Y. Gao[48], Y. S. Gao[29,m], F. M. Garay Walls[142a], C. García[169], J. E. García Navarro[169], J. A. García Pascual[13a], M. Garcia-Sciveres[16], R. W. Gardner[35], D. Garg[75], R. B. Garg[149], S. Gargiulo[50], C. A. Garner[162], V. Garonne[27], S. J. Gasiorowski[144], P. Gaspar[78b], G. Gaudio[68a], P. Gauzzi[70a,70b], I. L. Gavrilenko[107], A. Gavrilyuk[119], C. Gay[170], G. Gaycken[44], E. N. Gazis[9], A. A. Geanta[25b], C. M. Gee[141], C. N. P. Gee[139], J. Geisen[94], M. Geisen[96], C. Gemme[53b], M. H. Genest[56], S. Gentile[70a,70b], S. George[91], W. F. George[19], T. Geralis[42], L. O. Gerlach[51], P. Gessinger-Befurt[34], M. Ghasemi Bostanabad[171], A. Ghosh[166], A. Ghosh[6], B. Giacobbe[21b], S. Giagu[70a,70b], N. Giangiacomi[162], P. Giannetti[69a], A. Giannini[67a,67b], S. M. Gibson[91], M. Gignac[141], D. T. Gil[81b], B. J. Gilbert[37], D. Gillberg[32], G. Gilles[115], N. E. K. Gillwald[44], D. M. Gingrich[2,ah], M. P. Giordani[64a,64c], P. F. Giraud[140], G. Giugliarelli[64a,64c], D. Giugni[66a], F. Giuli[71a,71b], I. Gkialas[8,h], P. Gkountoumis[9], L. K. Gladilin[109], C. Glasman[95], G. R. Gledhill[127], M. Glisic[127], I. Gnesi[39b,d], M. Goblirsch-Kolb[24], D. Godin[106], S. Goldfarb[101], T. Golling[52], D. Golubkov[118], J. P. Gombas[103], A. Gomes[135a,135b], R. Goncalves Gama[51], R. Gonçalo[135a,135c], G. Gonella[127], L. Gonella[19], A. Gongadze[77], F. Gonnella[19], J. L. Gonski[37], S. González de la Hoz[169], S. Gonzalez Fernandez[12], R. Gonzalez Lopez[88], C. Gonzalez Renteria[16], R. Gonzalez Suarez[167], S. Gonzalez-Sevilla[52], G. R. Gonzalvo Rodriguez[169], R. Y. González Andana[142a], L. Goossens[34], N. A. Gorasia[19], P. A. Gorbounov[119], H. A. Gordon[27], B. Gorini[34], E. Gorini[65a,65b], A. Gorišek[89], A. T. Goshaw[47], M. I. Gostkin[77], C. A. Gottardo[114], M. Gouighri[33b], V. Goumarre[44], A. G. Goussiou[144], N. Govender[31c], C. Goy[4], I. Grabowska-Bold[81a], K. Graham[32], E. Gramstad[129], S. Grancagnolo[17], M. Grandi[152], V. Gratchev[133], P. M. Gravila[25f], F. G. Gravili[65a,65b], H. M. Gray[16], C. Grefe[22], I. M. Gregor[44], P. Grenier[149], K. Grevtsov[44], C. Grieco[12], N. A. Grieser[124], A. A. Grillo[141], K. Grimm[29,l], S. Grinstein[12,u], J.-F. Grivaz[62], S. Groh[96], E. Gross[175], J. Grosse-Knetter[51], C. Grud[102], A. Grummer[113], J. C. Grundy[130], L. Guan[102], W. Guan[176], C. Gubbels[170], J. G. R. Guerrero Rojas[169], F. Guescini[111], D. Guest[17], R. Gugel[96], A. Guida[44], T. Guillemin[4], S. Guindon[34], F. Guo[13a],

J. Guo[58c], L. Guo[62], Y. Guo[102], R. Gupta[44], S. Gurbuz[22], G. Gustavino[124], M. Guth[52], P. Gutierrez[124], L. F. Gutierrez Zagazeta[132], C. Gutschow[92], C. Guyot[140], C. Gwenlan[130], C. B. Gwilliam[88], E. S. Haaland[129], A. Haas[121], M. Habedank[44], C. Haber[16], H. K. Hadavand[7], A. Hadef[96], S. Hadzic[111], M. Haleem[172], J. Haley[125], J. J. Hall[145], G. Halladjian[103], G. D. Hallewell[98], L. Halser[18], K. Hamano[171], H. Hamdaoui[33e], M. Hamer[22], G. N. Hamity[48], K. Han[58a], L. Han[13c], L. Han[58a], S. Han[16], Y. F. Han[162], K. Hanagaki[79,s], M. Hance[141], M. D. Hank[35], R. Hankache[97], E. Hansen[94], J. B. Hansen[38], J. D. Hansen[38], M. C. Hansen[22], P. H. Hansen[38], K. Hara[164], T. Harenberg[177], S. Harkusha[104], Y. T. Harris[130], P. F. Harrison[173], N. M. Hartman[149], N. M. Hartmann[110], Y. Hasegawa[146], A. Hasib[48], S. Hassani[140], S. Haug[18], R. Hauser[103], M. Havranek[137], C. M. Hawkes[19], R. J. Hawkings[34], S. Hayashida[112], D. Hayden[103], C. Hayes[102], R. L. Hayes[170], C. P. Hays[130], J. M. Hays[90], H. S. Hayward[88], S. J. Haywood[139], F. He[58a], Y. He[160], Y. He[131], M. P. Heath[48], V. Hedberg[94], A. L. Heggelund[129], N. D. Hehir[90], C. Heidegger[50], K. K. Heidegger[50], W. D. Heidorn[76], J. Heilman[32], S. Heim[44], T. Heim[16], B. Heinemann[44,af], J. G. Heinlein[132], J. J. Heinrich[127], L. Heinrich[34], J. Hejbal[136], L. Helary[44], A. Held[121], C. M. Helling[141], S. Hellman[43a,43b], C. Helsens[34], R. C. W. Henderson[87], L. Henkelmann[30], A. M. Henriques Correia[34], H. Herde[149], Y. Hernández Jiménez[151], H. Herr[96], M. G. Herrmann[110], T. Herrmann[46], G. Herten[50], R. Hertenberger[110], L. Hervas[34], N. P. Hessey[163a], H. Hibi[80], S. Higashino[79], E. Higón-Rodriguez[169], K. H. Hiller[44], S. J. Hillier[19], M. Hils[46], I. Hinchliffe[16], F. Hinterkeuser[22], M. Hirose[128], S. Hirose[164], D. Hirschbuehl[177], B. Hiti[89], O. Hladik[136], J. Hobbs[151], R. Hobincu[25e], N. Hod[175], M. C. Hodgkinson[145], B. H. Hodkinson[30], A. Hoecker[34], J. Hofer[44], D. Hohn[50], T. Holm[22], T. R. Holmes[35], M. Holzbock[111], L. B. A. H. Hommels[30], B. P. Honan[97], J. Hong[58c], T. M. Hong[134], Y. Hong[51], J. C. Honig[50], A. Hönle[111], B. H. Hooberman[168], W. H. Hopkins[5], Y. Horii[112], L. A. Horyn[35], S. Hou[154], J. Howarth[55], J. Hoya[86], M. Hrabovsky[126], A. Hrynevich[105], T. Hryn'ova[4], P. J. Hsu[61], S.-C. Hsu[144], Q. Hu[37], S. Hu[58c], Y. F. Hu[13a,13d,aj], D. P. Huang[92], X. Huang[13c], Y. Huang[58a], Y. Huang[13a], Z. Hubacek[137], F. Hubaut[98], M. Huebner[22], F. Huegging[22], T. B. Huffman[130], M. Huhtinen[34], S. K. Huiberts[15], R. Hulsken[56], N. Huseynov[77,y], J. Huston[103], J. Huth[57], R. Hyneman[149], S. Hyrych[26a], G. Iacobucci[52], G. Iakovidis[27], I. Ibragimov[147], L. Iconomidou-Fayard[62], P. Iengo[34], R. Iguchi[159], T. Iizawa[52], Y. Ikegami[79], A. Ilg[18], N. Ilic[162], H. Imam[33a], T. Ingebretsen Carlson[43a,43b], G. Introzzi[68a,68b], M. Iodice[72a], V. Ippolito[70a,70b], M. Ishino[159], W. Islam[176], C. Issever[17,44], S. Istin[11c,ak], J. M. Iturbe Ponce[60a], R. Iuppa[73a,73b], A. Ivina[175], J. M. Izen[41], V. Izzo[67a], P. Jacka[136], P. Jackson[1], R. M. Jacobs[44], B. P. Jaeger[148], C. S. Jagfeld[110], G. Jäkel[177], K. Jakobs[50], T. Jakoubek[175], J. Jamieson[55], K. W. Janas[81a], G. Jarlskog[94], A. E. Jaspan[88], T. Javůrek[34], M. Javurkova[99], F. Jeanneau[140], L. Jeanty[127], J. Jejelava[155a,z], P. Jenni[50,e], S. Jézéquel[4], J. Jia[151], Z. Jia[13c], Y. Jiang[58a], S. Jiggins[48], J. Jimenez Pena[111], S. Jin[13c], A. Jinaru[25b], O. Jinnouchi[160], H. Jivan[31f], P. Johansson[145], K. A. Johns[6], C. A. Johnson[63], D. M. Jones[30], E. Jones[173], R. W. L. Jones[87], T. J. Jones[88], J. Jovicevic[14], X. Ju[16], J. J. Junggeburth[34], A. Juste Rozas[12,u], S. Kabana[142d], A. Kaczmarska[82], M. Kado[70a,70b], H. Kagan[123], M. Kagan[149], A. Kahn[37], A. Kahn[132], C. Kahra[96], T. Kaji[174], E. Kajomovitz[156], C. W. Kalderon[27], A. Kamenshchikov[118], M. Kaneda[159], N. J. Kang[141], S. Kang[76], Y. Kano[112], D. Kar[31f], K. Karava[130], M. J. Kareem[163b], I. Karkanias[158], S. N. Karpov[77], Z. M. Karpova[77], V. Kartvelishvili[87], A. N. Karyukhin[118], E. Kasimi[158], C. Kato[58d], J. Katzy[44], S. Kaur[32], K. Kawade[146], K. Kawagoe[85], T. Kawaguchi[112], T. Kawamoto[140], G. Kawamura[51], E. F. Kay[171], F. I. Kaya[165], S. Kazakos[12], V. F. Kazanin[117a,117b], Y. Ke[151], J. M. Keaveney[31a], R. Keeler[171], J. S. Keller[32], A. S. Kelly[92], D. Kelsey[152], J. J. Kempster[19], J. Kendrick[19], K. E. Kennedy[37], O. Kepka[136], S. Kersten[177], B. P. Kerš/evan[89], S. Ketabchi Haghighat[162], M. Khandoga[131], A. Khanov[125], A. G. Kharlamov[117a,117b], T. Kharlamova[117a,117b], E. E. Khoda[144], T. J. Khoo[17], G. Khoriauli[172], E. Khramov[77], J. Khubua[155b], S. Kido[80], M. Kiehn[34], A. Kilgallon[127], E. Kim[160], Y. K. Kim[35], N. Kimura[92], A. Kirchhoff[51], D. Kirchmeier[46], C. Kirfel[22], J. Kirk[139], A. E. Kiryunin[111], T. Kishimoto[159], D. P. Kisliuk[162], C. Kitsaki[9], O. Kivernyk[22], T. Klapdor-Kleingrothaus[50], M. Klassen[59a], C. Klein[32], L. Klein[172], M. H. Klein[102], M. Klein[88], U. Klein[88], P. Klimek[34], A. Klimentov[27], F. Klimpel[111], T. Klingl[22], T. Klioutchnikova[34], F. F. Klitzner[110], P. Kluit[115], S. Kluth[111], E. Kneringer[74], T. M. Knight[162], A. Knue[50], D. Kobayashi[85], R. Kobayashi[83], M. Kocian[149], T. Kodama[159], P. Kodys[138], D. M. Koeck[152], P. T. Koenig[22], T. Koffas[32], N. M. Köhler[34], M. Kolb[140], I. Koletsou[4], T. Komarek[126], K. Köneke[50], A. X. Y. Kong[1], T. Kono[122], V. Konstantinides[92], N. Konstantinidis[92], B. Konya[94], R. Kopeliansky[63], S. Koperny[81a], K. Korcyl[82], K. Kordas[158], G. Koren[157], A. Korn[92], S. Korn[51], I. Korolkov[12], E. V. Korolkova[145], N. Korotkova[109], B. Kortman[115], O. Kortner[111], S. Kortner[111], W. H. Kostecka[116], V. V. Kostyukhin[147,161], A. Kotsokechagia[62],

A. Kotwal[47], A. Koulouris[34], A. Kourkoumeli-Charalampidi[68a,68b], C. Kourkoumelis[8], E. Kourlitis[5], O. Kovanda[152], R. Kowalewski[171], W. Kozanecki[140], A. S. Kozhin[118], V. A. Kramarenko[109], G. Kramberger[89], P. Kramer[96], D. Krasnopevtsev[58a], M. W. Krasny[131], A. Krasznahorkay[34], J. A. Kremer[96], J. Kretzschmar[88], K. Kreul[17], P. Krieger[162], F. Krieter[110], S. Krishnamurthy[99], A. Krishnan[59b], M. Krivos[138], K. Krizka[16], K. Kroeninger[45], H. Kroha[111], J. Kroll[136], J. Kroll[132], K. S. Krowpman[103], U. Kruchonak[77], H. Krüger[22], N. Krumnack[76], M. C. Kruse[47], J. A. Krzysiak[82], A. Kubota[160], O. Kuchinskaia[161], S. Kuday[3a], D. Kuechler[44], J. T. Kuechler[44], S. Kuehn[34], T. Kuhl[44], V. Kukhtin[77], Y. Kulchitsky[104,ac], S. Kuleshov[142c], M. Kumar[31f], N. Kumari[98], M. Kuna[56], A. Kupco[136], T. Kupfer[45], O. Kuprash[50], H. Kurashige[80], L. L. Kurchaninov[163a], Y. A. Kurochkin[104], A. Kurova[108], M. G. Kurth[13a,13d], E. S. Kuwertz[34], M. Kuze[160], A. K. Kvam[144], J. Kvita[126], T. Kwan[100], K. W. Kwok[60a], C. Lacasta[169], F. Lacava[70a,70b], H. Lacker[17], D. Lacour[131], N. N. Lad[92], E. Ladygin[77], R. Lafaye[4], B. Laforge[131], T. Lagouri[142d], S. Lai[51], I. K. Lakomiec[81a], N. Lalloue[56], J. E. Lambert[124], S. Lammers[63], W. Lampl[6], C. Lampoudis[158], E. Lançon[27], U. Landgraf[50], M. P. J. Landon[90], V. S. Lang[50], J. C. Lange[51], R. J. Langenberg[99], A. J. Lankford[166], F. Lanni[27], K. Lantzsch[22], A. Lanza[68a], A. Lapertosa[53a,53b], J. F. Laporte[140], T. Lari[66a], F. Lasagni Manghi[21b], M. Lassnig[34], V. Latonova[136], T. S. Lau[60a], A. Laudrain[96], A. Laurier[32], M. Lavorgna[67a,67b], S. D. Lawlor[91], Z. Lawrence[97], M. Lazzaroni[66a,66b], B. Le[97], B. Leban[89], A. Lebedev[76], M. LeBlanc[34], T. LeCompte[5], F. Ledroit-Guillon[56], A. C. A. Lee[92], G. R. Lee[15], L. Lee[57], S. C. Lee[154], S. Lee[76], L. L. Leeuw[31c], B. Lefebvre[163a], H. P. Lefebvre[91], M. Lefebvre[171], C. Leggett[16], K. Lehmann[148], N. Lehmann[18], G. Lehmann Miotto[34], W. A. Leight[44], A. Leisos[158,t], M. A. L. Leite[78c], C. E. Leitgeb[44], R. Leitner[138], K. J. C. Leney[40], T. Lenz[22], S. Leone[69a], C. Leonidopoulos[48], A. Leopold[150], C. Leroy[106], R. Les[103], C. G. Lester[30], M. Levchenko[133], J. Levêque[4], D. Levin[102], L. J. Levinson[175], D. J. Lewis[19], B. Li[13b], B. Li[58b], C. Li[58a], C-Q. Li[58c,58d], H. Li[58a], H. Li[58b], H. Li[58b], J. Li[58c], K. Li[144], L. Li[58c], M. Li[13a,13d], Q. Y. Li[58a], S. Li[58c,58d,c], T. Li[58b], X. Li[44], Y. Li[44], Z. Li[58b], Z. Li[130], Z. Li[100], Z. Li[88], Z. Liang[13a], M. Liberatore[44], B. Liberti[71a], K. Lie[60c], J. Lieber Marin[78b], K. Lin[103], R. A. Linck[63], R. E. Lindley[6], J. H. Lindon[2], A. Linss[44], E. Lipeles[132], A. Lipniacka[15], T. M. Liss[168,ag], A. Lister[170], J. D. Little[7], B. Liu[13a], B. X. Liu[148], J. B. Liu[58a], J. K. K. Liu[35], K. Liu[58c,58d], M. Liu[58a], M. Y. Liu[58a], P. Liu[13a], Q. Liu[58c,58d,144], X. Liu[58a], Y. Liu[44], Y. Liu[13c,13d], Y. L. Liu[102], Y. W. Liu[58a], M. Livan[68a,68b], J. Llorente Merino[148], S. L. Lloyd[90], E. M. Lobodzinska[44], P. Loch[6], S. Loffredo[71a,71b], T. Lohse[17], K. Lohwasser[145], M. Lokajicek[136], J. D. Long[168], I. Longarini[70a,70b], L. Longo[34], R. Longo[168], I. Lopez Paz[34], A. Lopez Solis[44], J. Lorenz[110], N. Lorenzo Martinez[4], A. M. Lory[110], A. Lösle[50], X. Lou[43a,43b], X. Lou[13a], A. Lounis[62], J. Love[5], P. A. Love[87], J. J. Lozano Bahilo[169], G. Lu[13a], M. Lu[58a], S. Lu[132], Y. J. Lu[61], H. J. Lubatti[144], C. Luci[70a,70b], F. L. Lucio Alves[13c], A. Lucotte[56], F. Luehring[63], I. Luise[151], L. Luminari[70a], O. Lundberg[150], B. Lund-Jensen[150], N. A. Luongo[127], M. S. Lutz[157], D. Lynn[27], H. Lyons[88], R. Lysak[136], E. Lytken[94], F. Lyu[13a], V. Lyubushkin[77], T. Lyubushkina[77], H. Ma[27], L. L. Ma[58b], Y. Ma[92], D. M. Mac Donell[171], G. Maccarrone[49], C. M. Macdonald[145], J. C. MacDonald[145], R. Madar[36], W. F. Mader[46], M. Madugoda Ralalage Don[125], N. Madysa[46], J. Maeda[80], T. Maeno[27], M. Maerker[46], V. Magerl[50], J. Magro[64a,64c], D. J. Mahon[37], C. Maidantchik[78b], A. Maio[135a,135b,135d], K. Maj[81a], O. Majersky[26a], S. Majewski[127], N. Makovec[62], V. Maksimovic[14], B. Malaescu[131], Pa. Malecki[82], V. P. Maleev[133], F. Malek[56], D. Malito[39a,39b], U. Mallik[75], C. Malone[30], S. Maltezos[9], S. Malyukov[77], J. Mamuzic[169], G. Mancini[49], J. P. Mandalia[90], I. Mandić[89], L. Manhaes de Andrade Filho[78a], I. M. Maniatis[158], M. Manisha[140], J. Manjarres Ramos[46], K. H. Mankinen[94], A. Mann[110], A. Manousos[74], B. Mansoulie[140], I. Manthos[158], S. Manzoni[115], A. Marantis[158,t], G. Marchiori[131], M. Marcisovsky[136], L. Marcoccia[71a,71b], C. Marcon[94], M. Marjanovic[124], Z. Marshall[16], S. Marti-Garcia[169], T. A. Martin[173], V. J. Martin[48], B. Martin dit Latour[15], L. Martinelli[70a,70b], M. Martinez[12,u], P. Martinez Agullo[169], V. I. Martinez Outschoorn[99], S. Martin-Haugh[139], V. S. Martoiu[25b], A. C. Martyniuk[92], A. Marzin[34], S. R. Maschek[111], L. Masetti[96], T. Mashimo[159], J. Masik[97], A. L. Maslennikov[117a,117b], L. Massa[21b], P. Massarotti[67a,67b], P. Mastrandrea[69a,69b], A. Mastroberardino[39a,39b], T. Masubuchi[159], D. Matakias[27], T. Mathisen[167], A. Matic[110], N. Matsuzawa[159], J. Maurer[25b], B. Maček[89], D. A. Maximov[117a,117b], R. Mazini[154], I. Maznas[158], S. M. Mazza[141], C. Mc Ginn[27], J. P. Mc Gowan[100], S. P. Mc Kee[102], T. G. McCarthy[111], W. P. McCormack[16], E. F. McDonald[101], A. E. McDougall[115], J. A. Mcfayden[152], G. Mchedlidze[155b], M. A. McKay[40], D. J. Mclaughlin[92], K. D. McLean[171], S. J. McMahon[139], P. C. McNamara[101], R. A. McPherson[171,x], J. E. Mdhluli[31f], Z. A. Meadows[99], S. Meehan[34], T. Megy[36], S. Mehlhase[110], A. Mehta[88], B. Meirose[41], D. Melini[156], B. R. Mellado Garcia[31f], A. H. Melo[51],

F. Meloni[44], A. Melzer[22], E. D. Mendes Gouveia[135a], A. M. Mendes Jacques Da Costa[19], H. Y. Meng[162], L. Meng[34], S. Menke[111], M. Mentink[34], E. Meoni[39a,39b], C. Merlassino[130], P. Mermod[52,*], L. Merola[67a,67b], C. Meroni[66a], G. Merz[102], O. Meshkov[107,109], J. K. R. Meshreki[147], J. Metcalfe[5], A. S. Mete[5], C. Meyer[63], J-P. Meyer[140], M. Michetti[17], R. P. Middleton[139], L. Mijović[48], G. Mikenberg[175], M. Mikestikova[136], M. Mikuž[89], H. Mildner[145], A. Milic[162], C. D. Milke[40], D. W. Miller[35], L. S. Miller[32], A. Milov[175], D. A. Milstead[43a,43b], T. Min[13c], A. A. Minaenko[118], I. A. Minashvili[155b], L. Mince[55], A. I. Mincer[121], B. Mindur[81a], M. Mineev[77], Y. Minegishi[159], Y. Mino[83], L. M. Mir[12], M. Miralles Lopez[169], M. Mironova[130], T. Mitani[174], V. A. Mitsou[169], M. Mittal[58c], O. Miu[162], P. S. Miyagawa[90], Y. Miyazaki[85], A. Mizukami[79], J. U. Mjörnmark[94], T. Mkrtchyan[59a], M. Mlynarikova[116], T. Moa[43a,43b], S. Mobius[51], K. Mochizuki[106], P. Moder[44], P. Mogg[110], A. F. Mohammed[13a], S. Mohapatra[37], G. Mokgatitswane[31f], B. Mondal[147], S. Mondal[137], K. Mönig[44], E. Monnier[98], L. Monsonis Romero[169], A. Montalbano[148], J. Montejo Berlingen[34], M. Montella[123], F. Monticelli[86], N. Morange[62], A. L. Moreira De Carvalho[135a], M. Moreno Llácer[169], C. Moreno Martinez[12], P. Morettini[53b], S. Morgenstern[173], D. Mori[148], M. Morii[57], M. Morinaga[159], V. Morisbak[129], A. K. Morley[34], A. P. Morris[92], L. Morvaj[34], P. Moschovakos[34], B. Moser[115], M. Mosidze[155b], T. Moskalets[50], P. Moskvitina[114], J. Moss[29,n], E. J. W. Moyse[99], S. Muanza[98], J. Mueller[134], R. Mueller[18], D. Muenstermann[87], G. A. Mullier[94], J. J. Mullin[132], D. P. Mungo[66a,66b], J. L. Munoz Martinez[12], F. J. Munoz Sanchez[97], M. Murin[97], P. Murin[26b], W. J. Murray[173,139], A. Murrone[66a,66b], J. M. Muse[124], M. Muškinja[16], C. Mwewa[27], A. G. Myagkov[118,ad], A. J. Myers[7], A. A. Myers[134], G. Myers[63], M. Myska[137], B. P. Nachman[16], O. Nackenhorst[45], A.Nag Nag[46], K. Nagai[130], K. Nagano[79], J. L. Nagle[27], E. Nagy[98], A. M. Nairz[34], Y. Nakahama[79], K. Nakamura[79], H. Nanjo[128], F. Napolitano[59a], R. Narayan[40], E. A. Narayanan[113], I. Naryshkin[133], M. Naseri[32], C. Nass[22], T. Naumann[44], G. Navarro[20a], J. Navarro-Gonzalez[169], R. Nayak[157], P. Y. Nechaeva[107], F. Nechansky[44], T. J. Neep[19], A. Negri[68a,68b], M. Negrini[21b], C. Nellist[114], C. Nelson[100], K. Nelson[102], S. Nemecek[136], M. Nessi[34,f], M. S. Neubauer[168], F. Neuhaus[96], J. Neundorf[44], R. Newhouse[170], P. R. Newman[19], C. W. Ng[134], Y. S. Ng[17], Y. W. Y. Ng[166], B. Ngair[33e], H. D. N. Nguyen[98], R. B. Nickerson[130], R. Nicolaidou[140], D. S. Nielsen[38], J. Nielsen[141], M. Niemeyer[51], N. Nikiforou[10], V. Nikolaenko[118,ad], I. Nikolic-Audit[131], K. Nikolopoulos[19], P. Nilsson[27], H. R. Nindhito[52], A. Nisati[70a], N. Nishu[2], R. Nisius[111], T. Nitta[174], T. Nobe[159], D. L. Noel[30], Y. Noguchi[83], I. Nomidis[131], M. A. Nomura[27], M. B. Norfolk[145], R. R. B. Norisam[92], J. Novak[89], T. Novak[44], O. Novgorodova[46], L. Novotny[137], R. Novotny[113], L. Nozka[126], K. Ntekas[166], E. Nurse[92], F. G. Oakham[32,ah], J. Ocariz[131], A. Ochi[80], I. Ochoa[135a], J. P. Ochoa-Ricoux[142a], S. Oda[85], S. Odaka[79], S. Oerdek[167], A. Ogrodnik[81a], A. Oh[97], C. C. Ohm[150], H. Oide[160], R. Oishi[159], M. L. Ojeda[44], Y. Okazaki[83], M. W. O'Keefe[88], Y. Okumura[159], A. Olariu[25b], L. F. Oleiro Seabra[135a], S. A. Olivares Pino[142d], D. Oliveira Damazio[27], D. Oliveira Goncalves[78a], J. L. Oliver[166], M. J. R. Olsson[166], A. Olszewski[82], J. Olszowska[82], Ö.O. Öncel[22], D. C. O'Neil[148], A. P. O'neill[18], A. Onofre[135a,135e], P. U. E. Onyisi[10], R. G. Oreamuno Madriz[116], M. J. Oreglia[35], G. E. Orellana[86], D. Orestano[72a,72b], N. Orlando[12], R. S. Orr[162], V. O'Shea[55], R. Ospanov[58a], G. Otero y Garzon[28], H. Otono[85], P. S. Ott[59a], G. J. Ottino[16], M. Ouchrif[33d], J. Ouellette[27], F. Ould-Saada[129], A. Ouraou[140,*], Q. Ouyang[13a], M. Owen[55], R. E. Owen[139], K. Y. Oyulmaz[11c], V. E. Ozcan[11c], N. Ozturk[7], S. Ozturk[11c], J. Pacalt[126], H. A. Pacey[30], K. Pachal[47], A. Pacheco Pages[12], C. Padilla Aranda[12], S. Pagan Griso[16], G. Palacino[63], S. Palazzo[48], S. Palestini[34], M. Palka[81b], P. Palni[81a], D. K. Panchal[10], C. E. Pandini[52], J. G. Panduro Vazquez[91], P. Pani[44], G. Panizzo[64a,64c], L. Paolozzi[52], C. Papadatos[106], S. Parajuli[40], A. Paramonov[5], C. Paraskevopoulos[9], D. Paredes Hernandez[60b], S. R. Paredes Saenz[130], B. Parida[175], T. H. Park[162], A. J. Parker[29], M. A. Parker[30], F. Parodi[53a,53b], E. W. Parrish[116], V. A. Parrish[48], J. A. Parsons[37], U. Parzefall[50], L. Pascual Dominguez[157], V. R. Pascuzzi[16], F. Pasquali[115], E. Pasqualucci[70a], S. Passaggio[53b], F. Pastore[91], P. Pasuwan[43a,43b], J. R. Pater[97], A. Pathak[176], J. Patton[88], T. Pauly[34], J. Pearkes[149], M. Pedersen[129], L. Pedraza Diaz[114], R. Pedro[135a], T. Peiffer[51], S. V. Peleganchuk[117a,117b], O. Penc[136], C. Peng[60b], H. Peng[58a], M. Penzin[161], B. S. Peralva[78a], A. P. Pereira Peixoto[135a], L. Pereira Sanchez[43a,43b], D. V. Perepelitsa[27], E. Perez Codina[163a], M. Perganti[9], L. Perini[66a,66b], H. Pernegger[34], S. Perrella[34], A. Perrevoort[115], K. Peters[44], R. F. Y. Peters[97], B. A. Petersen[34], T. C. Petersen[38], E. Petit[98], V. Petousis[137], C. Petridou[158], P. Petroff[62], F. Petrucci[72a,72b], A. Petrukhin[147], M. Pettee[178], N. E. Pettersson[34], K. Petukhova[138], A. Peyaud[140], R. Pezoa[142e], L. Pezzotti[34], G. Pezzullo[178], T. Pham[101], P. W. Phillips[139], M. W. Phipps[168], G. Piacquadio[151], E. Pianori[16], F. Piazza[66a,66b], A. Picazio[99], R. Piegaia[28], D. Pietreanu[25b], J. E. Pilcher[35], A. D. Pilkington[97], M. Pinamonti[64a,64c], J. L. Pinfold[2], C. Pitman Donaldson[92], D. A. Pizzi[32], L. Pizzimento[71a,71b],

A. Pizzini[115], M.-A. Pleier[27], V. Plesanovs[50], V. Pleskot[138], E. Plotnikova[77], P. Podberezko[117a,117b], R. Poettgen[94], R. Poggi[52], L. Poggioli[131], I. Pogrebnyak[103], D. Pohl[22], I. Pokharel[51], G. Polesello[68a], A. Poley[148,163a], A. Policicchio[70a,70b], R. Polifka[137], A. Polini[21b], C. S. Pollard[130], Z. B. Pollock[123], V. Polychronakos[27], D. Ponomarenko[108], L. Pontecorvo[34], S. Popa[25a], G. A. Popeneciu[25d], L. Portales[4], D. M. Portillo Quintero[163a], S. Pospisil[137], P. Postolache[25c], K. Potamianos[130], I. N. Potrap[77], C. J. Potter[30], H. Potti[1], T. Poulsen[44], J. Poveda[169], T. D. Powell[145], G. Pownall[44], M. E. Pozo Astigarraga[34], A. Prades Ibanez[169], P. Pralavorio[98], M. M. Prapa[42], S. Prell[76], D. Price[97], M. Primavera[65a], M. A. Principe Martin[95], M. L. Proffitt[144], N. Proklova[108], K. Prokofiev[60c], F. Prokoshin[77], G. Proto[71a,71b], S. Protopopescu[27], J. Proudfoot[5], M. Przybycien[81a], D. Pudzha[133], P. Puzo[62], D. Pyatiizbyantseva[108], J. Qian[102], Y. Qin[97], T. Qiu[90], A. Quadt[51], M. Queitsch-Maitland[34], G. Rabanal Bolanos[57], F. Ragusa[66a,66b], J. A. Raine[52], S. Rajagopalan[27], K. Ran[13a,13d], D. F. Rassloff[59a], D. M. Rauch[44], S. Rave[96], B. Ravina[55], I. Ravinovich[175], M. Raymond[34], A. L. Read[129], N. P. Readioff[145], D. M. Rebuzzi[68a,68b], G. Redlinger[27], K. Reeves[41], D. Reikher[157], A. Reiss[96], A. Rej[147], C. Rembser[34], A. Renardi[44], M. Renda[25b], M. B. Rendel[111], A. G. Rennie[55], S. Resconi[66a], M. Ressegotti[53a,53b], E. D. Resseguie[16], S. Rettie[92], B. Reynolds[123], E. Reynolds[19], M. Rezaei Estabragh[177], O. L. Rezanova[117a,117b], P. Reznicek[138], E. Ricci[73a,73b], R. Richter[111], S. Richter[44], E. Richter-Was[81b], M. Ridel[131], P. Rieck[111], P. Riedler[34], O. Rifki[44], M. Rijssenbeek[151], A. Rimoldi[68a,68b], M. Rimoldi[44], L. Rinaldi[21a,21b], T. T. Rinn[168], M. P. Rinnagel[110], G. Ripellino[150], I. Riu[12], P. Rivadeneira[44], J. C. Rivera Vergara[171], F. Rizatdinova[125], E. Rizvi[90], C. Rizzi[52], B. A. Roberts[173], B. R. Roberts[16], S. H. Robertson[100,x], M. Robin[44], D. Robinson[30], C. M. Robles Gajardo[142e], M. Robles Manzano[96], A. Robson[55], A. Rocchi[71a,71b], C. Roda[69a,69b], S. Rodriguez Bosca[59a], Y. Rodriguez Garcia[20a], A. Rodriguez Rodriguez[50], A. M. Rodríguez Vera[163b], S. Roe[34], A. R. Roepe[124], J. Roggel[177], O. Røhne[129], R. A. Rojas[171], B. Roland[50], C. P. A. Roland[63], J. Roloff[27], A. Romaniouk[108], M. Romano[21b], A. C. Romero Hernandez[168], N. Rompotis[88], M. Ronzani[121], L. Roos[131], S. Rosati[70a], B. J. Rosser[132], E. Rossi[162], E. Rossi[4], E. Rossi[67a,67b], L. P. Rossi[53b], L. Rossini[44], R. Rosten[123], M. Rotaru[25b], B. Rottler[50], D. Rousseau[62], D. Rousso[30], G. Rovelli[68a,68b], A. Roy[10], A. Rozanov[98], Y. Rozen[156], X. Ruan[31f], A. J. Ruby[88], T. A. Ruggeri[1], F. Rühr[50], A. Ruiz-Martinez[169], A. Rummler[34], Z. Rurikova[50], N. A. Rusakovich[77], H. L. Russell[34], L. Rustige[36], J. P. Rutherfoord[6], E. M. Rüttinger[145], K. Rybacki[87], M. Rybar[138], E. B. Rye[129], A. Ryzhov[118], J. A. Sabater Iglesias[52], P. Sabatini[169], L. Sabetta[70a,70b], H.F-W. Sadrozinski[141], R. Sadykov[77], F. Safai Tehrani[70a], B. Safarzadeh Samani[152], M. Safdari[149], S. Saha[100], M. Sahinsoy[111], A. Sahu[177], M. Saimpert[140], M. Saito[159], T. Saito[159], D. Salamani[34], G. Salamanna[72a,72b], A. Salnikov[149], J. Salt[169], A. Salvador Salas[12], D. Salvatore[39a,39b], F. Salvatore[152], A. Salzburger[34], D. Sammel[50], D. Sampsonidis[158], D. Sampsonidou[58c,58d], J. Sánchez[169], A. Sanchez Pineda[4], V. Sanchez Sebastian[169], H. Sandaker[129], C. O. Sander[44], I. G. Sanderswood[87], J. A. Sandesara[99], M. Sandhoff[177], C. Sandoval[20b], D. P. C. Sankey[139], M. Sannino[53a,53b], A. Sansoni[49], C. Santoni[36], H. Santos[135a,135b], S. N. Santpur[16], A. Santra[175], K. A. Saoucha[145], A. Sapronov[77], J. G. Saraiva[135a,135d], J. Sardain[98], O. Sasaki[79], K. Sato[164], C. Sauer[59b], F. Sauerburger[50], E. Sauvan[4], P. Savard[162,ah], R. Sawada[159], C. Sawyer[139], L. Sawyer[93], I. Sayago Galvan[169], C. Sbarra[21b], A. Sbrizzi[21a,21b], T. Scanlon[92], J. Schaarschmidt[144], P. Schacht[111], D. Schaefer[35], U. Schäfer[96], A. C. Schaffer[62], D. Schaile[110], R. D. Schamberger[151], E. Schanet[110], C. Scharf[17], N. Scharmberg[97], V. A. Schegelsky[133], D. Scheirich[138], F. Schenck[17], M. Schernau[166], C. Schiavi[53a,53b], L. K. Schildgen[22], Z. M. Schillaci[24], E. J. Schioppa[65a,65b], M. Schioppa[39a,39b], B. Schlag[96], K. E. Schleicher[50], S. Schlenker[34], K. Schmieden[96], C. Schmitt[96], S. Schmitt[44], L. Schoeffel[140], A. Schoening[59b], P. G. Scholer[50], E. Schopf[130], M. Schott[96], J. Schovancova[34], S. Schramm[52], F. Schroeder[177], H-C. Schultz-Coulon[59a], M. Schumacher[50], B. A. Schumm[141], Ph. Schune[140], A. Schwartzman[149], T. A. Schwarz[102], Ph. Schwemling[140], R. Schwienhorst[103], A. Sciandra[141], G. Sciolla[24], F. Scuri[69a], F. Scutti[101], C. D. Sebastiani[88], K. Sedlaczek[45], P. Seema[17], S. C. Seidel[113], A. Seiden[141], B. D. Seidlitz[27], T. Seiss[35], C. Seitz[44], J. M. Seixas[78b], G. Sekhniaidze[67a], S. J. Sekula[40], L. P. Selem[4], N. Semprini-Cesari[21a,21b], S. Sen[47], C. Serfon[27], L. Serin[62], L. Serkin[64a,64b], M. Sessa[72a,72b], H. Severini[124], S. Sevova[149], F. Sforza[53a,53b], A. Sfyrla[52], E. Shabalina[51], R. Shaheen[150], J. D. Shahinian[132], N. W. Shaikh[43a,43b], D. Shaked Renous[175], L. Y. Shan[13a], M. Shapiro[16], A. Sharma[34], A. S. Sharma[1], S. Sharma[44], P. B. Shatalov[119], K. Shaw[152], S. M. Shaw[97], P. Sherwood[92], L. Shi[92], C. O. Shimmin[178], Y. Shimogama[174], J. D. Shinner[91], I. P. J. Shipsey[130], S. Shirabe[52], M. Shiyakova[77], J. Shlomi[175], M. J. Shochet[35], J. Shojaii[101], D. R. Shope[150], S. Shrestha[123], E. M. Shrif[31f], M. J. Shroff[171], E. Shulga[175], P. Sicho[136], A. M. Sickles[168], E. Sideras Haddad[31f],

O. Sidiropoulou[34], A. Sidoti[21b], F. Siegert[46], Dj. Sijacki[14], J. M. Silva[19], M. V. Silva Oliveira[34], S. B. Silverstein[43a], S. Simion[62], R. Simoniello[34], N. D. Simpson[94], S. Simsek[11c], S. Sindhu[51], P. Sinervo[162], V. Sinetckii[109], S. Singh[148], S. Singh[162], S. Sinha[44], S. Sinha[31f], M. Sioli[21a,21b], I. Siral[127], S.Yu. Sivoklokov[109], J. Sjölin[43a,43b], A. Skaf[51], E. Skorda[94], P. Skubic[124], M. Slawinska[82], K. Sliwa[165], V. Smakhtin[175], B. H. Smart[139], J. Smiesko[138], S.Yu. Smirnov[108], Y. Smirnov[108], L. N. Smirnova[109,r], O. Smirnova[94], E. A. Smith[35], H. A. Smith[130], M. Smizanska[87], K. Smolek[137], A. Smykiewicz[82], A. A. Snesarev[107], H. L. Snoek[115], S. Snyder[27], R. Sobie[171,x], A. Soffer[157], C. A. Solans Sanchez[34], E.Yu. Soldatov[108], U. Soldevila[169], A. A. Solodkov[118], S. Solomon[50], A. Soloshenko[77], O. V. Solovyanov[118], V. Solovyev[133], P. Sommer[145], H. Son[165], A. Sonay[12], W. Y. Song[163b], A. Sopczak[137], A. L. Sopio[92], F. Sopkova[26b], S. Sottocornola[68a,68b], R. Soualah[120c], A. M. Soukharev[117a,117b], Z. Soumaimi[33e], D. South[44], S. Spagnolo[65a,65b], M. Spalla[111], M. Spangenberg[173], F. Spanò[91], D. Sperlich[50], G. Spigo[34], M. Spina[152], S. Spinali[87], D. P. Spiteri[55], M. Spousta[138], A. Stabile[66a,66b], B. L. Stamas[116], R. Stamen[59a], M. Stamenkovic[115], A. Stampekis[19], M. Standke[22], E. Stanecka[82], B. Stanislaus[34], M. M. Stanitzki[44], M. Stankaityte[130], B. Stapf[44], E. A. Starchenko[118], G. H. Stark[141], J. Stark[98], D. M. Starko[163b], P. Staroba[136], P. Starovoitov[59a], S. Stärz[100], R. Staszewski[82], G. Stavropoulos[42], P. Steinberg[27], A. L. Steinhebel[127], B. Stelzer[148,163a], H. J. Stelzer[134], O. Stelzer-Chilton[163a], H. Stenzel[54], T. J. Stevenson[152], G. A. Stewart[34], M. C. Stockton[34], G. Stoicea[25b], M. Stolarski[135a], S. Stonjek[111], A. Straessner[46], J. Strandberg[150], S. Strandberg[43a,43b], M. Strauss[124], T. Strebler[98], P. Strizenec[26b], R. Ströhmer[172], D. M. Strom[127], L. R. Strom[44], R. Stroynowski[40], A. Strubig[43a,43b], S. A. Stucci[27], B. Stugu[15], J. Stupak[124], N. A. Styles[44], D. Su[149], S. Su[58a], W. Su[58c,58d,144], X. Su[58a], K. Sugizaki[159], V. V. Sulin[107], M. J. Sullivan[88], D. M. S. Sultan[73a,73b], L. Sultanaliyeva[107], S. Sultansoy[3c], T. Sumida[83], S. Sun[102], S. Sun[176], X. Sun[97], O. Sunneborn Gudnadottir[167], C. J. E. Suster[153], M. R. Sutton[152], M. Svatos[136], M. Swiatlowski[163a], T. Swirski[172], I. Sykora[26a], M. Sykora[138], T. Sykora[138], D. Ta[96], K. Tackmann[44,v], A. Taffard[166], R. Tafirout[163a], R. H. M. Taibah[131], R. Takashima[84], K. Takeda[80], T. Takeshita[146], E. P. Takeva[48], Y. Takubo[79], M. Talby[98], A. A. Talyshev[117a,117b], K. C. Tam[60b], N. M. Tamir[157], A. Tanaka[159], J. Tanaka[159], R. Tanaka[62], J. Tang[58c], Z. Tao[170], S. Tapia Araya[76], S. Tapprogge[96], A. Tarek Abouelfadl Mohamed[103], S. Tarem[156], K. Tariq[58b], G. Tarna[25b], G. F. Tartarelli[66a], P. Tas[138], M. Tasevsky[136], E. Tassi[39a,39b], G. Tateno[159], Y. Tayalati[33e], G. N. Taylor[101], W. Taylor[163b], H. Teagle[88], A. S. Tee[176], R. Teixeira De Lima[149], P. Teixeira-Dias[91], H. Ten Kate[34], J. J. Teoh[115], K. Terashi[159], J. Terron[95], S. Terzo[12], M. Testa[49], R. J. Teuscher[162,x], N. Themistokleous[48], T. Theveneaux-Pelzer[17], O. Thielmann[177], D. W. Thomas[91], J. P. Thomas[19], E. A. Thompson[44], P. D. Thompson[19], E. Thomson[132], E. J. Thorpe[90], Y. Tian[51], V. O. Tikhomirov[107,ae], Yu.A. Tikhonov[117a,117b], S. Timoshenko[108], E. X. L. Ting[1], P. Tipton[178], S. Tisserant[98], S. H. Tlou[31f], A. Tnourji[36], K. Todome[21a,21b], S. Todorova-Nova[138], S. Todt[46], M. Togawa[79], J. Tojo[85], S. Tokár[26a], K. Tokushuku[79], E. Tolley[123], R. Tombs[30], M. Tomoto[79,112], L. Tompkins[149], P. Tornambe[99], E. Torrence[127], H. Torres[46], E. Torró Pastor[169], M. Toscani[28], C. Tosciri[35], J. Toth[98,w], D. R. Tovey[145], A. Traeet[15], C. J. Treado[121], T. Trefzger[172], A. Tricoli[27], I. M. Trigger[163a], S. Trincaz-Duvoid[131], D. A. Trischuk[170], W. Trischuk[162], B. Trocmé[56], A. Trofymov[62], C. Troncon[66a], F. Trovato[152], L. Truong[31c], M. Trzebinski[82], A. Trzupek[82], F. Tsai[151], M. Tsai[102], A. Tsiamis[158], P. V. Tsiareshka[104], A. Tsirigotis[158,t], V. Tsiskaridze[151], E. G. Tskhadadze[155a], M. Tsopoulou[158], Y. Tsujikawa[83], I. I. Tsukerman[119], V. Tsulaia[16], S. Tsuno[79], O. Tsur[156], D. Tsybychev[151], Y. Tu[60b], A. Tudorache[25b], V. Tudorache[25b], A. N. Tuna[34], S. Turchikhin[77], I. Turk Cakir[3a], R. J. Turner[19], R. Turra[66a], P. M. Tuts[37], S. Tzamarias[158], P. Tzanis[9], E. Tzovara[96], K. Uchida[159], F. Ukegawa[164], P. A. Ulloa Poblete[142b], G. Unal[34], M. Unal[10], A. Undrus[27], G. Unel[166], F. C. Ungaro[101], K. Uno[159], J. Urban[26b], P. Urquijo[101], G. Usai[7], R. Ushioda[160], M. Usman[106], Z. Uysal[11d], V. Vacek[137], B. Vachon[100], K. O. H. Vadla[129], T. Vafeiadis[34], C. Valderanis[110], E. Valdes Santurio[43a,43b], M. Valente[163a], S. Valentinetti[21a,21b], A. Valero[169], R. A. Vallance[19], A. Vallier[98], J. A. Valls Ferrer[169], T. R. Van Daalen[144], P. Van Gemmeren[5], S. Van Stroud[92], I. Van Vulpen[115], M. Vanadia[71a,71b], W. Vandelli[34], M. Vandenbroucke[140], E. R. Vandewall[125], D. Vannicola[157], L. Vannoli[53a,53b], R. Vari[70a], E. W. Varnes[6], C. Varni[16], T. Varol[154], D. Varouchas[62], K. E. Varvell[153], M. E. Vasile[25b], L. Vaslin[36], G. A. Vasquez[171], F. Vazeille[36], D. Vazquez Furelos[12], T. Vazquez Schroeder[34], J. Veatch[51], V. Vecchio[97], M. J. Veen[115], I. Veliscek[130], L. M. Veloce[162], F. Veloso[135a,135c], S. Veneziano[70a], A. Ventura[65a,65b], A. Verbytskyi[111], M. Verducci[69a,69b], C. Vergis[22], M. Verissimo De Araujo[78b], W. Verkerke[115], A. T. Vermeulen[115], J. C. Vermeulen[115], C. Vernieri[149], P. J. Verschuuren[91], M. Vessella[99], M. L. Vesterbacka[121], M. C. Vetterli[148,ah], A. Vgenopoulos[158],

N. Viaux Maira[142e], T. Vickey[145], O. E. Vickey Boeriu[145], G. H. A. Viehhauser[130], L. Vigani[59b], M. Villa[21a,21b], M. Villaplana Perez[169], E. M. Villhauer[48], E. Vilucchi[49], M. G. Vincter[32], G. S. Virdee[19], A. Vishwakarma[48], C. Vittori[21a,21b], I. Vivarelli[152], V. Vladimirov[173], E. Voevodina[111], M. Vogel[177], P. Vokac[137], J. Von Ahnen[44], E. Von Toerne[22], B. Vormwald[34], V. Vorobel[138], K. Vorobev[108], M. Vos[169], J. H. Vossebeld[88], M. Vozak[97], L. Vozdecky[90], N. Vranjes[14], M. Vranjes Milosavljevic[14], V. Vrba[137,*], M. Vreeswijk[115], N. K. Vu[98], R. Vuillermet[34], O. V. Vujinovic[96], I. Vukotic[35], S. Wada[164], C. Wagner[99], W. Wagner[177], S. Wahdan[177], H. Wahlberg[86], R. Wakasa[164], M. Wakida[112], V. M. Walbrecht[111], J. Walder[139], R. Walker[110], S. D. Walker[91], W. Walkowiak[147], A. M. Wang[57], A. Z. Wang[176], C. Wang[58a], C. Wang[58c], H. Wang[16], J. Wang[60a], P. Wang[40], R.-J. Wang[96], R. Wang[57], R. Wang[116], S. M. Wang[154], S. Wang[58b], T. Wang[58a], W. T. Wang[75], W. X. Wang[58a], X. Wang[13c], X. Wang[168], X. Wang[58c], Y. Wang[58a], Z. Wang[102], Z. Wang[47,58c,58d], Z. Wang[102], C. Wanotayaroj[34], A. Warburton[100], C. P. Ward[30], R. J. Ward[19], N. Warrack[55], A. T. Watson[19], M. F. Watson[19], G. Watts[144], B. M. Waugh[92], A. F. Webb[10], C. Weber[27], M. S. Weber[18], S. A. Weber[32], S. M. Weber[59a], C. Wei[58a], Y. Wei[130], A. R. Weidberg[130], J. Weingarten[45], M. Weirich[96], C. Weiser[50], T. Wenaus[27], B. Wendland[45], T. Wengler[34], S. Wenig[34], N. Wermes[22], M. Wessels[59a], S. Westhoff[179], K. Whalen[127], A. M. Wharton[87], A. S. White[57], A. White[7], M. J. White[1], D. Whiteson[166], L. Wickremasinghe[128], W. Wiedenmann[176], C. Wiel[46], M. Wielers[139], N. Wieseotte[96], C. Wiglesworth[38], L. A. M. Wiik-Fuchs[50], D. J. Wilbern[124], H. G. Wilkens[34], L. J. Wilkins[91], D. M. Williams[37], H. H. Williams[132], S. Williams[30], S. Willocq[99], P. J. Windischhofer[130], I. Wingerter-Seez[4], F. Winklmeier[127], B. T. Winter[50], M. Wittgen[149], M. Wobisch[93], A. Wolf[96], R. Wölker[130], J. Wollrath[166], M. W. Wolter[82], H. Wolters[135a,135c], V. W. S. Wong[170], A. F. Wongel[44], S. D. Worm[44], B. K. Wosiek[82], K. W. Woźniak[82], K. Wraight[55], J. Wu[13a,13d], S. L. Wu[176], X. Wu[52], Y. Wu[58a], Z. Wu[58a,140], J. Wuerzinger[130], T. R. Wyatt[97], B. M. Wynne[48], S. Xella[38], L. Xia[13c], M. Xia[13b], J. Xiang[60c], X. Xiao[102], M. Xie[58a], X. Xie[58a], I. Xiotidis[152], D. Xu[13a], H. Xu[58a], H. Xu[58a], L. Xu[58a], R. Xu[132], W. Xu[102], Y. Xu[13b], Z. Xu[58b], Z. Xu[149], B. Yabsley[153], S. Yacoob[31a], N. Yamaguchi[85], Y. Yamaguchi[160], M. Yamatani[159], H. Yamauchi[164], T. Yamazaki[16], Y. Yamazaki[80], J. Yan[58c], S. Yan[130], Z. Yan[23], H. J. Yang[58c,58d], H. T. Yang[16], S. Yang[58a], T. Yang[60c], X. Yang[58a], X. Yang[13a], Y. Yang[159], Z. Yang[58a,102], W-M. Yao[16], Y. C. Yap[44], H. Ye[13c], J. Ye[40], S. Ye[27], I. Yeletskikh[77], M. R. Yexley[87], P. Yin[37], K. Yorita[174], K. Yoshihara[76], C. J. S. Young[50], C. Young[149], M. Yuan[102], R. Yuan[58b,i], X. Yue[59a], M. Zaazoua[33e], B. Zabinski[82], G. Zacharis[9], E. Zaid[48], A. M. Zaitsev[118,ad], T. Zakareishvili[155b], N. Zakharchuk[32], S. Zambito[34], D. Zanzi[50], O. Zaplatilek[137], S. V. Zeißner[45], C. Zeitnitz[177], J. C. Zeng[168], D. T. Zenger Jr[24], O. Zenin[118], T. Ženiš[26a], S. Zenz[90], S. Zerradi[33a], D. Zerwas[62], B. Zhang[13c], D. F. Zhang[145], G. Zhang[13b], J. Zhang[5], K. Zhang[13a], L. Zhang[13c], M. Zhang[168], R. Zhang[176], S. Zhang[102], X. Zhang[58c], X. Zhang[58b], Z. Zhang[62], P. Zhao[47], T. Zhao[58b], Y. Zhao[141], Z. Zhao[58a], A. Zhemchugov[77], Z. Zheng[149], D. Zhong[168], B. Zhou[102], C. Zhou[176], H. Zhou[6], N. Zhou[58c], Y. Zhou[6], C. G. Zhu[58b], C. Zhu[13a,13d], H. L. Zhu[58a], H. Zhu[13a], J. Zhu[102], Y. Zhu[58a], X. Zhuang[13a], K. Zhukov[107], V. Zhulanov[117a,117b], D. Zieminska[63], N. I. Zimine[77], S. Zimmermann[50,*], J. Zinsser[59b], M. Ziolkowski[147], L. Živković[14], A. Zoccoli[21a,21b], K. Zoch[52], T. G. Zorbas[145], O. Zormpa[42], W. Zou[37], L. Zwalinski[34]

---

[1] Department of Physics, University of Adelaide, Adelaide, Australia

[2] Department of Physics, University of Alberta, Edmonton, AB, Canada

[3] (a)Department of Physics, Ankara University, Ankara, Turkey; (b)Application and Research Center for Advanced Studies, Istanbul Aydin University, Istanbul, Turkey; (c)Division of Physics, TOBB University of Economics and Technology, Ankara, Turkey

[4] LAPP, Univ. Savoie Mont Blanc, CNRS/IN2P3, Annecy, France

[5] High Energy Physics Division, Argonne National Laboratory, Argonne, IL, USA

[6] Department of Physics, University of Arizona, Tucson, AZ, USA

[7] Department of Physics, University of Texas at Arlington, Arlington, TX, USA

[8] Physics Department, National and Kapodistrian University of Athens, Athens, Greece

[9] Physics Department, National Technical University of Athens, Zografou, Greece

[10] Department of Physics, University of Texas at Austin, Austin, TX, USA

[11] (a)Bahcesehir University, Faculty of Engineering and Natural Sciences, Istanbul, Turkey; (b)Istanbul Bilgi University, Faculty of Engineering and Natural Sciences, Istanbul, Turkey; (c)Department of Physics, Bogazici University, Istanbul, Turkey; (d)Department of Physics Engineering, Gaziantep University, Gaziantep, Turkey

[12] Institut de Física d'Altes Energies (IFAE), Barcelona Institute of Science and Technology, Barcelona, Spain

[13] [a] Institute of High Energy Physics, Chinese Academy of Sciences, Beijing, China; [b] Physics Department, Tsinghua University, Beijing, China; [c] Department of Physics, Nanjing University, Nanjing, China; [d] University of Chinese Academy of Science (UCAS), Beijing, China

[14] Institute of Physics, University of Belgrade, Belgrade, Serbia

[15] Department for Physics and Technology, University of Bergen, Bergen, Norway

[16] Physics Division, Lawrence Berkeley National Laboratory and University of California, Berkeley, CA, USA

[17] Institut für Physik, Humboldt Universität zu Berlin, Berlin, Germany

[18] Albert Einstein Center for Fundamental Physics and Laboratory for High Energy Physics, University of Bern, Bern, Switzerland

[19] School of Physics and Astronomy, University of Birmingham, Birmingham, UK

[20] [a] Facultad de Ciencias y Centro de Investigaciónes, Universidad Antonio Nariño, Bogotá, Colombia; [b] Departamento de Física, Universidad Nacional de Colombia, Bogotá, Colombia

[21] [a] Dipartimento di Fisica e Astronomia A. Righi, Università di Bologna, Bologna, Italy; [b] INFN Sezione di Bologna, Bologna, Italy

[22] Physikalisches Institut, Universität Bonn, Bonn, Germany

[23] Department of Physics, Boston University, Boston, MA, USA

[24] Department of Physics, Brandeis University, Waltham, MA, USA

[25] [a] Transilvania University of Brasov, Brasov, Romania; [b] Horia Hulubei National Institute of Physics and Nuclear Engineering, Bucharest, Romania; [c] Department of Physics, Alexandru Ioan Cuza University of Iasi, Iasi, Romania; [d] Physics Department, National Institute for Research and Development of Isotopic and Molecular Technologies, Cluj-Napoca, Romania; [e] University Politehnica Bucharest, Bucharest, Romania; [f] West University in Timisoara, Timisoara, Romania

[26] [a] Faculty of Mathematics, Physics and Informatics, Comenius University, Bratislava, Slovakia; [b] Department of Subnuclear Physics, Institute of Experimental Physics of the Slovak Academy of Sciences, Kosice, Slovak Republic

[27] Physics Department, Brookhaven National Laboratory, Upton, NY, USA

[28] Departamento de Física (FCEN) and IFIBA, Universidad de Buenos Aires and CONICET, Buenos Aires, Argentina

[29] California State University, Long Beach, CA, USA

[30] Cavendish Laboratory, University of Cambridge, Cambridge, UK

[31] [a] Department of Physics, University of Cape Town, Cape Town, South Africa; [b] iThemba Labs, Western Cape, South Africa; [c] Department of Mechanical Engineering Science, University of Johannesburg, Johannesburg, South Africa; [d] National Institute of Physics, University of the Philippines, Diliman, Philippines; [e] University of South Africa, Department of Physics, Pretoria, South Africa; [f] School of Physics, University of the Witwatersrand, Johannesburg, South Africa

[32] Department of Physics, Carleton University, Ottawa, ON, Canada

[33] [a] Faculté des Sciences Ain Chock, Réseau Universitaire de Physique des Hautes Energies, Université Hassan II, Casablanca, Morocco; [b] Faculté des Sciences, Université Ibn-Tofail, Kenitra, Morocco; [c] Faculté des Sciences Semlalia, Université Cadi Ayyad, LPHEA, Marrakech, Morocco; [d] LPMR, Faculté des Sciences, Université Mohamed Premier, Oujda, Morocco; [e] Faculté des sciences, Université Mohammed V, Rabat, Morocco; [f] Mohammed VI Polytechnic University, Ben Guerir, Morocco

[34] CERN, Geneva, Switzerland

[35] Enrico Fermi Institute, University of Chicago, Chicago, IL, USA

[36] LPC, Université Clermont Auvergne, CNRS/IN2P3, Clermont-Ferrand, France

[37] Nevis Laboratory, Columbia University, Irvington, NY, USA

[38] Niels Bohr Institute, University of Copenhagen, Copenhagen, Denmark

[39] [a] Dipartimento di Fisica, Università della Calabria, Rende, Italy; [b] INFN Gruppo Collegato di Cosenza, Laboratori Nazionali di Frascati, Frascati, Italy

[40] Physics Department, Southern Methodist University, Dallas, TX, USA

[41] Physics Department, University of Texas at Dallas, Richardson, TX, USA

[42] National Centre for Scientific Research "Demokritos", Agia Paraskevi, Greece

[43] [a] Department of Physics, Stockholm University, Stockholm, Sweden; [b] Oskar Klein Centre, Stockholm, Sweden

[44] Deutsches Elektronen-Synchrotron DESY, Hamburg and Zeuthen, Germany

[45] Lehrstuhl für Experimentelle Physik IV, Technische Universität Dortmund, Dortmund, Germany

46 Institut für Kern- und Teilchenphysik, Technische Universität Dresden, Dresden, Germany

47 Department of Physics, Duke University, Durham, NC, USA

48 SUPA-School of Physics and Astronomy, University of Edinburgh, Edinburgh, UK

49 INFN e Laboratori Nazionali di Frascati, Frascati, Italy

50 Physikalisches Institut, Albert-Ludwigs-Universität Freiburg, Freiburg, Germany

51 II. Physikalisches Institut, Georg-August-Universität Göttingen, Göttingen, Germany

52 Département de Physique Nucléaire et Corpusculaire, Université de Genève, Geneva, Switzerland

53 (a)Dipartimento di Fisica, Università di Genova, Genoa, Italy; (b)INFN Sezione di Genova, Genoa, Italy

54 II. Physikalisches Institut, Justus-Liebig-Universität Giessen, Giessen, Germany

55 SUPA-School of Physics and Astronomy, University of Glasgow, Glasgow, UK

56 LPSC, Université Grenoble Alpes, CNRS/IN2P3, Grenoble INP, Grenoble, France

57 Laboratory for Particle Physics and Cosmology, Harvard University, Cambridge, MA, USA

58 (a)Department of Modern Physics and State Key Laboratory of Particle Detection and Electronics, University of Science and Technology of China, Hefei, China; (b)Institute of Frontier and Interdisciplinary Science and Key Laboratory of Particle Physics and Particle Irradiation (MOE), Shandong University, Qingdao, China; (c)School of Physics and Astronomy, Key Laboratory for Particle Astrophysics and Cosmology (MOE), SKLPPC, Shanghai Jiao Tong University, Shanghai, China; (d)Tsung-Dao Lee Institute, Shanghai, China

59 (a)Kirchhoff-Institut für Physik, Ruprecht-Karls-Universität Heidelberg, Heidelberg, Germany; (b)Physikalisches Institut, Ruprecht-Karls-Universität Heidelberg, Heidelberg, Germany

60 (a)Department of Physics, Chinese University of Hong Kong, Shatin, N.T., Hong Kong; (b)Department of Physics, University of Hong Kong, Pokfulam, Hong Kong; (c)Department of Physics and Institute for Advanced Study, Hong Kong University of Science and Technology, Clear Water Bay, Kowloon, Hong Kong, China

61 Department of Physics, National Tsing Hua University, Hsinchu, Taiwan

62 IJCLab, Université Paris-Saclay, CNRS/IN2P3, 91405 Orsay, France

63 Department of Physics, Indiana University, Bloomington, IN, USA

64 (a)INFN Gruppo Collegato di Udine, Sezione di Trieste, Udine, Italy; (b)ICTP, Trieste, Italy; (c)Dipartimento Politecnico di Ingegneria e Architettura, Università di Udine, Udine, Italy

65 (a)INFN Sezione di Lecce, Lecce, Italy; (b)Dipartimento di Matematica e Fisica, Università del Salento, Lecce, Italy

66 (a)INFN Sezione di Milano, Milan, Italy; (b)Dipartimento di Fisica, Università di Milano, Milan, Italy

67 (a)INFN Sezione di Napoli, Naples, Italy; (b)Dipartimento di Fisica, Università di Napoli, Naples, Italy

68 (a)INFN Sezione di Pavia, Pavia, Italy; (b)Dipartimento di Fisica, Università di Pavia, Pavia, Italy

69 (a)INFN Sezione di Pisa, Pisa, Italy; (b)Dipartimento di Fisica E. Fermi, Università di Pisa, Pisa, Italy

70 (a)INFN Sezione di Roma, Rome, Italy; (b)Dipartimento di Fisica, Sapienza Università di Roma, Rome, Italy

71 (a)INFN Sezione di Roma Tor Vergata, Rome, Italy; (b)Dipartimento di Fisica, Università di Roma Tor Vergata, Rome, Italy

72 (a)INFN Sezione di Roma Tre, Rome, Italy; (b)Dipartimento di Matematica e Fisica, Università Roma Tre, Rome, Italy

73 (a)INFN-TIFPA, Povo, Italy; (b)Università degli Studi di Trento, Trento, Italy

74 Institut für Astro- und Teilchenphysik, Leopold-Franzens-Universität, Innsbruck, Austria

75 University of Iowa, Iowa City, IA, USA

76 Department of Physics and Astronomy, Iowa State University, Ames, IA, USA

77 Joint Institute for Nuclear Research, Dubna, Russia

78 (a)Departamento de Engenharia Elétrica, Universidade Federal de Juiz de Fora (UFJF), Juiz de Fora, Brazil; (b)Universidade Federal do Rio De Janeiro COPPE/EE/IF, Rio de Janeiro, Brazil; (c)Instituto de Física, Universidade de São Paulo, São Paulo, Brazil

79 KEK, High Energy Accelerator Research Organization, Tsukuba, Japan

80 Graduate School of Science, Kobe University, Kobe, Japan

81 (a)AGH University of Science and Technology, Faculty of Physics and Applied Computer Science, Krakow, Poland; (b)Marian Smoluchowski Institute of Physics, Jagiellonian University, Krakow, Poland

82 Institute of Nuclear Physics Polish Academy of Sciences, Krakow, Poland

83 Faculty of Science, Kyoto University, Kyoto, Japan

84 Kyoto University of Education, Kyoto, Japan

85 Research Center for Advanced Particle Physics and Department of Physics, Kyushu University, Fukuoka , Japan

86 Instituto de Física La Plata, Universidad Nacional de La Plata and CONICET, La Plata, Argentina

[87] Physics Department, Lancaster University, Lancaster, UK

[88] Oliver Lodge Laboratory, University of Liverpool, Liverpool, UK

[89] Department of Experimental Particle Physics, Jožef Stefan Institute and Department of Physics, University of Ljubljana, Ljubljana, Slovenia

[90] School of Physics and Astronomy, Queen Mary University of London, London, UK

[91] Department of Physics, Royal Holloway University of London, Egham, UK

[92] Department of Physics and Astronomy, University College London, London, UK

[93] Louisiana Tech University, Ruston, LA, USA

[94] Fysiska Institutionen, Lunds Universitet, Lund, Sweden

[95] Departamento de Física Teorica C-15 and CIAFF, Universidad Autónoma de Madrid, Madrid, Spain

[96] Institut für Physik, Universität Mainz, Mainz, Germany

[97] School of Physics and Astronomy, University of Manchester, Manchester, UK

[98] CPPM, Aix-Marseille Université, CNRS/IN2P3, Marseille, France

[99] Department of Physics, University of Massachusetts, Amherst, MA, USA

[100] Department of Physics, McGill University, Montreal, QC, Canada

[101] School of Physics, University of Melbourne, Melbourne, VIC, Australia

[102] Department of Physics, University of Michigan, Ann Arbor, MI, USA

[103] Department of Physics and Astronomy, Michigan State University, East Lansing, MI, USA

[104] B.I. Stepanov Institute of Physics, National Academy of Sciences of Belarus, Minsk, Belarus

[105] Research Institute for Nuclear Problems of Byelorussian State University, Minsk, Belarus

[106] Group of Particle Physics, University of Montreal, Montreal, QC, Canada

[107] P.N. Lebedev Physical Institute of the Russian Academy of Sciences, Moscow, Russia

[108] National Research Nuclear University MEPhI, Moscow, Russia

[109] D.V. Skobeltsyn Institute of Nuclear Physics, M.V. Lomonosov Moscow State University, Moscow, Russia

[110] Fakultät für Physik, Ludwig-Maximilians-Universität München, Munich, Germany

[111] Max-Planck-Institut für Physik (Werner-Heisenberg-Institut), Munich, Germany

[112] Graduate School of Science and Kobayashi-Maskawa Institute, Nagoya University, Nagoya, Japan

[113] Department of Physics and Astronomy, University of New Mexico, Albuquerque, NM, USA

[114] Institute for Mathematics, Astrophysics and Particle Physics, Radboud University/Nikhef, Nijmegen, The Netherlands

[115] Nikhef National Institute for Subatomic Physics and University of Amsterdam, Amsterdam, The Netherlands

[116] Department of Physics, Northern Illinois University, DeKalb, IL, USA

[117] (a)Budker Institute of Nuclear Physics and NSU, SB RAS, Novosibirsk, Russia; (b)Novosibirsk State University, Novosibirsk, Russia

[118] Institute for High Energy Physics of the National Research Centre, Kurchatov Institute, Protvino, Russia

[119] Institute for Theoretical and Experimental Physics named by A.I. Alikhanov of National Research Centre "Kurchatov Institute", Moscow, Russia

[120] (a)New York University Abu Dhabi, Abu Dhabi, United Arab Emirates; (b)United Arab Emirates University, Al Ain, United Arab Emirates; (c)University of Sharjah, Sharjah, United Arab Emirates

[121] Department of Physics, New York University, New York, NY, USA

[122] Ochanomizu University, Otsuka, Bunkyo-ku, Tokyo, Japan

[123] Ohio State University, Columbus, OH, USA

[124] Homer L. Dodge Department of Physics and Astronomy, University of Oklahoma, Norman, OK, USA

[125] Department of Physics, Oklahoma State University, Stillwater, OK, USA

[126] Palacký University, Joint Laboratory of Optics, Olomouc, Czech Republic

[127] Institute for Fundamental Science, University of Oregon, Eugene, OR, USA

[128] Graduate School of Science, Osaka University, Osaka, Japan

[129] Department of Physics, University of Oslo, Oslo, Norway

[130] Department of Physics, Oxford University, Oxford, UK

[131] LPNHE, Sorbonne Université, Université de Paris, CNRS/IN2P3, Paris, France

[132] Department of Physics, University of Pennsylvania, Philadelphia, PA, USA

[133] Konstantinov Nuclear Physics Institute of National Research Centre "Kurchatov Institute", PNPI, St. Petersburg, Russia

[134] Department of Physics and Astronomy, University of Pittsburgh, Pittsburgh, PA, USA

135 (a)Laboratório de Instrumentação e Física Experimental de Partículas - LIP, Lisbon, Portugal; (b)Departamento de Física, Faculdade de Ciências, Universidade de Lisboa, Lisbon, Portugal; (c)Departamento de Física, Universidade de Coimbra, Coimbra, Portugal; (d)Centro de Física Nuclear da Universidade de Lisboa, Lisbon, Portugal; (e)Departamento de Física, Universidade do Minho, Braga, Portugal; (f)Departamento de Física Teórica y del Cosmos, Universidad de Granada, Granada, Spain; (g)Instituto Superior Técnico, Universidade de Lisboa, Lisbon, Portugal

136 Institute of Physics of the Czech Academy of Sciences, Prague, Czech Republic

137 Czech Technical University in Prague, Prague, Czech Republic

138 Charles University, Faculty of Mathematics and Physics, Prague, Czech Republic

139 Particle Physics Department, Rutherford Appleton Laboratory, Didcot, UK

140 IRFU, CEA, Université Paris-Saclay, Gif-sur-Yvette, France

141 Santa Cruz Institute for Particle Physics, University of California Santa Cruz, Santa Cruz, CA, USA

142 (a)Departamento de Física, Pontificia Universidad Católica de Chile, Santiago, Chile; (b)Universidad de la Serena, La Serena, Chile; (c)Universidad Andres Bello, Department of Physics, Santiago, Chile; (d)Instituto de Alta Investigación, Universidad de Tarapacá, Arica, Chile; (e)Departamento de Física, Universidad Técnica Federico Santa María, Valparaíso, Chile

143 Universidade Federal de São João del Rei (UFSJ), São João del Rei, Brazil

144 Department of Physics, University of Washington, Seattle, WA, USA

145 Department of Physics and Astronomy, University of Sheffield, Sheffield, UK

146 Department of Physics, Shinshu University, Nagano, Japan

147 Department Physik, Universität Siegen, Siegen, Germany

148 Department of Physics, Simon Fraser University, Burnaby, BC, Canada

149 SLAC National Accelerator Laboratory, Stanford, CA, USA

150 Department of Physics, Royal Institute of Technology, Stockholm, Sweden

151 Departments of Physics and Astronomy, Stony Brook University, Stony Brook, NY, USA

152 Department of Physics and Astronomy, University of Sussex, Brighton, UK

153 School of Physics, University of Sydney, Sydney, Australia

154 Institute of Physics, Academia Sinica, Taipei, Taiwan

155 (a)E. Andronikashvili Institute of Physics, Iv. Javakhishvili Tbilisi State University, Tbilisi, Georgia; (b)High Energy Physics Institute, Tbilisi State University, Tbilisi, Georgia

156 Department of Physics, Technion, Israel Institute of Technology, Haifa, Israel

157 Raymond and Beverly Sackler School of Physics and Astronomy, Tel Aviv University, Tel Aviv, Israel

158 Department of Physics, Aristotle University of Thessaloniki, Thessaloniki, Greece

159 International Center for Elementary Particle Physics and Department of Physics, University of Tokyo, Tokyo, Japan

160 Department of Physics, Tokyo Institute of Technology, Tokyo, Japan

161 Tomsk State University, Tomsk, Russia

162 Department of Physics, University of Toronto, Toronto, ON, Canada

163 (a)TRIUMF, Vancouver, BC, Canada; (b)Department of Physics and Astronomy, York University, Toronto, ON, Canada

164 Division of Physics and Tomonaga Center for the History of the Universe, Faculty of Pure and Applied Sciences, University of Tsukuba, Tsukuba, Japan

165 Department of Physics and Astronomy, Tufts University, Medford, MA, USA

166 Department of Physics and Astronomy, University of California Irvine, Irvine, CA, USA

167 Department of Physics and Astronomy, University of Uppsala, Uppsala, Sweden

168 Department of Physics, University of Illinois, Urbana, IL, USA

169 Instituto de Física Corpuscular (IFIC), Centro Mixto Universidad de Valencia-CSIC, Valencia, Spain

170 Department of Physics, University of British Columbia, Vancouver, BC, Canada

171 Department of Physics and Astronomy, University of Victoria, Victoria, BC, Canada

172 Fakultät für Physik und Astronomie, Julius-Maximilians-Universität Würzburg, Würzburg, Germany

173 Department of Physics, University of Warwick, Coventry, UK

174 Waseda University, Tokyo, Japan

175 Department of Particle Physics and Astrophysics, Weizmann Institute of Science, Rehovot, Israel

176 Department of Physics, University of Wisconsin, Madison, WI, USA

177 Fakultät für Mathematik und Naturwissenschaften, Fachgruppe Physik, Bergische Universität Wuppertal, Wuppertal, Germany

[178] Department of Physics, Yale University, New Haven, CT, USA

[179] Associated at Institut für Theoretische Physik, Universität Heidelberg, Heidelberg, Germany

[a] Also at Borough of Manhattan Community College, City University of New York, New York, NY, USA

[b] Also at Bruno Kessler Foundation, Trento, Italy

[c] Also at Center for High Energy Physics, Peking University, China

[d] Also at Centro Studi e Ricerche Enrico Fermi, Rome, Italy

[e] Also at CERN, Geneva, Switzerland

[f] Also at Département de Physique Nucléaire et Corpusculaire, Université de Genève, Geneva, Switzerland

[g] Also at Departament de Fisica de la Universitat Autonoma de Barcelona, Barcelona, Spain

[h] Also at Department of Financial and Management Engineering, University of the Aegean, Chios, Greece

[i] Also at Department of Physics and Astronomy, Michigan State University, East Lansing, MI, USA

[j] Also at Department of Physics and Astronomy, University of Louisville, Louisville, KY, USA

[k] Also at Department of Physics, Ben Gurion University of the Negev, Beer Sheva, Israel

[l] Also at Department of Physics, California State University, East Bay, USA

[m] Also at Department of Physics, California State University, Fresno, USA

[n] Also at Department of Physics, California State University, Sacramento, USA

[o] Also at Department of Physics, King's College London, London, UK

[p] Also at Department of Physics, St. Petersburg State Polytechnical University, St. Petersburg, Russia

[q] Also at Department of Physics, University of Fribourg, Fribourg, Switzerland

[r] Also at Faculty of Physics, M.V. Lomonosov Moscow State University, Moscow, Russia

[s] Also at Graduate School of Science, Osaka University, Osaka, Japan

[t] Also at Hellenic Open University, Patras, Greece

[u] Also at Institucio Catalana de Recerca i Estudis Avancats, ICREA, Barcelona, Spain

[v] Also at Institut für Experimentalphysik, Universität Hamburg, Hamburg, Germany

[w] Also at Institute for Particle and Nuclear Physics, Wigner Research Centre for Physics, Budapest, Hungary

[x] Also at Institute of Particle Physics (IPP), Victoria, Canada

[y] Also at Institute of Physics, Azerbaijan Academy of Sciences, Baku, Azerbaijan

[z] Also at Institute of Theoretical Physics, Ilia State University, Tbilisi, Georgia

[aa] Also at Instituto de Fisica Teorica, IFT-UAM/CSIC, Madrid, Spain

[ab] Also at Department of Physics, Istanbul University, Istanbul, Turkey

[ac] Also at Joint Institute for Nuclear Research, Dubna, Russia

[ad] Also at Moscow Institute of Physics and Technology State University, Dolgoprudny, Russia

[ae] Also at National Research Nuclear University MEPhI, Moscow, Russia

[af] Also at Physikalisches Institut, Albert-Ludwigs-Universität Freiburg, Freiburg, Germany

[ag] Also at The City College of New York, New York, NY, USA

[ah] Also at TRIUMF, Vancouver, BC, Canada

[ai] Also at Universita di Napoli Parthenope, Naples, Italy

[aj] Also at University of Chinese Academy of Sciences (UCAS), Beijing, China

[ak] Also at Physics Department, Yeditepe University, Istanbul, Turkey

[*] Deceased